

# **CHARACTERIZATION OF THE DYNAMIC ONSET OF FIBRIC DAMAGE IN TYPE I COLLAGEN FASCICLES**

by

Edward Herger

A thesis submitted in partial fulfillment of the requirements for the degree of

**MASTER OF SCIENCES  
In  
MECHANICAL ENGINEERING**

**UNIVERSITY OF PUERTO RICO  
MAYAGÜEZ CAMPUS  
2009**

Approved by:

---

Paul A. Sundaram, Ph.D.  
President, Graduate Committee

---

Date

---

Vijay K. Goyal, Ph.D.  
Member, Graduate Committee

---

Date

---

Rick Valentin, Ph.D.  
Member, Graduate Committee

---

Date

---

Pablo Caceres Valencia, Ph.D.  
Chairperson of the Department

---

Date

---

Dr. Surinder Singh  
Representative of Graduate Studies

---

Date

## **Abstract**

The mechanical properties of collagen in the form of Type I fascicles obtained from rat tail tendons were determined under dynamic loading conditions. Experimental procedures and apparatus were developed to establish a relationship between parameters of dynamic loading and the ability of collagen to resist damage. The viscoelastic behavior of the fascicles under sinusoidal tensile loading was characterized in terms of loss tangent and dynamic modulus and in terms of models developed specifically to explain the observed results. Dynamic analysis showed an average loss tangent of approximately 0.3 at 0.5 hertz, a value which agrees well with literature. Type I collagen fascicles were able to withstand higher amounts of impulse, defined by area under the force-time curve of the loading function, at higher frequencies for the range tested. Detailed strain analysis revealed two distinct behaviors, a linear hysteric progression of strain which dominates at low loading frequencies and a saturating curve behavior which prevails at high loading frequencies. Computational and mechanistic models have been established for each case. The action of an intermolecular chain mechanism caused by the addition of strain energy affecting the state of cross linking in the material is hypothesized to explain the observed phenomena. Support for this hypothesis is based on the definitive results indicating higher order time-mechanical behavior prevalence with increasing loading frequency.

## Resumen

Las propiedades de fibras de colágeno Tipo I obtenidas de los tendones de la cola de rata fueron investigadas. Procedimientos experimentales y equipos especiales fueron desarrollados para establecer la relación entre las características de carga dinámica y la resistencia de la fibra contra daño. El comportamiento viscoelástico de las fibras fue definido en términos de “loss tangent” y “dynamic modulus” y también con modelos desarrollados según los resultados específicos. Análisis dinámico dio 0.3 para “loss tangent” a frecuencia de 0.5 hertzios, un valor que tenga buena correlación con otros valores publicados. Fue observado que fibras de colágeno Tipo I soportan más impulso cuando cargadas a mayor frecuencia. Un análisis detallado de deformación mostró dos comportamientos de progresión de deformación distintos. Típicamente con variación de carga a bajas frecuencias, la progresión de deformación fue lineal. Por lo tanto, con altas frecuencias, progresión de deformación mostró típicamente un comportamiento curvado. Varios modelos han sido establecidos para caracterizar el comportamiento observado. Una hipótesis está ofrecida explicando el comportamiento a través de un modelo que se enfoca en el proceso de aumentación de energía de deformación que provoca actividad entre enlaces transversos conectando las cadenas de moléculas.

## **Acknowledgements**

I would especially like to thank my advisor Dr. Paul Sundaram for providing great support as well as freedom in this project. His unique ability to combine creative vision with supreme technical knowledge allowed this project to reach its potential. Also, I must thank the energetic and dedicated individuals of the Mechanical Engineering and Biology Departments at the University of Puerto Rico Mayagüez. Their spirit and attitude made this project not only successful, but a joy to undertake. Further, I would like to express my appreciation to all of those who have been close to me for many years and those who have become close to me in recent times. You provide strength, inspiration, motivation and challenge, but more than anything invaluable friendship. Finally, I would like to recognize all those who display, encourage and spread the bold open-mindedness that drives the evolution of science and humanity. If we lose our desire for knowledge and experience, we lose what it is to be human.

# Contents

<b>List of Equations.....</b>	<b>ix</b>
<b>List of Figures.....</b>	<b>x</b>
<b>List of Tables.....</b>	<b>xii</b>
<b>Chapter 1: Introduction and Breadth of Project.....</b>	<b>1</b>
1.1 Overview.....	1
1.2 Purpose and Scope of Work.....	2
1.3 Basic Methodology.....	3
1.4 Report Format.....	3
1.5 Ethical Concerns.....	4
<b>Chapter 2: Technical Background.....</b>	<b>5</b>
2.1 Overview.....	5
2.2 Collagen.....	5
2.3 Human Tendons.....	9
2.4 Inflammation and Tendon Pathologies.....	11
2.5 Anatomy and Biomechanics.....	13
2.6 ASTM F2212-08e1.....	14
<b>Chapter 3: Literature Review.....</b>	<b>16</b>
3.1 Overview.....	16
3.2 Quasi-static Mechanical Testing.....	16
3.3 Dynamic Mechanical Testing.....	18
3.4 Micro/Nano Indentation Techniques.....	19
3.5 Testing of Chemical-mechanical Relationships.....	21
3.6 Testing of Biological-mechanical Relationships.....	22
3.7 Non-mechanical Testing Methods.....	22
3.8 Testing of Engineered Collagen Biomaterials.....	24
3.9 Literature Review Summary.....	25
<b>Chapter 4: Methodology.....</b>	<b>26</b>
4.1 Overview.....	26
4.2 Pre-experimental Procedures.....	27
4.2.1 Defining Failure Mode.....	27
4.2.2 Defining General Test Procedures.....	28

4.2.3	Addressing Validity of Results.....	29
4.2.4	Dehydration Induced Damage.....	30
4.3	Phase I.....	31
4.3.1	Selecting a Tendon Substructure.....	31
4.3.2	Sourcing Collagenous Tendon Fascicles.....	32
4.3.3	Fascicle Extraction Procedures.....	32
4.3.4	Storage of Materials and Samples.....	33
4.4	Phase II.....	34
4.4.1	Test Apparatus Design Parameters.....	34
4.4.2	General Design Specifications.....	36
4.4.3	Voice Coil Linear Motor Specifications.....	37
4.4.4	Linear Bearing Guide and Linkage.....	38
4.4.5	Sensor and Data Acquisition Specifications.....	39
4.4.6	Clamp Design.....	41
4.4.7	Platform Schematic.....	42
4.5	Phase III.....	43
4.5.1	Visualizing Sample Failure.....	43
4.5.2	Microscope and Related Equipment.....	44
4.5.3	Point of Failure.....	45
4.6	Phase IV.....	46
4.6.1	Replication of in-vivo Conditions.....	46
4.6.2	Maintenance of Temperature.....	46
4.6.3	Maintaining Stable Chemistry.....	47
4.6.4	Hydration of Exposed Collagen.....	47
4.7	Detailed Testing Procedures.....	48
4.7.1	Microscope Set-up.....	48
4.7.2	Sensor and Data Acquisition System Connections.....	48
4.7.3	Data Acquisition Calibration.....	49
4.7.4	Connecting Voice Coil Motor Power Supplies.....	49
4.7.5	Preparing Samples for Testing.....	50
4.7.6	Sample Mounting Procedure.....	50
4.7.7	Measurement of Initial Dimensions.....	51
4.7.8	Test Run Procedure.....	52
4.8	Post-experimental Procedures.....	52
4.8.1	Trimming the Data Points.....	52
4.8.2	Essential Result Set.....	53
4.8.3	Advanced Result Set.....	55

<b>Chapter 5: Basis for Interpreting Results and Reaching Conclusions.....</b>	<b>59</b>
5.1 Overview.....	59
5.2 Limitations in Interpreting Results.....	59
5.3 Developing Relevant Conclusions through Anatomy and Biomechanics.....	60
5.4 Load Bearing Fascicle Count.....	60
5.5 Biomechanical Loading Function.....	61
5.6 Suitable Candidates for Study.....	62
5.7 Tendon Injury Risk Coefficient.....	63
5.8 Final Formulation.....	64
5.9 Validation and Refinement of Results.....	65
<b>Chapter 6: Results.....</b>	<b>67</b>
6.1 Overview.....	67
6.2 Reported Results for Essential Interpretation.....	68
6.2.1 Results: 0.5 Hz Frequency; 0.5 N Amplitude; 0.5 N Preload.....	68
6.2.2 Results: 1.0 Hz Frequency; 0.5 N Amplitude; 0.5 N Preload.....	70
6.2.3 Results: 1.5 Hz Frequency; 0.5 N Amplitude; 0.5 N Preload.....	72
6.2.4 Results: 2.0 Hz Frequency; 0.5 N Amplitude; 0.5 N Preload.....	74
6.2.5 Results: 2.4 Hz Frequency; 0.5 N Amplitude; 0.5 N Preload.....	76
6.3 Essential Results Against Frequency.....	78
6.3.1 Basic Data Presentation.....	78
6.3.2 Linear Interpretation of Essential Results.....	79
6.3.3 Polynomial Fit to Essential Results.....	81
<b>Chapter 7: Advanced Results.....</b>	<b>83</b>
7.1 Overview.....	83
7.2 Dual Response Behavior.....	83
7.3 Variation of Instantaneous Strain Rate.....	88
7.4 Modulus Trends Corresponding to Split Behavior.....	90
7.5 Discussion of Mechanistic Model.....	93
7.6 Loss Angle; Loss Tangent; and Dynamic Modulus.....	98
7.7 Proposed Models and Correlation of Solutions.....	101
7.8 Quasi-physical Model.....	104
<b>Chapter 8: Conclusions and Continuation of Work.....</b>	<b>107</b>
8.1 Overview.....	107
8.2 Conclusions in Results.....	107
8.3 Conclusions in Advanced Results.....	108

8.4 Future Collagen Testing.....	109
<b>8.5 Testing of Fibers in General.....</b>	<b>110</b>
<b>References.....</b>	<b>111</b>
<b>Appendix A: Complete Strain per Time Results.....</b>	<b>117</b>
<b>Appendix B: Photographs.....</b>	<b>134</b>
<b>Appendix C: Review of Viscoelasticity.....</b>	<b>140</b>
C.1 Overview.....	140
C.2 Macro-mechanics of Viscoelastic Materials.....	141
C.3 Testing Methods for Viscoelastic Materials.....	144
C.4 Quasi-physical Viscoelastic Models.....	145
C.5 Model Solutions and Tensor Analysis.....	148

## List of Equations

4.1	Impulse per cross-section calculation.....	53
4.2	Calibrated load calculation.....	55
4.3	Measured transient stress calculation.....	56
4.4	Sample cross-sectional area calculation.....	56
4.5	Calibrated displacement calculation.....	56
4.6	Measured transient strain calculation.....	57
4.7	Transient stress calculation.....	57
4.8	Data point rate of strain calculation.....	58
5.1	Load per fascicle calculation.....	63
5.2	Example tendon injury risk coefficient calculation.....	64
5.3	Possible polynomial fit template.....	65
6.1	Linear approximation to durability.....	80
6.2	Polynomial fit to durability.....	82
7.1	Model of higher order strain trend.....	84
7.2	Computational strain template for linearly progressive behavior.....	101
7.3	Proposed computational strain model for linearly progressive behavior.....	101
7.4	Computational strain template for exponentially progressive behavior.....	102
7.5	Proposed computational strain model for exponentially progressive behavior.....	103
7.6	Kelvin-Voight input energy calculation.....	104
7.7	Kelvin-Voight output energy calculation.....	104
7.8	Final energy analysis equation for Kelvin-Voight model with hysteric damping.....	105
C.1	Ideal spring equation.....	148
C.2	Ideal damper equation.....	149
C.3	Adding mechanical elements in series.....	149
C.4	Adding mechanical elements in parallel.....	149
C.5	Coupled equations defining viscoelasticity.....	153
C.6	Phase angle calculation.....	154
C.7	Dynamic modulus relationships.....	154
C.8	Dynamic modulus relation to phase angle*.....	154

## List of Figures

2.1	Molecular Model of Collagen.....	6
2.2	D-band patterning.....	7
2.3	Cross-linking in collagen.....	8
2.4	Tendon hierarchy illustration.....	10
2.5	Image of scar tissue repair.....	13
4.1	SEM of parallel collagen fibrils.....	28
4.2	Biomechanical cycling of the knee joint.....	29
4.3	LVCM-051-089-01 Linear Voice Coil Motor.....	37
4.4	Omega Engineering LCFA-1KG Load Cell.....	39
4.5	Omega Engineering LD621-30 LVDT.....	40
4.6	Clamp design.....	41
4.7	Schematic of testing platform.....	42
4.8	Damaged collagen fascicles from previous research.....	44
4.9	Example of graphical result.....	55
6.1	Example applied loading function (10 cycles).....	68
6.2	Graphical representation of test series.....	69
6.3	Example applied loading function (10 cycles).....	70
6.4	Graphical representation of test series.....	71
6.5	Example applied loading function (10 cycles).....	72
6.6	Graphical representation of test series.....	73
6.7	Example applied loading function (10 cycles).....	74
6.8	Graphical representation of test series.....	75
6.9	Example applied loading function (10 cycles)*.....	76
6.10	Graphical representation of test series.....	77
6.11	Graphical representation of basic results.....	79
6.12	Linear representation of basic results.....	80
6.13	Polynomial representation of basic results.....	81
7.1	Trend distribution observed throughout testing.....	84
7.2	Examples of observed linear strain trend at various loading frequencies.....	85
7.3	Examples of observed exponential behavior at various loading frequencies.....	86
7.4	Observed average strain amplitude plotted against frequency.....	89
7.5	Maximum observed instantaneous strain rate verse frequency.....	90
7.6	Graphs showing modulus trend during higher order behavior at 1.0 hertz.....	91
7.7	Graphs showing modulus trend during linear behavior at 1.0 hertz.....	92
7.8	Dissipated and recoverable portion of strain cycles.....	94
7.9	Mechanistic model cycle for linear behavior.....	95
7.10	Mechanistic model cycle for higher order behavior.....	96

7.11	Assumed behavior of dynamic cross-link reestablishment.....	97
7.12	Distributions of loss angle and loss tangent against sample area .....	99
7.13	Example material characterization graph at 0.5 hertz loading frequency.....	100
7.14	Predicted linear behavior at 1.5 hertz loading frequency.....	102
7.15	Predicted exponential strain behavior at 1.5 hertz loading frequency.....	103
7.16	Strain behavior predicted by Kelvin-Voight model with hysteric damping*.....	105
C.1	Graphs demonstrating viscoelastic creep.....	141
C.2	Graph demonstrating viscoelastic stress relaxation selected biomaterials.....	142
C.3	Generic representation of a viscoelastic hysteresis loop.....	142
C.4	Cyclic test with controlled strain state demonstrating phase shift.....	143
C.5	Shear stress to strain rate graph for some special case viscoelastic materials.....	144
C.6	Maxwell Model.....	146
C.7	Kelvin-Voight Model.....	147
C.8	Standard Linear Solid Model.....	148
C.9	Graphical representation of solution to Maxwell Model*.....	150
C.10	Graphical representation of solution to Kelvin-Voight Model*.....	150
C.11	Graphical representation of solution to Standard Linear Solid Model*.....	151

## List of Tables

2.1	Specific strength values for engineering materials.....	8
2.2	Recommended treatments for inflammation.....	12
6.1	Full set of results tabulated for simplified reference.....	78

# Chapter 1

## Introduction and Breadth of Project

### 1.1 Overview

Physical testing of materials will always be one of the most essential aspects of engineering. Without defining elastic, thermal, magnetic, electrical and chemical properties and limits of engineering materials, the engineer can hardly begin the process of design.

The application of material properties in design development may be rather straight forward or particularly complicated. In essence, engineers define the parameters within which their design can safely operate using material properties which are often readily available, ubiquitous and standardized. Additionally, a factor of safety is always applied based on numerous aspects of the design's application and its critical nature. If loading on the structure exceeds the engineer's determined value, the system is considered to be operating in an unsafe condition. If loading continues to intensify, the structure, or a substructure will eventually fail. Similar to the factor of safety assigned to a design, the definition of failure is also subject to interpretation according to various aspects of the system in question. In some cases, complete breakage of a part may be the only important form of failure. In other cases, exceeding the elastic limit of the material and subsequent deformation and change in material properties constitutes failure. In the most critical applications, a part may be considered to have failed simply if it is in use for a period of time or number of cycles exceeding the predetermined design limit. The part may be in perfect condition, but is considered unsafe due to the critical nature of its role in the system [1].

The past half century has seen the rise in use of engineering composites to greatly enhance the design possibilities over use of conventional monolithic materials. Incorporation of composite design undoubtedly improves the engineer's capabilities of optimization and innovation. However, factor of safety and structural failure are not as easily defined. Composite materials are complicated to manufacture, often resulting in inconsistent properties and material limits. While numerous standards for material testing of composites do exist, the field is still

considered as much an art as a science. The design factor of safety must be adjusted accordingly and new characteristics and modes of failure are introduced [2].

The emerging field of bioengineering brings the complexity of defining material properties to yet another level. Monolithic organic materials such as lipids, proteins and polysaccharides are characterized by their complex time dependent properties and sensitivity to the delicate chemistry of the human body [3-5]. Further complicating the outlook, biological structures such as skin, bone, tendon and ligament are all composite materials. The final aspect of this complex problem is that each of the structures is part of a living creature and therefore, any stimulus to the structure results in a reaction of several of the body's systems [6]. It becomes apparent that the failure of an organic structure can be defined in a number of ways.

## **1.2 Purpose and Scope of Work**

The basic purpose of this work is to facilitate an in-vitro biomechanical test of the physical limits of collagen under dynamic tension. To effectively meet this goal, a mode of failure for a specific biological structural element is defined, and using an innovative dynamic testing method and apparatus, the properties and limits of the material are determined so that a factor of safety, or risk level can be predicted for a number of high intensity human activities especially in athletics.

Further, a detailed analysis of the cyclic mechanical response of collagen in tension is carried out. The instrumented platform which is used to induce failure of the material also provides transient stress/strain data which will be interpreted dynamically to create a series of models which characterize the behavior of collagen. Finally, a mechanistic model describing the molecular and super-molecular interactions which govern the physical behavior is hypothesized.

The structural element to be studied is the tendon fascicle substructure, a composite fiber (0.3 millimeter average diameter) consisting of micro-scale collagen fibrils bound in an organic matrix [7-9]. The final goal is to be able to offer a general guideline, useful not only to scientists and engineers, but to athletes and coaches as well, that suggests when intensity, duration or both

parameters of a repetitive training activity put the tendon at risk of minor damage and subsequent unfavorable inflammatory reaction or other chronic pathology.

### **1.3 Basic Methodology**

Individual collagen fascicles are sourced from commonly available rat tail tendons. They are removed by basic dissection of the tail. Each test consists of mounting a fascicle between two posts, one static and one free to translate along the axis of the sample, using custom designed clamps. The static post contains a load cell for measurement of the instantaneous tension while the mobile post is driven by a linear motor and contains a displacement sensor for measurement of strain.

Upon commencement of a test, the linear motor applies tension to the fiber in a sinusoidal pattern where the tension on the sample is never allowed to fall below zero. Testing occurs under an optical microscope at approximately 50X magnification which allows the observation of the development of damage within the fascicle so that the point of failure can be clearly defined during progressive loading cycles.

### **1.4 Report Format**

This report is divided into eight chapters with the intention of organizing and dividing distinct result sets and conclusions as well as presenting general concepts first followed by advanced concepts and conclusions based on initially developed ideas. An initial presentation of the work to be described and the type of results that will be reported is given in Chapter 1. Chapter 2 provides essential technical background of areas that are not well known to the mechanical engineer, but are important in this work and will be developed in detail later in the report. In Chapter 3 a thorough review of previous work that has been done in the field of testing

the mechanical properties of collagen is presented. Chapter 4 gives full detail of the experimental methodologies and equipment employed. A methodology for interpretation of results pertaining to the fiber's ability to resist damage where the final result provides an estimation of whether or not a specific activity or exercise is likely to cause damage in the tendon which is stressed is proposed in Chapter 5. Complete results obtained comparing collagen's ability to resist damage according to the frequency of the loading function is presented in Chapter 6. Chapter 7 presents the results of the detailed study of collagen's mechanical behavior under dynamic tension. Numerous models are also developed and presented in Chapter 8. Finally, Chapter 8 gives a brief conclusion highlighting all of the important points that are reported. Three appendices are included: Appendix A gives the complete set of strain versus time graphs for all tests; Appendix B displays various photographs taken during testing including magnified collagen fascicles; finally, Appendix C provides the reader with a detailed review of viscoelasticity, the analysis of viscoelastic materials and methods for modeling specific viscoelastic characteristics.

## **1.5 Ethical Concerns**

This project's intention is to establish a guideline which warns against conducting physical activity exceeding certain levels of intensity. Ethical questions are raised in relation to the possibility that certain classical athletic activities could be considered unsafe due to the conclusions put forth by this research. In the mind of the author, the establishment of such a conclusion is unacceptable. To avoid this conflict, the results will be related only to training type activities such as weightlifting and calisthenics. Practically speaking, these experiments will have a higher correlation to training type activities which are much more uniform and repetitive than competitive physical activities which are generally random and varied from a biomechanical point of view.

## **Chapter 2**

### **Technical Background**

#### **2.1 Overview**

A number of concepts outside the realm of common knowledge in mechanical engineering will be developed in this report. A detailed review of important topics is given in this chapter to allow for the effective presentation of advanced results and conclusions. The intention is to provide a complete background in the molecular/superstructural characteristics of collagen, as well as in areas of physiology and biomechanics. All of these will be used later to develop accurate, pertinent and reliable conclusions.

#### **2.2 Collagen**

Collagen is among the most abundant materials that can be found in any form of vertebrate life. It is a structural protein occurring in as many as twenty eight varieties described to date [7-9]. All variations are characterized by an amino acid chain type molecule similar to the model in Figure 2.1. Proline, hydroxyproline and glycine are the principal amino acid components. Differences in specific chemical composition and amino acid sequence are responsible for the many varieties. The characteristics and therefore functions change significantly among collagen's variations. In several types, the protein chain molecules form fibers. In others, the polymer molecules do not form into fibers, but the larger structure is known to be in the form of a fiber. Non-periodic, but structured networks are also formed by certain varieties of collagen [7-9].

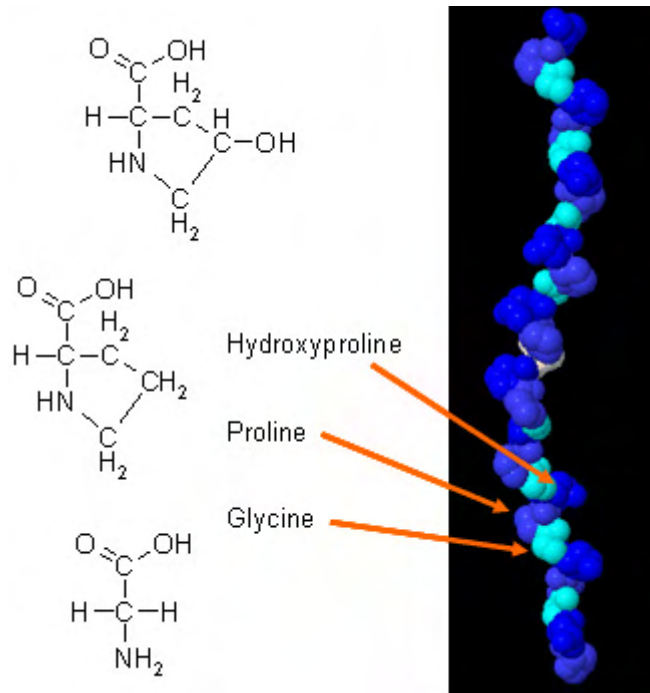


**Figure 2.1:** Molecular Model of Collagen

Individual molecules of collagen have been termed tropocollagens. Every tropocollagen is formed by three peptide strands which arrange into left-handed helical structures of 1.5 nanometer diameter and 300 nanometer length. In fibrous collagen varieties, tropocollagens form a periodic right-handed coil which becomes known as a micro-fibril. Micro-fibrils then associate to form higher structures and so on. The ends of tropocollagens have a uniform staggering of approximately 67nm, a value that can change due to dehydration of the structure. The result is a periodic structure referenced by the letter “D” represented schematically in Figure 2.2. A D-Period consists of four tropocollagens, but the result is a non-uniform sequence where some D-Periods contain five tropocollagens instead of four. This particular arrangement results in a band or wave pattern termed D-Banding. D-Bands can be observed on the microscopic level, and are visible to the naked eye in larger collagen structures [10, 11]. The cross-sectional arrangement is hexagonal or quasi-hexagonal with some covalent type cross-linking between tropocollagens. In nature, maturity of cross-links increases with age, that is, the collagenous structures of young creatures are not fully cross-linked on the super-molecular level [12].

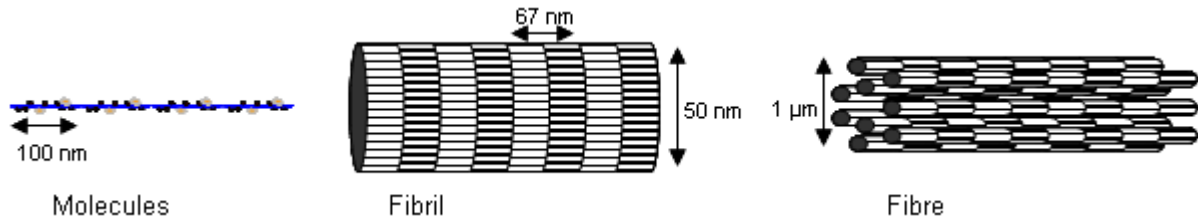


**Figure 2.2:** D-band patterning

It is important to note that collagen is not chemically inert. Proteins play important chemical roles in the human body through enzymatic mechanisms. Collagen has not only structural purposes, but conducts enzymatic functions as well. Specifically, these properties are responsible for controlling growth and repair of the body’s structural tissues as well as processes such as blood clotting [4].

The unique construction of collagen results in several characteristic physical properties. Most notably high stiffness to weight ratio, is observed in fibers of collagen [13, 14]. The results of this work show a stiffness to weight ratio for Type I collagen of approximately  $300 \frac{kN-m}{kg}$ . Values for various other materials are given in Table 2.1 for comparison. The above mentioned D-Periodic sequence results in a non-linear toe region in a stress-strain diagram at the initial application of tension on the fiber. The phenomenon is a result of a gradual straightening of the waves in collagen sub-fibers. Once sufficient tension is applied, the sub-fibers straighten fully and the stress-strain curve becomes linear until onset of failure [14]. The other particular mechanical property of collagen is viscoelasticity, a time dependent stress-strain relationship. The phenomenon may be attributed to the inconsistent breaking of covalent bonds between sub-fibers or adjacent tropocollagens as in Figure 2.3. These are termed “sacrificial bonds,” but tend to reconstruct themselves upon release of tension allowing the fiber to regain its original properties [15]. Collagen cross-links and/or the entire structure of collagen can be broken down by various methods. In bioengineering, for example, application of thermal, chemical and mechanical methods is used to create a collagen gel that can then serve as a raw material for numerous advanced applications [16-18].

**Table 2.1:** Specific strength values for engineering materials (units:  $\frac{kN-m}{kg}$ )

Rubber	16.3
Brass	67.8
Aluminum	222
Steel	254
Titanium	288
Glass Fiber	1307
Carbon Fiber	2457
Carbon Nanotube	46268

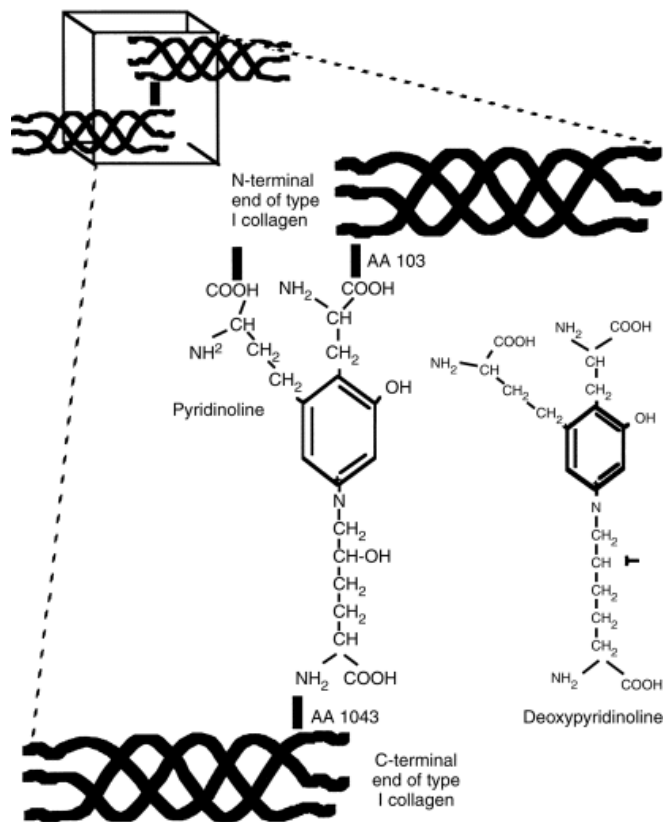


**Figure 2.3:** Cross-linking in collagen

When considering the structure of human beings, the most common form of collagen by far is Type I. It is of the fibrous nature with its tropocollagen polymer chains aligned in the axial direction, an arrangement that results in a particularly strong and resilient structural fiber. For this reason, many of the body's components are composites of Type I collagen. Tendon and ligament are nearly exclusively Type I collagen with only small amounts of matrix and sheathing material to organize the bundles of fiber. Bones and teeth are composites of Type I collagen and crystalline apatite forming a much more rigid structure. When collagen is combined with keratin, skin is formed. Types II, III, IV and V are also commonly found in various tissues and organs of the human body, and may have differing functions such as filtering of blood and matrix material for collagen fiber composite structures among others [3, 7, 8, 19].

## **2.3 Human Tendons**

As mentioned, the basic biological unit studied in this research is the collagenous tendon fascicle. A detailed description of the tendon must be given in order to fully justify the relationship to be established between the material properties of the fascicle and the functionality and capacity of the tendon as a unit.

Tendons are an integral part of the human skeletal system. They allow locomotion by serving as mechanical linkages between the body's skeletal muscles and bones. Tendons are formed by groupings of higher order fibrous Type I collagen structures as shown in Figure 2.4. Micro-fibrils converge in a parallel and in-phase arrangement to form collagen fibrils bound by matrix materials including proteoglycan, decorin and aggrecan. Fibrils then form parallel groups, become bound by endotenon and are then termed fascicles, the smallest structures that can be studied on the macroscopic level. Parallel bundles of fascicles are sheathed by epitenon and the final grouping is bound in peritenon and results in the tendon as a unit [7, 20]. The final dry weight composition of a typical tendon is approximately eighty six percent unidirectional Type I collagen with matrix materials making up the final fourteen percent [21]. Isolated human muscles are capable of producing only tensile force, their tendons with a rope-like structure,

operate efficiently only in tension, an obvious result since the majority of the composite fraction is parallel fiber.

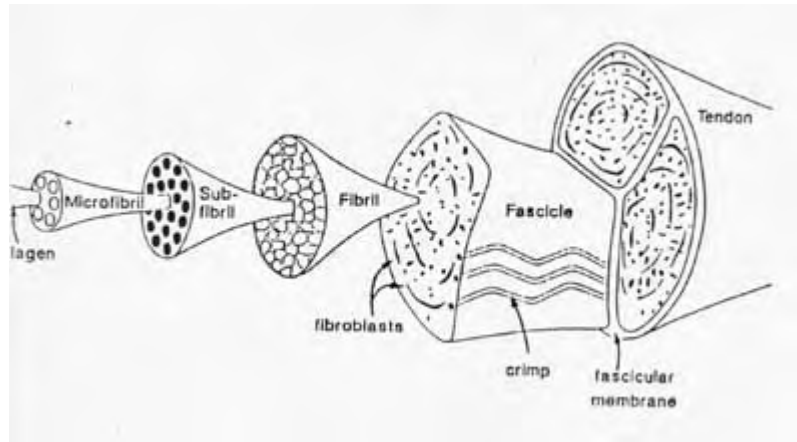


**Figure 2.4:** Tendon hierarchy illustration

Although strictly a structural component of the body, the tendon is truly living tissue and therefore completely integrated into human metabolic processes. Limited branching blood vessels are found in endotenon in a direction parallel to fiber alignment. While nerve cells are not found in tendon, nerve endings are attached to epitenon and peritenon. So called Golgi tendon organs are found in the region between muscle and tendon, and serve to communicate information relating the amount of force being generated by the muscle-tendon system to the central nervous system. Finally, collagen generating cells known as fibroblasts are found within all tendons as well as most other collagen based tissues [17, 22].

The tendon communicates its condition with the body's higher order systems chemically. Since proteins are active in the enzymatic sense, a broken or damaged protein strand produces a distinct chemistry that causes an inflammatory response in the area of the damage. Fibroblasts as living cells respond to the inflammation mechanisms of the body repairing the damage that has occurred in the tendon due to overuse or acute injury [17, 23]. Fibroblasts are thought to be sensitive to stress direction when producing tissue. Stress deprivation after injury can cause

disoriented tissue generation in tendon for example, resulting in a less than ideal repair formed by weak scar tissue whose fibers are not aligned with the load direction [17].

The specific structure of tendons, in conjunction with characteristic properties of collagen, is considered to yield various beneficial biomechanical phenomena related to human locomotion. The low initial modulus attributed to the un-stretched wave structure serves as a cushioning mechanism, attenuating shock transmitted through impacts, heavy foot falls, etc. This characteristic also reduces the load at the initiation of muscle contraction. The high, linear modulus of the pre-stretched tendon allows for fast reaction to intense muscle contraction as well as efficient energy transfer at high speed. Energy storage and return during rapid movement is an additional biomechanical benefit. As a unit the tendon has a relatively high degree of viscoelasticity which attenuates high intensity shock. Further, the viscoelastic properties of the tendon allow the muscle to continue contracting dynamically during isometric or static application of force. This reduces overall fatigue by gradually allowing more muscle fibers to activate over a period of time [11, 24, 25].

## **2.4 Inflammation and Tendon Pathologies**

To define a failure mode that results in an undesirable reaction of the body's immune mechanisms, the inflammatory processes must be understood. Micro-scale injury to tendon material results in a chemical change surrounding the damage site. The main triggering chemical is collagenase mRNA among other general syntheses of proteins including cytokine which is generally associated with inflammatory response [5, 26]. A subsequent series of chemical reactions communicates the signal to the immune system which in turn triggers a repair oriented response. The inflammatory response includes increased fluid and white blood cell presence in the area resulting in painful swelling. Fibroblast metabolism is increased to allow for the production of new tendon material. Further, fibroblasts regulate their activity through gene expression based on the general level of stress experienced by the tendon [5]. For this reason, both overuse and lack of use or stress deprivation cause undesirable effects.

The inflammation reaction, although a facilitator of tissue repair, is considered adverse in terms of athletic performance. The pain associated with the pathology alone prevents full athletic capacity. However, the tensile capacities of the tendon are also reduced during repair due to presence of collagenase in the tendon matrix [5, 28].

Treatment of tendon pathologies becomes a delicate process due to the various factors involved. Onsite swelling can be reduced by medications ranging from non-steroidal anti-inflammatories to potent cortical steroids. External processes such as cooling of the affected area and massage are also effective in reducing swelling [29]. Table 2.2 summarizes treatment options.

**Table 2.2:** Recommended treatments, their premises and drawbacks, for inflammation

<b>REST</b>	<b>AVOID PHYSICAL ACTIVITY THAT STRESSES THE AFFECTED AREA</b>	<b>LACK OF FIBROBLAST STIMULATION</b>
<b>ICING</b>	<b>COOL AFFECTED AREA BY APPLYING ICE OF COLD PACKS</b>	<b>REMOVAL OF BODY'S REPAIR MECHANISMS</b>
<b>NSAIDs</b>	<b>IBUPROPHEN; ACETYLSALICYLIC ACID; ACETAMINOPHEN; ETC.</b>	<b>REMOVAL OF BODY'S REPAIR MECHANISMS</b>
<b>CORTICOSTEROIDS</b>	<b>HYDROCORTISONE; CORTISONE ACETATE; PREDNISONE ETC.</b>	<b>CATABOLIC EFFECT ON TISSUE</b>
<b>PHYSICAL THERAPY</b>	<b>RESISTANCE TRAINING; STRETCHING; ULTRASOUND STIMULATION; ETC.</b>	<b>POSSIBILITY OF FURTHER DAMAGE</b>
<b>SURGERY</b>	<b>REPAIR OF RUPTURED TENDON BY TENDON GRAFT</b>	<b>COMPLICATIONS OF SURGERY; LONG HEALING TIME</b>

Of course reducing the inflammatory response is beneficial only in that pain is alleviated. Tissue repair slows when inflammation is inhibited, and so actions taken to reduce swelling also increase realistic healing time and put the patient in danger of advancing damage by continued

overuse [30]. Conversely, lack of activity is equally detrimental as insufficient stress stimulation will eliminate the necessary directional signals to fibroblasts which likely will result in formation of scar tissue repair, see Figure 2.5, instead of strong, properly oriented tissue.



**Figure 2.5:** Image of scar tissue repair

## 2.5 Anatomy and Biomechanics

In an effort to generate widely useful results that can be utilized by the general nonscientific population, this work seeks to relate general parameters of human activity to the capacity of the tendon to sustain that activity without damage. To this end, concepts in anatomy and biomechanics must be applied to determine the effects of large scale movements of the body on the individual fascicle and the effects of specific material properties of the fascicle on the body's movements. Advancing from this basis, the biological systems can be accurately modeled and replicated in the lab. Furthermore, necessary assumptions and generalizations can be made during subsequent analysis.

Several basic but important concepts relevant to this work come from anatomy and biomechanics. Basic mechanics of materials dictates that, given a specific exercise having a

certain rate, intensity and duration, a larger tendon will experience less mechanical stress than a smaller tendon. The muscle groups that are used and their respective tendons must be identified, and the size of these tendons in terms of cross-sectional area must be approximated or measured. As a function of the muscle-tendon-bone arrangement, the tendon as a unit transfers force as an in-series component. Tendons are not homogeneous structural units. They are formed of a composite material with directional mechanical properties and fraction of a mechanically dominant material. The actual load bearing portion of the tendon as a composite must be determined where the fascicle is assumed to be the first homogeneous unit in the hierarchy. Finally, the load on the tendon must be measured, approximated or reformulated to a more general value which may include the factors of rate and duration. Determination of the exact loading function that tendons experience is particularly difficult. Various simplifications will certainly have to be made to complete the final goal of this project. To retain high accuracy when transferring laboratory determined values to usable formulas and guidelines, the methodologies and approximations used must be carefully scrutinized under the principles of anatomy and biomechanics.

## **2.6 ASTM F2212-08e1**

ASTM (American Society for Testing and Materials) is a widely known international organization which publishes an enormous range of procedural and general standards for testing of engineering materials and devices. The scope of ASTM standards extends into the realm of biomaterials, and among many other bioengineering related guidelines, ASTM F2212-08e1 is known as the standard guide for characterization of Type I collagen as starting material for surgical implants and substrates for tissue engineered medical products. This standard deals mainly with the biocompatibility and quality of engineered collagen material, and not with properties of naturally structured collagen studied in this project. Direct relevance is very limited in this case since the immediate goals for this project do not include advancement of engineered tissue technology. However, the experimental procedures of the present work do include measurement of several specific properties of the Type I collagen fascicle, and so future

applications of this research could potentially include enhancement of bioengineering in applications of both artificial and processed natural biomaterials [18].

## **Chapter 3**

### **Literature Review**

#### **3.1 Overview**

The history of the study of collagen in terms of mechanical material properties extends from the mid-twentieth century to the present with enormous increases in science's understanding of this biomaterial and advancement of experimentation techniques. The larger field of investigation of mechanical properties can be divided into numerous subcategories based on scale, testing equipment utilized and developed and final application. These divisions will be treated individually to establish exactly where the presently discussed work best applies, and to establish the novel nature of the approach that is being employed in this project.

#### **3.2 Quasi-static Mechanical Testing**

The single most essential form of mechanical testing of materials is the basic quasi-static tensile test. Quasi-static refers to the application of increased load at a rate slow and uniform enough to effectively eliminate dynamic effects. Several material characteristics can be measured using this form of tensile testing including: elastic modulus, viscoelastic creep or stress relaxation and yield and ultimate strengths. Naturally, collagen fibers were first tested using these techniques.

The earliest reviewed study was undertaken in the late 1950's by Rigby, Hirai, Spikes and Eyring [31]. The research was based on simple quasi-static tensile testing of Type I fibrous collagen extracted from rat tail tendons. The fibers were found to suffer from reduced modulus after exceeding 4 percent strain; however, repetition of loading allowed strains of over 35% to be reached. Temperature was also controlled and determined to have no effect on mechanical

properties in the range of 0-37 degrees Celsius. Finally a simple model was proposed to aid in the further study of soft tissue disorders.

The scope of quasi-static collagen testing has since expanded to include various more specific collagen based structures under refined conditions. In a cooperative study conducted by a group of international universities, properties of collagen-elastin composite interactions with extracellular matrix in lung tissue were investigated by quasi-static testing. The flexibility and simplicity of the basic quasi-static tensile test allowed investigators to measure material properties in hypotonic, normal and hypertonic solutions. This work concluded that the characteristics of the interaction between collagen formations and extracellular matrix are dependent on the present osmolarity, and a combined effect of material properties and organization of the material's composite structure are responsible for the larger properties of lung tissue [32].

In a similar, highly specific study, the University of Pittsburgh departments of regenerative medicine and urology combined to conduct a bi-axial quasi-static test of high collagen content urinary bladder wall tissue harvested from Sprague-Drawley rats. Test and control groups of samples underwent different treatments. The control group was considered healthy tissue, while the test group was taken from rats that were intentionally injured at the thoracic portion of the spinal cord four weeks before sacrifice. Results were assumed to reflect the effect of human spinal cord on urinary bladder wall tissue and the ensuing complications. Definitively lower resistance to stress relaxation was seen in spinal cord injury samples [33].

Stella and Sacks conducted a novel study of isolated layers of heart valve leaflet materials each having distinct collagen derived material properties. The heart valve leaflets were separated into two layers, the fibrosa and ventricularis. They were tested individually under biaxial loading with highly sensitive sensing equipment. It was demonstrated that axial stress levels are much higher in the fibrosa layer, but the ventricularis controls circumferential distortion of the valve system. Highly complex bonding between layers was also observed indicating that heart valve operation depends on a system of interrelated anisotropic material properties [34].

Human medial collateral ligament properties were investigated in a General Motors study seeking data to more accurately computer model impacts of automobiles with pedestrians. Both

quasi-static loading and high strain rate (1 millimeter per millisecond) were applied to potted bone-ligament-bone samples. Although the high strain rate loading is very dynamic, the load was not varied, and each test proceeded to fix the sample at 3 millimeters deflection and observe stress relaxation phenomena. The material properties were then optimized for a quasi-linear viscoelastic material with anisotropic predominance assigned to the direction of collagen fiber alignment. The final virtual material with optimized properties was used in finite element simulation based studies [35].

A basic study centered on quasi-static tension application to whole rat tail tendon analyzed specific mechanisms by which the tendon as a unit generates strains on various sublevels. Confocal microscopy was used to observe cell nuclei within the tendon as markers for measuring the state of strain. The results of this study indicated that strain at the fascicle level is far lower than the overall strain of the tendon with a sliding mechanism of the extracellular matrix responsible for the majority of the strain observed in the tendon [36].

### **3.3 Dynamic Mechanical Testing**

Advancing from quasi-static techniques, dynamic application of stress for testing biomaterials is particularly important because of the very nature of human locomotion. Dynamic loads experienced by the body's musculo-skeletal system range from near quasi-static low intensity functions to particularly violent, high impact high rate transfers of energy. Structural tissues are forced to endure and absorb all types of load and shock on a daily basis. Despite such direct correlation between dynamic loading and human activity, work in this area of materials testing is relatively limited likely due to the added complexity and lack of precedent work.

Bone fracture at high strain rate and impact stress application was investigated in a study conducted by the University of California at San Diego. Fracture toughness analysis as well as fracture path were analyzed in relation to strain rate. Age of the equine samples was also considered as an independent variable in the research. Advanced confocal and scanning electron microscopy was used in observation of micro-structural variations in relation to fracture

toughness related mechanisms. The focal points of this work were catastrophic injuries related to sports, collisions or falls [37].

In an effort to define differences between static and dynamic loading, an orthopedic study compared quasi-static testing results with controlled impact testing. Here an instrumented drop tower was used to apply impact loads of precise energy levels to both sample cartilage and cartilage as attached to bone. Different substrates replaced the natural bone and the resultant effects on the cartilage behavior were determined. The elastic modulus of cartilage under impact strain rates of  $1100 \text{ s}^{-1}$  to  $1500 \text{ s}^{-1}$  was found to be two orders of magnitude higher than quasi-static based modulus. Further, it was found to vary non-linearly with changes in applied stress. Destructive testing in the same study showed that cartilage as a soft collagen based tissue has a higher survivability than bone, a mineralized collagen composite [38].

A series of small scale dynamic pressure fluctuation tests was carried out on rat arterial material to determine the effects of hypoxia induced by heart disease on blood vessel wall material properties. Pulmonary artery samples were extracted from a group of non-treated rats as a control group as well as rats treated at 10 days of hypoxia and a group treated for 15 days in hypoxic conditions. Samples were loaded by dynamic variation of fluid pressure within the artery, and measurements were taken with a visual system. Increase in arterial wall stiffness was observed in hypoxia treated samples and correlated with increased wall thickness and collagen content [39].

### **3.4 Micro/Nano Indentation Techniques**

Indentation techniques are most familiar as hardness tests for metals, and other monolithic materials, in the form of Rockwell hardness testing and other tests. They have been adapted to the micro scale for use with metals and some metal matrix composites. Most recently, indentation techniques have been adapted to the nano scale. Applications are numerous in the areas of composites and biomaterials where small structures and fibers are common. Indentation

is often used when working with these delicate materials over more traditional mechanical methods in the determination of elastic modulus especially.

Donnelly et al. conducted a study using nano-scale indentation on porous cancellous bone structures. Proportion, organization and orientation of collagen and mineral apatite were observed. The results of the mechanical indentation testing were then compared to facilitate proposal of interrelationship and correlations of cancellous bone structure with micro-scale material properties [40].

Engineered collagen gel was measured in terms of hardness and elasticity by an advanced nano-indentation technique at the Institute of Human Genetics. The study reported reduced scatter and higher repeatability over other similar techniques such as atomic force microscope based indentation. The improvement was attributed to finer resolution of indenter control, and the new technique has been suggested as a more reliable method for characterizing soft engineered biomaterials [41].

Atomic force microscopy was the foundation of a cutting edge study to dissect micro-scale collagen fibrils and subsequently measure the mechanical properties of both the shell and core using nano-indentation techniques. A scraping mechanism based in the atomic force microscopy equipment was used to separate the shell and core of each fibril. The core of the fibril was found to have the characteristic D-banding pattern common to fibrous collagen. A particularly significant result was found in that little difference was observed between material properties of the collagen fibril shell and core. This reflects that the fibril can be treated as a homogeneous structure and may imply that the properties of higher ordered fibrous collagen structures could also be controlled by less complex mechanisms [42].

Finally, a more straight forward study based on nano-indentation was conducted by scientists in the United Kingdom. The test samples were fibril structures of diameters ranging from 50 nanometers to 200 nanometers and taken from rat tail tendon. The reduced modulus of elasticity was measured and reported to range from 5 GPa to 11.5 GPa in a room temperature open environment. Observation of non-uniformities in the indentation pattern indicated that sub-fibril alignment matches overall fiber alignment and material properties as a result also align axially [43].

### 3.5 Testing of Chemical-mechanical Relationships

Since collagen is a structural protein, the possibility that mechanical influence on tissues containing collagen will result in change of physiological chemistry by peptide and amino acid triggers will always exist. Conversely, the properties of collagen, especially related to cross-linking, are highly affected by the presence or absence of various organic chemicals. Various previous studies have treated this phenomenon and this work seeks to expand on the chemical-mechanical relationship that manifests between collagen and the human body.

A highly relevant veterinary study using rat tail tendon derived Type I collagen fibers was reviewed in the early stages of this project. The study used quasi-static loading to induce fibrillar damage in fascicle structures. The samples were then chemically screened to detect the presence of MMP13 mRNA collagenase an inflammation trigger for collagen structures. Up-regulation of protein production was also measured with materials in culture conditions. Stress deprived cultures were also arranged and observed to act as controls. All results of this study were positive, that is, increases were seen in mRNA collagenase as well as protein production, while control samples showed significantly decreased metabolic activity [5].

To illustrate an example of the converse effect, a large research group conducted a study of bone properties in amino acid manipulated mice. Specifically, the ratio of pyridinoline to dehydrodihydroxynorleucine was controlled as an independent variable. The hypothesis speculated that subsequent effects on collagen cross-linking and bone mineral crystallinity would become apparent under three-point-bending type mechanical testing. While little effect was seen on material properties based on a strain analysis, a strong correlation was found between the level of collagen cross-linking and mineral crystallinity with respect to the specific amino acid ratio [44].

### **3.6 Testing of Biological-mechanical Relationships**

Significant research has been conducted under the hypothesis that collagen producing cells such as fibroblasts and osteoblasts are influenced in relation to their metabolism and activity level by mechanical stress application. Investigation has also looked into long term mechanical influences on previously formed collagen. This field of study is especially important in the future of biomaterials engineering as understanding these characteristic relationships provides a means of process control.

One such study, especially related to bioengineering, applied various cyclical stress loads to a prepared acellular collagen gel. Formation of larger collagen fibrils was associated with corresponding increase in number of applied stress cycles. Further, ultimate stress, ultimate strain and elastic modulus were all found to increase as the stress treatment was intensified. In fact, elastic modulus and ultimate stress increased in multiples between 2 and 4.5 during increase of applied stress cycles from 48 to 144 [45].

A recent population based study used two groupings of meat-type chickens to study the effect of physical activity on stimulation of tendon growth. A group of 180 chickens were given a daily exercise regimen where they were made to run on a treadmill. The control chicken group was raised normally. The study later analyzed several characteristics of both groups noting that while exercise did not change the material properties or internal structure of the gastrocnemius tendon, increased tendon size was in fact observed [46].

### **3.7 Non-mechanical Testing Methods**

Several advanced techniques and technologies that can be applied for visualizing collagen structures in-vivo or at extremely high optical definition have recently been developed. Advantages to observation of collagen in vivo include the ability to determine dimensions and strains in a completely biologically accurate state as opposed to a simulated biological state. Use

of high resolution optical microscopy complements use of scanning electron and atomic force microscopy where detailed visual interpretations by the scientist are not possible under physical microscopy methods.

Collagen substructures were found to be ideal candidates for study by Second Harmonic Generation microscopy. The non-centrosymmetric organization of fibrillar collagen is deemed to be the main contributing factor for the high subjectivity to this microscopic technique. This study claims that sub-micron resolution can be obtained with optical images produced. Characteristic property variations among mature and immature collagen fibrils, differentiated by the level of molecular cross-linking, were scrutinized in this research. It was found that fibrillogenesis can be studied in great detail by use of Second Harmonic Generation in the fibril shell [47].

Ultrasound imaging and measurement technology was used to observe the Achilles tendon and aponeurosis of the human gastrocnemius muscle for in-vivo strain relationships among the two mechanically parallel structures. Several subjects were tested by isolation, resistance and electrical stimulation of the muscle. Ultrasound images provided real-time strain information for both the tendon and its aponeurosis. Results showed strains as high as 5.1 percent in the tendon and 5.9 percent in the aponeurosis. The study concluded that the tendon/aponeurosis system is stretched homogeneously and the results as such have various functional effects in-vivo [24].

While advanced ultrasound imaging is used to determine tendon properties in-vivo, ultrasound technology was used in the early 1980's to directly estimate material properties of rat tail collagen. One hundred megahertz frequency sound was passed through saline containing a collagen fiber sample. The resulting interferogram showed that velocity of sound axially passing through the fiber was 2.1 kilometers per second. Further, axial velocity in the collagen samples was found to be 82.6 percent of the axial velocity showing distinct directionality and effect of matrix material in the composite structure of the fiber. Values of mechanical properties in relation to the ultrasound determined velocities were not presented [25].

### 3.8 Testing of Engineered Collagen Biomaterials

Engineered collagen as a biomaterial is the result of relatively recent advances in research and processing. However, standards are already being established with respect to testing of collagen for biomaterial use. ASTM Standard F2212-08e1 was mentioned earlier and is a prominent example of the foreseen importance of bioengineered collagen and the need to establish precedent and control for testing and verification of its material properties.

One rather comprehensive project attempted to impose strain induced alignment of fibers in an engineered collagen gel. Stress was applied directly through glass cylinders under the control of linear transducers. Fiber alignment was found to be established permanently in the direction of applied stress for non-cross linked gel. However, when the collagen gel was made to cross link by chemical stimulation before application of stress, fiber direction would match the load direction, but could be recovered to its previous state after removal of the load [48].

Recent research was presented to characterize properties of extruded collagen based scaffolding biomaterials for use in ligament repair. Mechanical properties were found to vary greatly with fiber diameter, with fibers of diameter 125 micron having properties most akin to human ligament. However, the engineered fibers did not match native human collagen in terms of viscoelasticity. The study went on to show that engineered collagen cultured with fibroblasts present had more resilient mechanical material properties [49].

Within the same study, two types of collagen based cell scaffold substrates were prepared, one based on extruded collagen fibers and the other on fiber embedded in collagen gel. Each was cultured with rat skin fibroblasts and controls were prepared with natural rat tail collagen fibers. The engineered substrates were successful as promoters of cell growth, but could not match the mechanical properties as tested in quasi-static loading of the natural collagen based materials. The presence of cells in the substrate after time did in fact greatly improve the mechanical properties over acellular engineered substrate [49].

### **3.9 Literature Review Summary**

Clearly, the testing of collagen as a biomaterial is extensive, highly varied and specialized to numerous applications. Several important points established from the literature reviewed in this chapter will carry through this report. For instance, control of environmental parameters is critical when testing collagen. Information presented above is used to make decisions in experimental design relating to the level of environmental control that must be established to arrive at valid results. Also, biochemistry and the mechanical state of collagen are interrelated. That is, mechanical input to collagen affects biochemistry and change in biochemistry affects the mechanical properties of collagen. This relationship establishes the basis for justifying this work. Review of the variety of reported results assures that the results of this project will play a valuable role in expanding science's understanding of collagen.

## **Chapter 4**

### **Methodology**

#### **4.1 Overview**

This project is a unique application of dynamic tension to fibrous Type I collagen where the definition of failure is the occurrence of microstructural damage. To effectively complete this research, a four phase methodology for experimental design has been developed.

Phase I is selection of a suitable tendon substructure. This fiber must be of a large enough diameter to be easy to handle and resistant to any damage that may be incurred during handling. However, the structure must also be of small enough diameter to allow for observation of damage induced in the microstructure by the application of load. Consideration is also given to availability of samples as well as sample preparation and storage over time.

Phase II is the design and construction of a device that can apply biologically accurate load functions. That is, the fiber being tested should experience the same load that it would in-vivo and at the same frequency for the same possible durations. This apparatus must utilize clamping methods that will secure the sample with no slippage, but cannot induce any site damage to the sample or cause a concentration of stress at the clamp point. Finally, the platform must incorporate sensors that measure load and displacement in real-time so that various properties and parameters can be measured for each test.

Phase III is the determination of a method and protocol for fixing the point during each test that the fiber is considered to have failed. The exact definition of this point in the most detailed form possible is critical to accuracy and validity of results.

Phase IV is the specification of methods which ensure the best possible in-vitro conditions. Given the nature and sensitivity of the materials to be tested, temperature, chemical environment and hydration must all be considered.

In addition to experimental design and experimental procedures, several pre and post-experimental procedures must also be completed to ensure the highest possible quality and reliability of results.

## **4.2 Pre-experimental Procedures**

### **4.2.1 Defining Failure Mode**

This work seeks to reveal the critical point where micro-scale tendon damage occurs, thus triggering the body's inflammatory response at the site of injury. Although it is not clear that the collagen fibril is the smallest unit for which damage to this substructure can chemically trigger inflammation, other practical experimental parameters and limitations prevent analysis of smaller fibers.

Advanced microscopy techniques including Atomic Force Microscopy (AFM) and Scanning Electron Microscopy (SEM) as seen in Figure 4.1, have been used extensively to examine collagen on the molecular level [50, 51]. However, these techniques prohibit analysis in real-time and greatly limit the area that can be viewed. For this reason, light microscopy will be used to view the sample in real-time under various series of dynamic loads. Previous studies have shown that damage to collagen fibrils can be observed through the general condition of a larger substructure, such as the fascicle, under a basic light microscope [5].

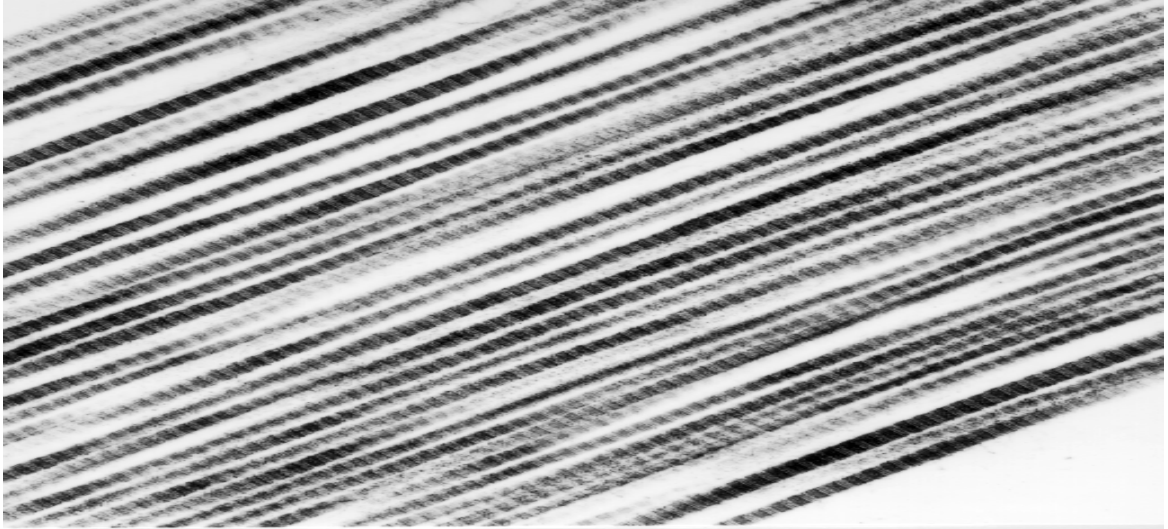


**Figure 4.1:** SEM of parallel collagen fibrils

This research will consider failure to be the point at which rupture of the fibril is first observed under the microscope. The moment of damage onset and exactly how damage is defined in terms of what can be viewed under the microscope will be described fully as part of Phase III.

The project's final conclusions are based on the assumption that failure of the sample as defined above would result in the triggering of inflammation if the fascicle were actually part of a human tendon. All data is taken from the time that dynamic loading is initially applied to the point that the first signs of damage are observed.

#### **4.2.2 Defining General Test Procedures**

General testing procedures have been developed in an effort to simulate the load that the tendon sub-unit would be expected to experience if it were a part of a functioning tendon. The parameters to be varied and controlled respectively are: frequency of loading and unloading and amplitude of mechanical tension that the sample experiences. The variation of load is sinusoidal

with no negative load and a slight tensile preload always maintained on the sample. A sinusoidal variation, similar to Figure 4.2, is thought to be the most biomechanically realistic given the rotational motion of the joints of the body [52]. That is to say that for constant load on a particular joint as the full range of motion is realized, the necessary muscle effort decreases as the muscle reaches a fully contracted state due to increased length of the moment arm between the point of rotation and the distal insertion of the tendon (the tendon's connection to the bone).

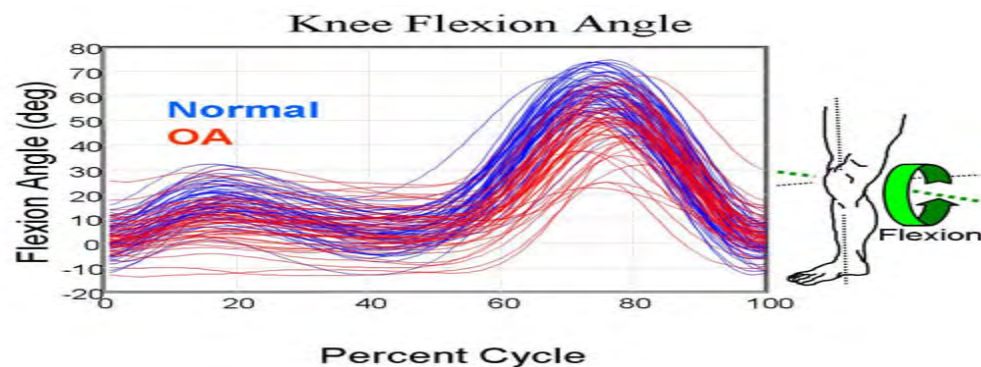


**Figure 4.2:** Biomechanical cycling of the knee joint

In terms of frequency, practically any repetitive motion that the human musculo-skeletal system conducts falls into a range of 0.5 to 2.5 cycles per second. Based on this, five test variations will be conducted varying frequency alone from 0.5 hertz to 2.5 hertz in half hertz steps. The parameters are set so that a collagen structure's sensitivities to load cycle frequency at high intensity in sustaining damage can be identified.

### **4.2.3 Addressing Validity of Results**

Refinement of experimental preparation, techniques and procedures as well as application of statistical standards when determining the proper number of redundant tests must all be applied in order to establish valid conclusions from this work.

Internal validity is defined as an inductive estimate of the degree to which conclusions drawn from experimentation are likely to be true, and so relies on careful design and adherence to experimental protocols [53, 54]. In this work meticulous revision of all aspects of experimental design ensures the highest possible internal validity. Replication of in-vivo conditions in terms of hydration, chemistry, realistic stress intensities and frequencies and mechanical influences are the main concerns when assuring the best possible internal validity in the present work.

While attention to detail in experimental design assures high validity of results, complete biological validity cannot be claimed for this project. Naturally, maximum internal validity is not possible since these tests seek to simulate the biological state in-vitro, and are not occurring in-vivo. Maximum internal validity, in this case is only possible where testing is conducted in-vivo, or where the sample is still in its natural environment as part of a living creature.

In an effort to establish highly significant results, the number of redundant tests will be set at ten for each loading frequency. This will reduce statistical t-values thus adding significance to correlations and distinctions observed between dependent variables as a result of variation of independent variables [53, 54].

#### **4.2.4 Dehydration Induced Damage**

The possibility that damage to the material may occur due to exposure to air and subsequent drying during a test run must be considered. To create a definitive distinction, control testing must be conducted to determine what observations may indicate that the collagen was damaged by dehydration and not by mechanical loading as desired.

A group of ten control fascicles are extracted, stored in a refrigerator and treated the same as all other mechanically tested samples. They are then mounted in the apparatus under the microscope. However, no mechanical load is applied. The samples are simply observed under magnification until visible signs of dehydration become apparent. The visual characteristics of

degradation are noted simultaneously and considered when analyzing damage that has been assumed to have been caused exclusively by the application of tension.

## **4.3 Phase I**

### **4.3.1 Selecting a Tendon Substructure**

Numerous factors must be considered when determining which collagenous tendon structure should be used in this project. From the above definition of failure mode, the substructure must be of appropriate dimensions so that rupture of the fibril is visible or at least visibly apparent under a light microscope. The substructure must be easy to extract from readily available sources. A fiber with properties that allow it to be mounted using a simple clamp design is very important since the reliability and set-up speed of the clamping system is critical. It must be thick enough to handle with fingers or tweezers and robust enough that it cannot be damaged during handling and clamping. Maintenance of the extracted samples is also important both during a test and for extended storage.

Testing of an individual fibril is impractical due to the extremely small diameter. Extraction of viable fibril specimens is particularly difficult. Further, handling and storage of samples is complicated since the fibers are thin and have a tendency to coagulate. Finally, a device to test on the fibrillar scale would have to be capable of generating and detecting minute loads, adding further complication and expense.

The next higher order structure of the tendon is the fascicle. The fascicle is an excellent choice for several reasons. Previous work on mechanical loading and visualization of internal damage of collagenous tendon fascicles has been successfully conducted [5]. The state of the internal structure (the reinforcing fibrils) can be observed through a low magnification light microscope. With an average diameter of 0.3 millimeter, these fibers can be extracted and handled easily. Previous work shows that an average fascicle can withstand well over one Newton of force without incurring any damage [31]. Assuming careful handling of the

specimens, each fascicle can be extracted and clamped with no damage. As a larger substructure, when stored as individual samples, fascicles will have a less pronounced tendency to coagulate attributable to their smaller surface area to mass ratio.

### **4.3.2 Sourcing Collagenous Tendon Fascicles**

Based on previous related projects that were researched, the majority of natural fibrous collagen structures used in research and biomedical applications comes from the tendons found in tails of laboratory rats. Availability is particularly good since rats are commonly used in numerous scientific applications [55].

For this project, fifty frozen individually packaged male Sprague-Drawley rat tails with a minimum length of thirteen centimeters were sourced from Bioreclamation Inc. a Long Island, New York based company. Each tail contains four independent tendons running the full length from root to tip. Five to ten fascicles can be extracted from each tendon, so the sample yield from each tail is between twenty and forty viable fascicles.

### **4.3.3 Fascicle Extraction Procedures**

Specific procedures are developed for this project based on information from several sources involved in similar operations. Fascicle extraction procedures are as follows:

- A whole rat tail is removed from frozen storage and, without removing the tail from the zip-lock bag, submerged in room temperature water for five minutes to thaw.
- The tail is removed from water and then removed from the zip-lock bag, and placed on a section of laboratory mat.
- With a new scalpel, the tail is severed transversely one centimeter from the root and two centimeters from the tip. This severs any internal attachments which connect fascicles.

- From the distal end (tip) the skin is sliced longitudinally two centimeters.
- The skin is peeled back to expose the four tendons.
- The longitudinal cut is continued three additional centimeters carefully avoiding the tendons.
- The tendon is sliced from below between two vertebrae approximately ten centimeters from the root using the scalpel.
- The scalpel is worked toward the tip of the tail severing the tendon before the vertebral connection.
- The loose end of the tendon is pinched between fingertips and firmly pulled to extract fascicles; this is repeated several times until as many fascicles as possible are removed.
- Upon removing a fascicle or bundle of fascicles, the samples are immediately submerged in Phosphate Buffered Saline (PBS).
- This procedure is applied to all four tendons and as many viable samples as possible are extracted.
- All materials (except the scalpel) are disposed of in a biological waste container and the scalpel is disposed of in a sharps waste container.

#### **4.3.4 Storage of Materials and Samples**

To ensure the most biologically accurate material properties at the time of testing, care is taken in storing both prepared samples and frozen tails. According to the supplier, rat tails should be stored as supplied frozen at negative twenty degrees Celsius or below. The tails remain viable for a minimum of two years under these conditions. Since an acceptable freezer is not available in the mechanical engineering facilities, upon arrival, the rat tail materials are transported to the facilities of the biology department for proper long term storage.

Prepared samples, upon extraction, are immediately placed in a Pyrex jar containing a small amount of PBS. If not used immediately, the samples are refrigerated at 4 degrees Celsius. Prepared samples are never refrozen, and they are never kept for more than three days before use.

## **4.4 Phase II**

### **4.4.1 Test Apparatus Design Parameters**

To begin the process of designing the unique device that will facilitate this experimentation, a series of parameters are established. A source of dynamic tension is to be specified according to the desired range of loading functions. From numerous historical studies of collagen, the collagen fascicle may have an ultimate tensile strength as high as 100 MPa. For an average diameter fascicle, the corresponding load is slightly under eight Newtons, and this value will therefore be used as the minimum design parameter. The tension source must be capable of producing at least eight Newtons of force. Further, the source of tension must be able to supply and vary this load at a rate of 2.5 Hz minimum at a low duty cycle to ensure consistent loading. To accurately measure viscoelastic properties, any moving parts of the tension source should have low mass and low friction so that the mechanical parts have a reduced effect on the natural movement of the sample. As mentioned, collagen is highly viscoelastic and strains as high as 40 percent before failure have been observed [31]. Assuming an un-stretched, initial sample length of five centimeters, the tension source must operate over a minimum stroke of two and a half centimeters.

The tension source and anchor point must be supported on a rigid platform. The structure must be completely stable on a flat surface and should have a large mass relative to the mass of moving parts to prevent vibration. Finally, the platform must allow for the sample to be viewed under a microscope during testing. The design of the platform must accommodate a microscope with a base of seven inches width and one and a half inches height minimum.

In order to gather large amounts of accurate real-time data, a series of sensors must be designed into the platform. The first sensor must measure real-time displacement, and the other real-time sample tension. High resolution is very important especially in measuring tension since load variations will probably not exceed one Newton. However, keeping in mind that the device may be used for other projects, the tension sensor must have a minimum capacity of at least eight Newtons, and if possible more if the same resolution can be maintained. When designing and constructing the platform, alignment of the tension source, sample fiber and load sensor is critical for accurate results. Any misalignment will result in reduced accuracy of the measured data. The displacement sensor must have a stroke capacity of at least two and a half centimeters given that the design calls for accommodation of fifty percent strain. Again, since the device could be used in the future for testing much stiffer materials, the resolution of the displacement sensor must also be high to allow accurate detection of small strains.

Efficient and effective sample mounting is critical to the accuracy and reliability of the results of this study. Given the slipperiness and fragility of the collagen samples, the design of suitable clamps is challenging. The clamping system must be firm enough to secure the fiber from slipping but must not pinch the fascicle causing damage or failure at the clamp. Simplicity and speed of mounting are also important since fibers are thin and difficult to handle.

When working with biological materials, choice of structural materials that will come in contact with the specimens must be carefully considered. Since many parts of the device may come into contact with saline solution, all parts should be made from corrosion resistant metals, plastics or rubber [56]. Corrosion of parts will not only jeopardize performance of the machine, but may also contaminate samples. Particular care should be taken when sourcing sensors. These are the most delicate parts of the design, and must be able to withstand the corrosion factors that will be present during testing. Use of lubricant on moving parts of the machine could easily contaminate test samples, and so the design must not use any moving parts that require additional lubrication.

The test apparatus is unique, and so will have to be constructed as a prototype. To save cost, the design should be developed such that all parts can be made and assembled using on-site facilities in the mechanical engineering department. Necessary manufacturing processes should

be limited to milling, turning, drilling, tapping, grinding and any other basic process that can be completed in-house.

#### **4.4.2 General Design Specifications**

The collagen fascicle dynamic tensile test apparatus is based on a solid aluminum platform three inches wide, one and a half inches thick and twenty one inches long. Two blocks with a total of three height adjustable points raise the platform over the base of the microscope and insure that the platform is level and stable.

Dynamic tension is generated by a voice coil linear motor. Voice coil motors provide a relatively linear mechanical response to direct current input over a long stroke. They are capable of supplying high dynamic loads as well as consistent static loads both at low response times. The voice coil motor housing is affixed to a precision aluminum block which fits tightly into a recess machined into the platform. Two stainless steel bolts fix the block to the platform.

The voice coil linear motor, as supplied has no support or guide for the movement of the armature within the housing. A custom designed linear bearing and precision aluminum guide rod is designed to serve as the support structure. The oversized linear bearing and thin aluminum arm add only minimal friction and mass to the moving parts.

Tension measurement is conducted through a load cell placed in series with the sample between the stationary anchoring block and the stationary fiber clamp. The load cell attaches to the anchoring block by threading into a tapped hole, while the anchoring block is fixed to the platform in the same manner as the voice coil housing block. Displacement is measured by a linear variable displacement transducer (LVDT) mounted in parallel between the voice coil housing block and the voice coil armature.

Clamps are a very basic design, each consisting of a stainless steel machine screw with a small transverse groove cut to the center and a stack of stainless steel and rubber washers pressed

together with a stainless steel nut. The sample passes through the transverse central diameter of the screw by means of the groove, and the stack of washers secures the fiber.

#### 4.4.3 Voice Coil Linear Motor Specifications

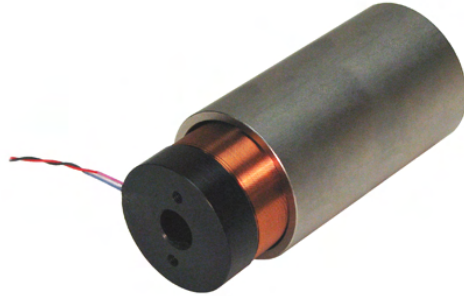


**Figure 4.3:** LVCM-051-089-01 Linear Voice Coil Motor

The linear voice coil motor specified for this project is the LVCM-051-089-01, model from Moticont based in Van Nuys, California, Figure 4.3. It utilizes a two inch diameter by three and a half inch length magnet housing fixed from the rear by three tapped holes. The armature coil has a 57.2 millimeter stroke and a 2 inch diameter face to which additional linkages can be mounted by two tapped holes. This voice coil motor is capable of producing 82.7 Newtons of immediate force at 10 percent duty cycle. Overall the motor has a power capacity of 40 watts. Maximum continuous force is rated at 26.2 Newtons. The force per input constant is 10.1 Newtons per ampere at 25 degrees Celsius. Armature mass is 195 grams while the magnet housing mass is 1155 grams. The large difference in mass between moving parts and stationary parts is beneficial in reducing vibration.

The voice coil motor's response linearity is high especially near mid-stroke. For this reason, the motor is specified with double the necessary stroke. Motion is positively limited to half of the motor's stroke capacity, but response throughout the entire movement is highly linear. For similar reasons, the motor's force producing capacity is actually ten times the minimum

specified requirement. These factors allow highly accurate reproduction of the electrical signal as a mechanical signal.

The variable power supply to the voice coil motor is a common function generator. A BK Precision model 3011B two megahertz function generator is selected for its capability to operate accurately at sub one hertz frequency. The function generator is connected directly to the voice coil leads. An EZ GP-4303GP direct current power supply is also connected to the circuit in parallel. The function of the direct current source is to supply a small preload to the sample, for calibration of the displacement sensor before each test and also to standardize measurement of diameter of the sample.

#### **4.4.4 Linear Bearing Guide and Linkage**

The Moticont LVCM-051-089-01 is supplied as two separate parts that must be supported individually. The magnet housing, in this system is the stationary part and so mounting is simple. However, since the voice coil armature must move in a strictly linear path within the magnet housing given only 0.38 millimeter clearance per side, a special support structure is developed.

The linear bearing guide consists of six ABEC 7 specification rotary ball bearings [57]. Three bearings support and restrict motion in the horizontal plane and three bearings operate in the vertical plane to provide the same effect. High quality, high precision bearings are used since the linear bearing is the only fixture on the entire device where moving parts come into contact with each other and smooth operation must be ensured without the use of lubricants. The bearings contact a precisely machined and polished square cross-section guide rod. The bearing contact force is controlled using horizontal and vertical machine screws. Alignment of the armature within the magnet housing is facilitated by three adjustable support screws. The guide rod serves to mechanically connect the face of the voice coil armature to the mobile sample clamp. A positive stroke limiting feature is designed into the guide rod and acts in conjunction with a recess machined into the platform. Stroke must be limited so that the armature cannot

impact the magnet housing in the event of sample breakage under high load, and more importantly so that the limits of the displacement sensor are not exceeded.

#### **4.4.5 Sensor and Data Acquisition Specifications**

A complete sensing and data acquisition system is sourced in from Omega Engineering Incorporated. The load sensor mounted in series with the collagen fascicle is the LCFA-1KG, Figure 4.4. The capacity of the load cell is 1 kilogram or 9.8 Newtons. A foil type strain gauge is the core of the sensing mechanism and is considered to have infinite resolution. The load cell is powered by a 10 volt direct current source PSS-10 also supplied by Omega Engineering. Construction is entirely stainless steel with inline threaded connections on the fixed and sensing ends. The factory supplies the sensor pre-calibrated to zero output voltage at zero load using a ballast resistor. The calibration coefficient and non-linearity for this particular sensor are: 495 Newtons per volt and 0.03% respectively.



**Figure 4.4:** Omega Engineering LCFA-1KG Load Cell

Displacement of the sample is measured by Omega Engineering LVDT LD621-30, Figure 4.5. Stroke capacity is 30 millimeters again with infinite resolution. The electrical excitement for this model is 20 volts direct current supplied by Omega Engineering U24Y101 direct current voltage source. Similar to the load cell, the LVDT is constructed of stainless steel.

A cylindrical housing facilitates clamping while the sensing rod has a threaded end to affix to the moving linkage. The sensing rod has a low mass and low friction movement. A return spring is supplied with the sensor, but is removed to avoid interference with the motion of the tension mechanism. The calibration constant and non-linearity for this model are: 0.003 meters per volt and 0.053% respectively.



**Figure 4.5:** Omega Engineering LD621-30 LVDT

Data acquisition is handled in real-time by an Omega OMB-DAQ-54 DAQ module. Sensor output leads connect into the module and information is then relayed to a PC or laptop via a USB connection. Personal DAQ View software serves as the interface for collecting and processing data. The resolution of the software is extremely high at  $10^{-6}$  volts. An “add-in” is provided that tabulates data directly into an Excel spreadsheet for further processing. The particular configuration used allows a maximum scan rate of slightly more than 4.6 hertz; therefore care must be taken to verify data collected during higher frequency load variation. False harmonic readings can result due to the cyclic sensor outputs interacting with the cyclic series of scans taken by the DAQ system.

#### 4.4.6 Clamp Design

Fixtures developed to secure both ends of the collagen fascicle are designed to be simple to manufacture and operate in the lab. The design is based on a stainless steel #10-32 Allen head machine screw one inch in threaded length. A thin stainless steel washer is first added to the screw followed by a thicker rubber washer of the same outer diameter. A transverse groove whose center is at the level of the exposed surface of the rubber washer is then made. Mounting a fiber involves sliding the sample along the surface of the rubber washer until it reaches the base of the transverse groove. The fascicle is now aligned with the center of the clamp. A second rubber washer is now added clamping the sample between the two rubber surfaces. Another stainless steel washer is added followed by a stainless steel nut to apply sufficient pressure to the rubber washers supported by the stainless steel washers. The soft rubber washers grip the sample without creating stress concentrations. Finally a spacer nut is added to the screw so that the sample can be aligned when placed in the test apparatus. The design of the clamping system is depicted in Figure 4.6.

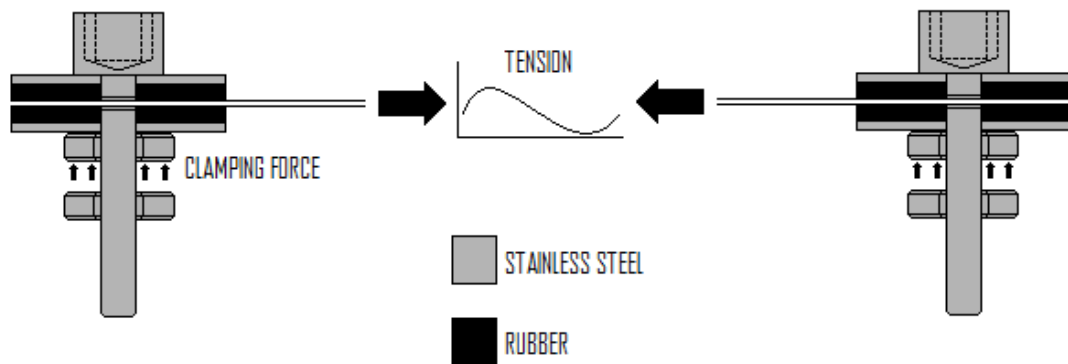


**Figure 4.6:** Clamp design

The mobile clamp will attach to a platform which is part of the voice coil armature guide using the spacer nut and a wing nut to create a secure mounting. The stationary clamp will attach to a platform threaded onto the sensing side of the load cell using the same spacer nut and wing nut configuration. A custom jig was constructed to aid in preparing samples of uniform length. Two hex shaped posts fitting the Allen head of each clamp are pressed into an aluminum block at a distance of approximately five centimeters. The jig holds two clamps upright, fixed against rotation and at a set distance apart so that the sample fiber can be mounted quickly.

#### 4.4.7 Platform Schematic

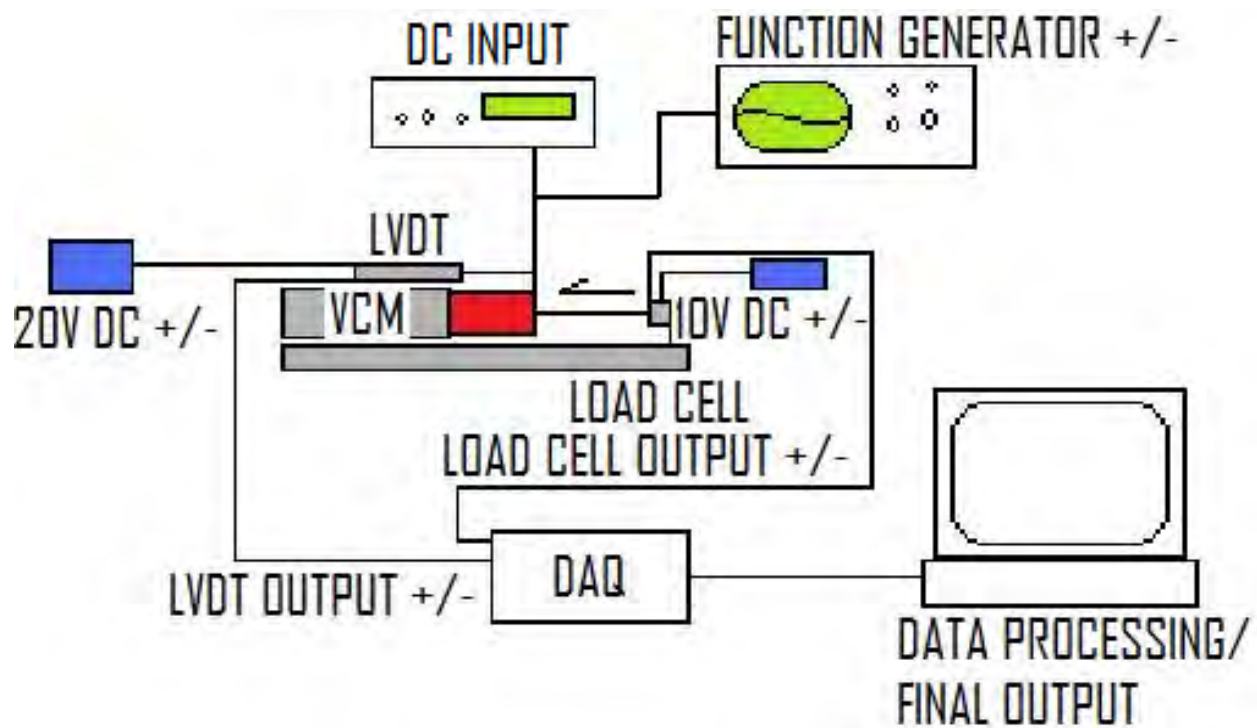


**Figure 4.7:** Schematic of testing platform

Figure 4.7 shows the complete testing system in schematic form. The function generator and DC input energize the voice coil motor according to the desired pattern of tension. The DC

input also ensures that positive tension, or preload, is always acting on the fiber. This ensures that during any given test, the fiber is never allowed to re-crimp which would introduce the complication of nonlinear stress versus strain behavior. The LVDT is connected mechanically in parallel with the mobile section of the platform. However, the load cell is fixed to a static post. Finally, sensor outputs are processed by the data acquisition module and recorded in spreadsheet form.

## **4.5 Phase III**

### **4.5.1 Visualizing Sample Failure**

Procurement of consistent and accurate results in this study relies heavily on identification of a definitive point of failure in terms of what can be observed under the microscope. Previous studies show that mechanical damage to collagen fascicles becomes apparent under magnification by a standard light microscope. The research describes a visible change to the surface of the fascicle due to reoccurrence of the easily identified D-Band pattern resulting from the release of tension on internal substructures indicating ruptured fibrils. Internal damage is also reported to manifest as sharp notches which become visible on the edge of the fiber, Figure 4.8 [5].

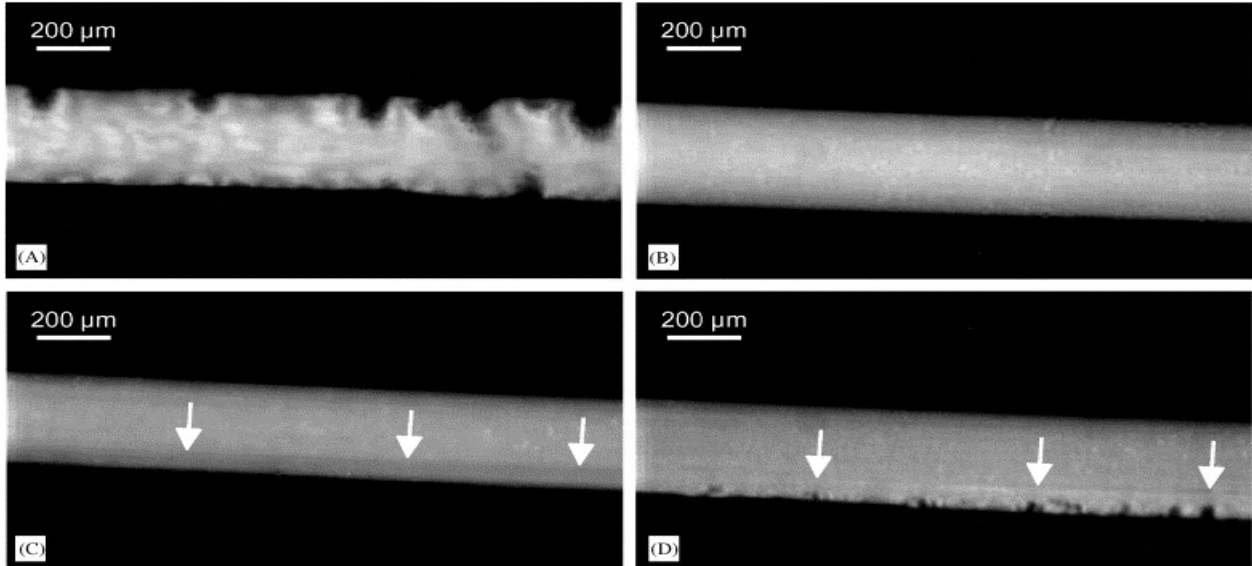


**Figure 4.8:** Damaged collagen fascicles from previous research [5]

#### 4.5.2 Microscope and Related Equipment

Previous work has successfully used low magnification microscopy, approximately fifty times magnification, to study collagen fibers on the fascicle level [5]. This experiment employs a NikonSMZ-10 stereomicroscope. The large objective lens allows the equipment to focus on the sample from a long distance compared to other microscopes. This is beneficial since the wide space between the base and lens allows the test platform to enter and exit the viewing area without having to raise the upper portion of the microscope. Illumination comes from a fiber optic ring source surrounding the lens and not from below thus greatly simplifying the design of the platform and set-up procedures. To improve viewing of the test, a Sony CCD-IRIS/RGB video camera adapter is connected to the microscope, so that the image of the sample can be seen on a computer monitor. Sample diameter however, can only be measured using the eyepiece, which contains a calibrated scale, even with the video camera installed.

### 4.5.3 Point of Failure

The most fundamental piece of data to be measured for each test is the exact time that the sample withstands every particular loading variation. Standards for determining the exact time zero and time of damage are precisely defined. Data is collected as a series of points each at a particular time increment. The independent variable time and the reading of each sensor at that time increment, the dependent variables comprise a data point. Given a scan rate of 4.63 hertz, the time increment will be 0.216 seconds.

Time zero is considered the first data point to show an increase in tension through the load cell. Note that each test begins in a state of zero tension. Determination of time zero therefore is only calculated after completion of a test run or series of test runs as a part of data post-processing.

Time of damage is more difficult to determine since observation by eye alone is the means of determining when the sample has been damaged. A standardized procedure must be developed and adhered to during testing. A test commences by triggering the data acquisition to record followed by initiation of the loading function. As the test proceeds, the state of the sample is observed under the microscope. When any sign of damage is observed, the recording of data is immediately stopped. Obviously the exact point of damage is not the final point in the recorded data stream. For this reason, the point of damage is taken as the peak strain point closest to the end of the data series.

## **4.6 Phase IV**

### **4.6.1 Replication of in-vivo Conditions**

Great consideration must be given to the specific steps and procedures that must be applied to maintain life-like material properties of the samples. If the collagen is exposed to a high temperature, unbalanced chemistry or dry conditions for any extended period of time, the samples will become nonviable. Procedures, treatments and precautions will be given for each factor.

### **4.6.2 Maintenance of Temperature**

Once prepared, samples are refrigerated in phosphate buffered saline contained in a sealed Pyrex jar for storage. Shortly before use, samples, along with solution are transferred from the jar to a Petri dish exposed to room temperature. Sufficient time is allowed to pass so that the fluid and collagen can be considered to have warmed to room temperature. Since tests are being conducted in a non-air conditioned laboratory in a tropical climate, room temperature is considered acceptable. To support this assumption, a long standing trend in research results shows that collagen's material properties are unaffected in a wide range of temperatures below 37 degrees Celsius.

Conducting tests at body temperature would require the entire test apparatus to be contained in a heated environmental chamber. Such a set-up is not immediately available, and will only come at high cost besides adding further complications when conducting tests. A more practical option may be to heat the fluid in which the collagen is contained before testing. However, given the thin diameter and low mass of the fibers, samples would quickly cool approaching room temperature as soon as they are removed from the solution for testing.

### **4.6.3 Maintaining Stable Chemistry**

Experimentation for this project results in the fact that each sample will be exposed to the open environment from the moment that the sample is mounted on the test platform until the end of the test run. For this reason, control over the chemical state of the collagen is lost from the point that the fiber is removed from the Petri dish. The choice of fluid for storing the samples in a hydrated and chemically stable state is of the highest importance. Phosphate buffered saline is selected as the only liquid to contact the samples from the point of extraction of each fascicle to the end of testing. PBS is a solution of salts including sodium chloride and sodium phosphate. Solution pH is stabilized by potassium chloride and/or potassium phosphate buffers. The most important characteristic of PBS is that it is generally isotonic in the human body.

Molecular mechanisms cause water to form a film around a foreign protein structure submerged in PBS. The film of water molecules prevents inherent instabilities in the protein from manifesting into structural changes [58]. Collagen, as a protein based substance is well suited to phosphate buffered saline as a moderately long term storage fluid.

### **4.6.4 Hydration of Exposed Collagen**

Knowing that the collagen will be exposed to drying upon contact with air during testing, procedures are defined to rehydrate the sample when possible during the period of exposure. During the course of each test run, the fascicle is exposed to air twice. Once while being fixed to the clamps and the second and final time when it is mounted on the apparatus through the clamps and tested until damaged. To prevent false readings, no physical contact will be attempted to the sample during measurement of initial properties or during dynamic testing. The fiber is gently wetted manually with a finger or cotton swab containing PBS during the short period between measurement of static properties and initiation of dynamic testing.

## **4.7 Detailed Testing Procedures**

### **4.7.1 Microscope Set-up**

Several steps are required to ready the microscope and computer monitor viewing program. The video camera must be mounted on the proper adapter and affixed to the vertical port of the microscope. The computer, computer monitor, camera monitor, camera power source and microscope light source must all be switched to the power on position. The FBG 32 microscope viewing program must also be initialized. At this point, the microscope image will be visible in real-time on the computer monitor.

### **4.7.2 Sensor and Data Acquisition System Connections**

Numerous connections must be made to supply the sensing and DAQ system with power and to accurately convey the sensor outputs to the computer. All signal sensor leads are to be connected before supplying power to the sensors. The load cell red lead connects to the positive terminal of the ten volt power supply and the black lead to the power supply ground. The load cell white lead connects to the 1L terminal of the DAQ module and the green lead to the common terminal of the module. The LVDT red lead connects to the positive terminal of the twenty volt power supply and the blue lead to the power supply ground. The yellow lead connects to the 1H terminal of the DAQ module and the green lead to the common terminal of the module. The DAQ module is connected to the computer via a USB cable and connection by which it receives power to operate using the computer as a source. The direct current power supplies can now be connected to alternating current wall output. Upon opening the Personal DAQ View program, the output voltages of each sensor can be viewed, calibrated and recorded.

### **4.7.3 Data Acquisition Calibration**

Data is collected as signal voltage and later converted to actual load and displacement. However, the zero point of each sensor must be set in the DAQ software. With the voice coil at its zero point, that is in contact with the sample side positive stop, the zeroing value that returns the LVDT sensor output to zero volts must be calculated and entered in the program. Ensuring that the sensing side of the load cell is free from any external force, the same procedure must be repeated to zero the tension output reading. The data recording feature is also adjusted at this time. Since the default setting records only 100 data points, the number of recorded points is set to 1,000 for each test run.

### **4.7.4 Connecting Voice Coil Motor Power Supplies**

The voice coil motor leads must be connected to both a direct current power supply and to a function generator, both previously specified. Before connecting the function generator, the frequency and amplitude of the output signal must be verified. Amplitude is verified by a pre-test run and is based on load cell read-out. Frequency is monitored on the function generator itself.

Leads from both the direct current supply and function generator have alligator clip terminals. The direct current source is clipped directly to the voice coil armature leads. In this case, the red lead of the voice coil motor is attached to the negative of the power supply so that the voice coil applies tension and not compression. The function generator leads are then fixed to the alligator clips of the direct current source.

#### **4.7.5 Preparing Samples for Testing**

Assuming that samples have been previously extracted and refrigerated, they must be transferred to a site where they can be separated and mounted before any testing. Samples, along with the PBS in which they are stored are transferred to a plastic Petri dish from the Pyrex jar. This step is done at least fifteen minutes before any test is performed so that samples reach a stable temperature. Collagen fibers have a tendency to coagulate in fluid and are handled more easily from a Petri dish as opposed to a jar. Once the samples have reached near room temperature, they are ready for testing.

#### **4.7.6 Sample Mounting Procedure**

After completion of the procedures described above, samples are now mounted according to the following list of steps:

- Two clamps are placed in the mounting jig.
- A stainless steel washer is first placed on each clamp screw followed by a rubber washer on each.
- A second rubber washer is placed on each clamp leaving at least one centimeter gap between rubber washers.
- A second stainless steel washer is placed over each rubber washer.
- Two stainless steel nuts are threaded onto each clamping screw.
- Tweezers are used to separate and remove a fascicle from the Petri dish.
- The sample is strung over the surface of the lower rubber washers and into the notch of each clamp.
- The upper two washers of each clamp are forced onto the lower washers and the first stainless steel nuts are tightened over the stainless steel washers of each clamp.
- A wrench is used to tighten the first stainless steel nut an additional 90 degrees only.

- The second stainless steel nut remains loose and is used later to align the fiber.
- Both clamps and the sample are transferred as a unit back into the Petri dish containing PBS.
- A moment is taken to ensure that all equipment is ready for commencement of the test run, and especially that the mechanism is at the zero point of its stroke.
- When the test is fully ready to begin, the sample is removed by handling the clamps from the PBS.
- One clamp enters the mounting point of the guide rod and the other the mounting point of the load cell.
- The alignment of the fiber is made parallel to the voice coil motor and load cell using the second set of stainless steel nuts.
- The clamps are fixed using stainless steel wing nuts tightened by hand.

#### **4.7.7 Measurement of Initial Dimensions**

The pre-loaded length of the sample and the fiber diameter are measured at this time. After mounting, the sample will be in a loose state between the mounts of the apparatus. The guide rod is moved by hand only far enough to remove slack from the sample. The direct current power source to the voice coil motor is switched on and adjusted to 0.2 volts. The LVDT output voltage is read quickly as the sample, although under only slight tension will show creep. The LVDT reading is recorded for use in later data processing. The diameter is now measured and recorded using the microscope's calibrated scale. Voltage applied to the voice coil is returned to zero, the source is switched off and the sample is rehydrated as described above.

### **4.7.8 Test Run Procedure**

Only after completing all previous procedures can the actual test run begin. The exact procedures are as follows:

- The guide rod is adjusted carefully by hand to remove any slack that may be present in the fiber.
- The direct current power supply is switched on.
- The microscope focus is adjusted to view the sample clearly.
- The data acquisition record procedure is triggered.
- A moment must pass before data recording actually begins.
- Once data recording commences, the function generator is switched on.
- The fascicle is viewed attentively under magnification until the first sign of damage is observed.
- Data recording is stopped immediately at this time.
- Power to the apparatus is switched off and the sample is removed.
- Test runs are repeated as called for above.

## **4.8 Post-experimental Procedures**

### **4.8.1 Trimming the Data Points**

Three columns of concurrent data result from each test run. The first column is the data point number which corresponds to a particular time increment during the test. The second and third columns represent the output signals in volts for each time increment of the load cell and LVDT respectively. These columns must be trimmed according to the standards previously set forth on test initialization and point of failure.

The top portion of the columns is discarded above the first point where the first valid increase in load cell signal voltage is observed. This eliminates the part of the data record where the function generator was not yet switched on and no tension was applied to the sample.

All points after the final peak that is observed in the LVDT output are also discarded. The purpose of removing these points is to standardize the point of failure to a known characteristic physical phenomenon related to the reaction of the fascicle.

#### 4.8.2 Essential Result Set

In order to arrive at the final goal of defining the risk level of a physical activity with a particular frequency and intensity, an essential parameter is defined for each series of tests, a series of tests in this work being ten successful tests under the same loading function. The key parameter sought after each series of tests is defined as area under loading function divided by cross-sectional area of the fascicle. Area under the loading function may be considered impulse since time is the independent variable [1, 59]. Division by cross-sectional area corrects for discrepancy in number of fibrils that are sustaining the tension in the fascicle. Equation 4.1 is used for the above described calculation:

$$C_s = \frac{4 \sum_{n=0.1}^K \{[\delta_V + a_P(\sin(2\pi f_P t_n))] - [\delta_V + a_P(\sin(2\pi f_P t_{n-1}))]\} x (t_n - t_{n-1})}{\pi D^2}$$

**Equation 4.1:** Impulse per cross-section calculation

where:  $C_s$  is the damage characteristic of the test;  $K$  is the number of points used to calculate the area under the curve, and is equal to the adjusted test duration in seconds multiplied by 10;  $\delta_V$  is the vertical shift of the loading function equal to the preload of the test in newtons;  $a_P$  is the

amplitude of the loading function in Newtons;  $f_p$  is the frequency of the loading function;  $t_n$  is the point time or independent variable; and  $D$  is the measured sample diameter.

The series of tests and ten corresponding data sets are processed in a separate spreadsheet. The area under the loading function is calculated numerically using only amplitude, frequency and time duration of the test run. This eliminates possible error caused by adverse harmonic interaction between the rate of sensor signal fluctuation and data acquisition rate. Fiber cross-sectional area is calculated from the previously measured diameter. In this case, area reduction caused by strain of the sample is not considered since the purpose of the area value is to approximate number of reinforcing fibrils relative to other samples only.

Once all ten data sets have been processed, each test run will yield a value of area under loading function and fiber cross-sectional area. For each data point, area under the loading function is divided by cross-sectional area to yield a characteristic value. This value may be considered the specific impulse that the typical collagen fiber can withstand at the tested frequency and intensity of loading. The average value is calculated and as such is considered the most important result for the series of tests. The standard deviation is also calculated to partially characterize the quality of the results.

These ten data points are then graphed with area under loading function as the dependent variable and cross-sectional area as the independent variable as in Figure 4.9. The degree of non-linearity of the resulting plot is an indication of validity and correlation between dependent and independent variables. The slope of the linear regression of the data points indicates the sensitivity of the sample to be damaged in relation to the area of the sample for the given parameters of the loading function.

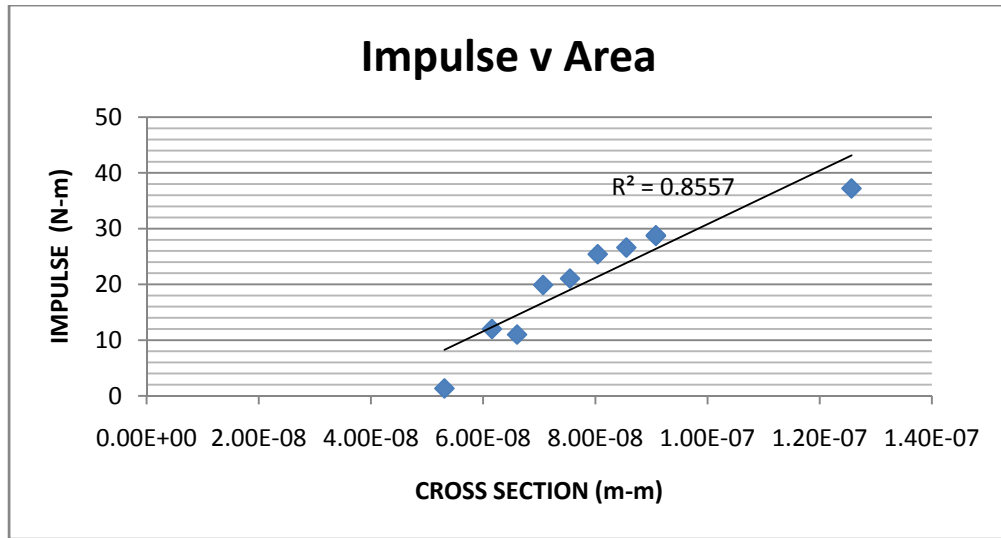


**Figure 4.9:** Example of graphical result for impulse versus area

### 4.8.3 Advanced Result Set

While the essential results are used to arrive at the general goal of defining tendon durability as a function of loading variables, numerous other properties are calculated from the recorded data. Trimmed data sets are copied into a more complicated series of spreadsheets for this post-experimental procedure.

From each data point, several real-time values are computed. The load cell output voltage is converted to force measured in Newtons using the appropriate calibration coefficient and the basic formula given in Equation 4.2:

$$P(t) = V_{LC} \times C_{LC}$$

**Equation 4.2:** Calibrated load calculation

Where:  $P(t)$  is the tension in the fiber in Newtons,  $V_{LC}$  is the data point load cell output in volts and  $C_{LC}$  is the load cell calibration coefficient in Newtons per volt.

Stress is then calculated for each data point using the formulation of equation 4.3:

$$\sigma(t) = \frac{P(t)}{Ax10^6}$$

**Equation 4.3:** Measured transient stress calculation

Where:  $\sigma(t)$  is the mechanical stress in MPa and  $A$  is the fascicle cross-sectional area in square meters calculated by the basic formula given in Equation 4.4:

$$A = \frac{\pi D^2}{4}$$

**Equation 4.4:** Sample cross-sectional area calculation

Where:  $D$  is the measured sample diameter.

Actual displacement is converted from the LVDT signal voltage using Equation 4.5:

$$d(t) = V_{LVDT} \times C_{LVDT}$$

**Equation 4.5:** Calibrated displacement calculation

Where:  $d(t)$  is the physical displacement of the fiber from the preload position,  $V_{LVDT}$  is the LVDT output in volts and  $C_{LVDT}$  is the LVDT calibration coefficient in meters per volt. While the sensors are calibrated, the platform is not due to complication with the dynamic nature of the testing and the lack of correlation to calibration by a quasistatic test. In this case, validity will be addressed by comparison of the transient data for modulus with published Young's modulus values for collagen.

Engineering strain is calculated from physical displacement and preload sample length using Equation 4.6:

$$\varepsilon(t) = \frac{d(t)}{L}$$

**Equation 4.6:** Measured transient strain calculation

Where:  $\varepsilon(t)$  is the engineering strain for the data point,  $d(t)$  is the physical displacement of the fascicle and  $L$  is the preload length of the sample measured before testing.

Engineering stress and engineering strain are used to calculate the instantaneous modulus of the fiber by the following formula given as Equation 4.7:

$$E = \frac{\sigma(t)}{\varepsilon(t)}$$

**Equation 4.7:** Transient modulus calculation

Where  $E$  is the modulus for the data point corresponding to time  $(t)$ ,  $\sigma(t)$  is previously calculated stress at time  $(t)$  and  $\varepsilon(t)$  is the engineering strain calculated for the data point.

Engineering strain rate is calculated to assist in quantifying the viscoelastic nature of the collagen fascicle. It is calculated by Equation 4.8:

$$\varepsilon'(t_n) = \frac{\varepsilon(t_n) - \varepsilon(t_{n-1})}{t_n - t_{n-1}}$$

**Equation 4.8:** Data point rate of strain calculation

Essentially, this equation finds the amount of change in engineering strain from one data point to the next and standardizes that value to the basic time interval. Alternatively, this property is better reported as the slope of the linear fit to the strain output for the duration of the test divided by the cross sectional area of the sample to account for the influence of varying fiber diameters.

Apart from calculation of standard engineering values, the harmonic input to the sample which corresponds to the LVDT signal, is plotted against the harmonic output of the sample, the load cell signal. Note that the system is in series, the LVDT is connected to the mechanical input source, the voice coil motor, via a rigid link, while the load cell is connected to the mechanical input through the sample. Phase shift of the peaks of the graph are analyzed to further qualify viscoelastic properties according to concepts developed later in this report. The final goal of the advanced analysis is to propose a uniaxial mathematical model for the mechanical behavior of the typical collagen fascicle.

## **Chapter 5**

### **Basis for Interpreting Results and Reaching Conclusions**

#### **5.1 Overview**

In keeping with the main goal of this project to create a generally useful guide both within and outside of the scientific community, a proposed methodology is offered to transform the empirical results of this research. Many of the techniques and their related fields discussed in this section are highly inter-disciplinary and hence further refinements are expected from this initial work. Nevertheless, the following is presented so that the connection between the in-vitro experimental simulations of loading on collagen substructures and the application to common human activity is developed in detail.

#### **5.2 Limitations in Interpreting Results**

This work focuses on defining the capacity of human tendons operating at the upper limits of tension to which they are subjected. Testing collagen samples at lower intensities is complicated by the increased time that the sample must be exposed to air before damage occurs. The current experimental platform cannot sustain sample viability for a long enough period of time to allow accurate testing at low tension levels. Based on this factor, special consideration will be given to the general conclusions that are drawn from this project.

Lack of data corresponding to low intensity fatigue prevents the development of a complete scheme of limitations to the operational capacities of tendons. However, collecting and interpreting data at what is considered 100 percent intensity allows for the development of particularly relevant conclusions. In terms of athletic training intensity, activities conducted at the full force capacity of the body's musculo-skeletal system represent one high risk grouping of exercise parameters. The other grouping of high risk parameters is activity conducted at low

force capacity for long periods of time. The latter grouping will not be considered in this work for the above reason.

### **5.3 Developing Relevant Conclusions through Anatomy and Biomechanics**

A critical step in arriving at the desired conclusions of this project is the development of the best possible model for applying the properties of the fascicle to the tendon as a unit. Two key values must be measured and/or defined and/or assumed to successfully arrive at this step. The first value, the number of load bearing fascicles that a particular tendon contains, comes from anatomical study. The second value, the body's physical output that constitutes full intensity, is determined from biomechanics. Both values are subject to approximations and assumptions that are found to be either necessary or practical when the information presented in this work is used in real-world applications.

### **5.4 Load Bearing Fascicle Count**

A major difficulty to overcome in creating a widely useful guideline from this research is the determination of the various cross-sectional areas of an athlete's tendons. The critical value is the number of fascicles being employed by the tendon to transfer force from the muscle to the skeleton. Obviously the exact number is, for practical purposes, impossible to determine, but using various methods this value can be estimated with reasonable accuracy. The assumption is made that the tendon to be analyzed is in perfectly healthy condition. That is all fascicles bear the same portion of the entire load.

The most accessible method is to offer general values for tendon cross-sectional area from statistical data based on sex, body mass, height and other relevant physiological parameters. A more accurate, although less accessible method is to use ultrasound imaging to measure the

cross-sectional areas of specific tendons of an individual athlete [24, 60]. While ultrasound imaging is the less available option, its availability is not completely restrictive. Ultrasound technology is becoming more widespread and economical with time. Ultrasound medical imaging has been used in several biomechanical studies to date, with the specific purpose of measuring tendon length and area. It would not be prohibitive for a high level or professional athlete especially, to undergo a quick and unobtrusive ultrasound imaging process for these purposes.

Once the tendon's area is known, the fascicle count is calculated from the relatively non-varying fraction of fascicles per unit area (tendon un-stretched) determined from the average measured fascicle diameter multiplied by 0.86 to account for the mass fraction of fiber to matrix. For simplicity, the final formulation will include cross-sectional area only.

## **5.5 Biomechanical Loading Function**

The other major difficulty is determining the forcing function that the tendon experiences. The first assumption to be made is the representation of the form of this function as a sine wave. While any interpretation of the complex motions of the human body as a uniform cyclic function will never be completely accurate, a sine function fits well to any mechanical system where a linear source of energy drives a rotating linkage. For the purposes of this project, the biomechanical system will be modeled as linear tension applied by the muscle-tendon structure operating the rotating skeletal joint, thus justifying the interpretation of the sine wave model for the loading function. Peak tension is seen at the joint's full flexion and minimum tension at full extension. This relationship however, will not always be correct and may actually be reversed as in the case of joint flexion versus joint extension.

Since the function's general form has now been specified, the two basic parameters of the function can also be defined. Any repeating sine wave can be fully described by the values of frequency and amplitude alone [52, 61]. In this research, frequency requires no further attention

since it is an independent variable in terms of data and in that it is not affected by anatomical or biomechanical variables.

Interpreting the amplitude of the dynamic tension that a tendon experiences in-vivo is complicated as many anatomical and biomechanical factors exert influence. The principal anatomical/biomechanical factor affecting the durability of any tendon is the size of the tendon's cross-section in relation to the capacity to generate force of its respective muscle. Disregarding the natural progression of events that leads to the state of an individual's muscle-tendon systems, three possible conditions can exist for a sufficiently large group of individuals.

## **5.6 Suitable Candidates for Study**

In the first group of subjects, the individuals' tendon cross-section is large enough and/or his/her muscle capacity is low enough that even at full muscle tension, fascicle damage will not occur in a short period of time. Those identified to fit into this category are not subject to analysis using the results of this study since the intensity of the load on their tendons will not cause fascicle damage within the time frames that are considered.

The second possibility is where the subjects' muscle capacity greatly exceeds the corresponding capacity determined by the cross-section of their tendons. These individuals are highly susceptible to tendon injury during short duration, high intensity exercise. The application of the results presented here is less direct as the assumption must be made that this athlete does not often use full muscle capacity, perhaps only 90-95 percent leaving a vague correlation.

This work best applies to those individuals who fall into a third category. These subjects are determined to have muscle capacity that corresponds well to tendon durability based on cross-section. To give a standard definition, these individuals, when conducting an exercise at full capacity will experience tendon damage within a period of time that falls within the range of duration times observed in these experimental tests.

## 5.7 Tendon Injury Risk Coefficient

The final step is to define a value that reflects muscle capacity compared to tendon durability and the ranges of this value that separate each of the three groupings. All experiments in this work apply a varying load with a maximum value of one Newton and a nominal tensile minimum value. Individuals, whose muscles can generate a maximum of one Newton of force for each fascicle contained in the muscle's corresponding tendon, or within a reasonable range above or below this value, are the best candidates for application of the results of this study. To define a formula that estimates the force experienced by each fascicle Equation 5.1 is given:

$$R_A = \frac{F_{max}}{N_f}$$

**Equation 5.1:** Load per fascicle calculation

Where  $R_A$  is the absolute tendon injury risk coefficient in Newtons per fascicle,  $F_{max}$  is the maximum linear force that the muscle can generate in Newtons and  $N_f$  is the estimated number of fascicles which comprise the tendon.

Assuming procedures to estimate fascicle count as described above have been completed, the maximum force that the corresponding muscle or muscle group experiences must also be estimated. This can be done using heavy resistance exercise of isolated muscle groups. The maximum muscle force can be roughly estimated by a competent athlete or coach using exercises done on common gymnasium equipment, or measured more accurately in a kinesiology lab or other facility with advanced equipment.

Once tendon cross-sectional area has been estimated or measured, a general tendon injury risk coefficient can be formulated by Equation 5.2:

$$R = \frac{F_{max}}{1000A_{tendon}}$$

**Equation 5.2:** Example tendon injury risk coefficient calculation

Where R is the general tendon injury risk coefficient,  $F_{max}$  again is the maximum pull force that the muscle can generate in Newtons and  $A_{tendon}$  is the value obtained for the tendon cross sectional area in square centimeters. The above formula estimates a value of 1000 fascicles per square centimeter. This number was arrived at by taking the area of the average fascicle based on a diameter of 0.3 millimeters; assuming initially that the tendon cross-section is one hundred percent fiber; then multiplying by 0.86 the given dry weight fraction of collagen fiber in tendon material, and finally assuming twenty percent fluid content in the cross-section. At this point, it is assumed that all test subjects will have a tendon injury risk coefficient reasonably close to one Newton per fascicle. The term cannot be precisely defined in a reasonable manner given the scope of this work, but with a conservative approach, +/- 10% variation could be assumed based on fascicle testing parameters and observed fluctuation of the measured load experienced by each sample.

## 5.8 Final Formulation

The final step to unification of the essential results of this work is incorporation of tension variation frequency, the general independent variable among test variations. A risk factor based on frequency can now be defined with a direct basis in experimental results. Frequency dependent risk factor will be given in terms of time that an individual who meets the

above outlined criteria can safely perform a maximum intensity exercise at a given frequency of cycling.

Presentation of the final working results is possible by three options. An equation of the form shown in Equation 5.3:

$$t_{safe} = C_1 + C_2f + C_3f^2 \dots$$

**Equation 5.3:** Possible polynomial fit template

For example, where  $t_{safe}$  is the nominal time or number of cycles,  $C_n$  are constants and  $f$  is frequency can be fitted to the resulting data points with frequency as the independent variable and either time that an activity can be sustained safely or number of cycles that can be safely completed as the dependent variable [62]. The same equation can be plotted with frequency on the x-axis and time or sustainable cycles on the y-axis and used as a visual tool in place of mathematical formulation. Results may also be tabulated to various degrees of resolution for general ease of use combined with improved accuracy over the graphical method.

Keeping in mind that these results are to be usable by non-scientific individuals, the presentation of results as graphs and tables are most important. Further, the speed and ease of use of pre-calculated tables or graphs will be advantageous in encouraging use of this information during training.

## 5.9 Validation and Refinement of Results

Due to the various assumptions and approximations that are employed to reach a point where the results of this research can be used in the intended environment, extensive population based statistical testing must be undertaken to confirm the validity of the conclusions reached and adjust the key values as found necessary. The initial guideline produced by this work is

based entirely in laboratory simulated conditions, and real-world trials of these standards are entirely necessary to reach an acceptable level of applicability.

A test group of subjects with sufficient size and variation or similarity of physical characteristics must be tested retroactively after having experienced tendon inflammation pathologies presumably due to overtraining or overuse. A control group must also be established by testing at a level determined to be slightly below what is predicted to cause inflammation. All individuals of the test group must perform the activity at the same frequency and full intensity. A conclusive result will be either affirmative, inflammation was caused in the majority of subjects, negative by inflammation not reported in the majority of individuals or negative where inflammation was reported in the majority of members of the control group. Subsequent tests must be conducted to find the correction factor to the guideline at the frequency tested. Further repetitions of the cycle must be undertaken for various increments of the frequency range before the results are fully refined and validated.

Several aspects of the final result must be scrutinized by controlled population based study of the application of the proposed information in the intended environment [63]. It may be revealed that calculation of the tendon injury risk coefficient calculation must be modified because of evidence that the fascicle count per area assumptions are in error or because an improved method of calculating maximum muscle force generation is developed. The curve fitted to the results may require modification of its general form or adjustment of the various characteristic constants defined above as  $C_n$ . Finally, the general magnitude and range in which the results are presented may be found to be too high or too low. A constant coefficient multiplication or addition can be applied to correct the result, but the source of error should be determined on the biological level.

## Chapter 6

### Results

#### 6.1 Overview

As previously described, the essential results of this work focus on providing very specific information on the durability of collagen fascicles under repeated fatigue loading that varies only in frequency. The information presented in this section is centered on the key value of total impulse, or area under the curve of the loading function in Newtons versus time, applied to the fiber until failure then corrected by division by the measured cross-sectional area of each sample. Moving forward, the value of impulse will be represented by  $I_f$  and as noted in Section 4.8.2, the impulse divided by the area of the fiber becomes  $C_s$  and is termed the Damage Characteristic.

Example loading function graphs are given to show the first 10 cycles in terms of tension versus time. These are the templates that are used for calculation of impulse. They are provided because the templates differ slightly from the actual functions at higher frequencies.

Establishment of a linear relationship between the total impulse and measured cross-sectional area is critical to define the validity of these results. For this reason, each series of tests is accompanied by a graphical linearity analysis of the ten final data points for a given frequency. Zero intercepts and correlation coefficients of the data are given in the graphs; however, non-linearity values are calculated separately. The slope of the linear regression is reported as an indication of sensitivity to the fascicle cross-section which may have implications in a physiological sense. The zero intercept may be construed as a third parameter in description of the characteristics of the collagen sample, but has a less direct application in a physiological sense. Finally, the value of  $C_s$  for a given load cycle frequency is calculated as the mean of the  $C_s$  value for each test in the series. Data scatter is then reported on in terms of standard deviation of the ten observed values for  $C_s$  at the frequency in question.

Average fascicle diameter must also be noted and must be reasonably near the assumed value of 0.3 millimeters to provide validity to subsequent interpretation based on the proposed methods of Chapter 5. This data will be reported along with standard deviation for the data set.

## 6.2 Reported Results for Essential Interpretation

Figures 6.1 through 6.10 give examples of the force-time function used to calculate impulse as well as graphical results for all 10 tests at each frequency. Results are summarized in Table 6.1.

### 6.2.1 Results: 0.5 Hz Frequency; 0.5 N Amplitude; 0.5 N Preload

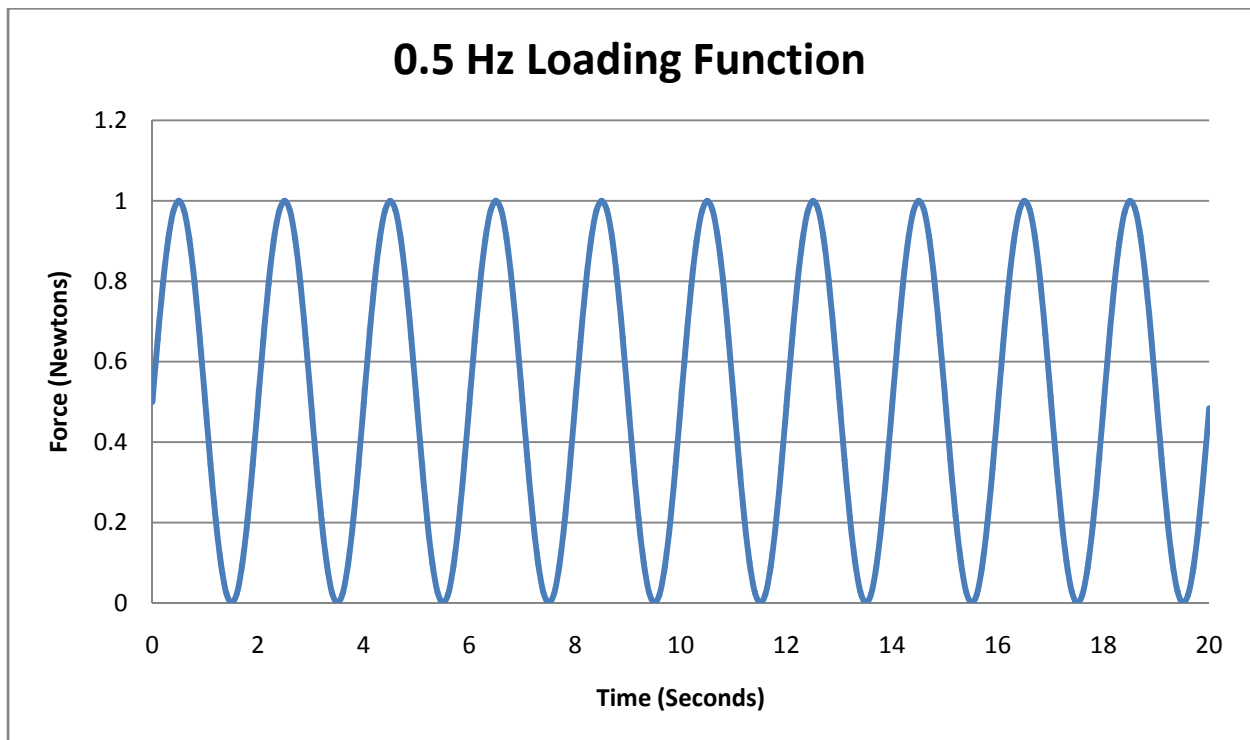


**Figure 6.1:** Example applied loading function (10 cycles)

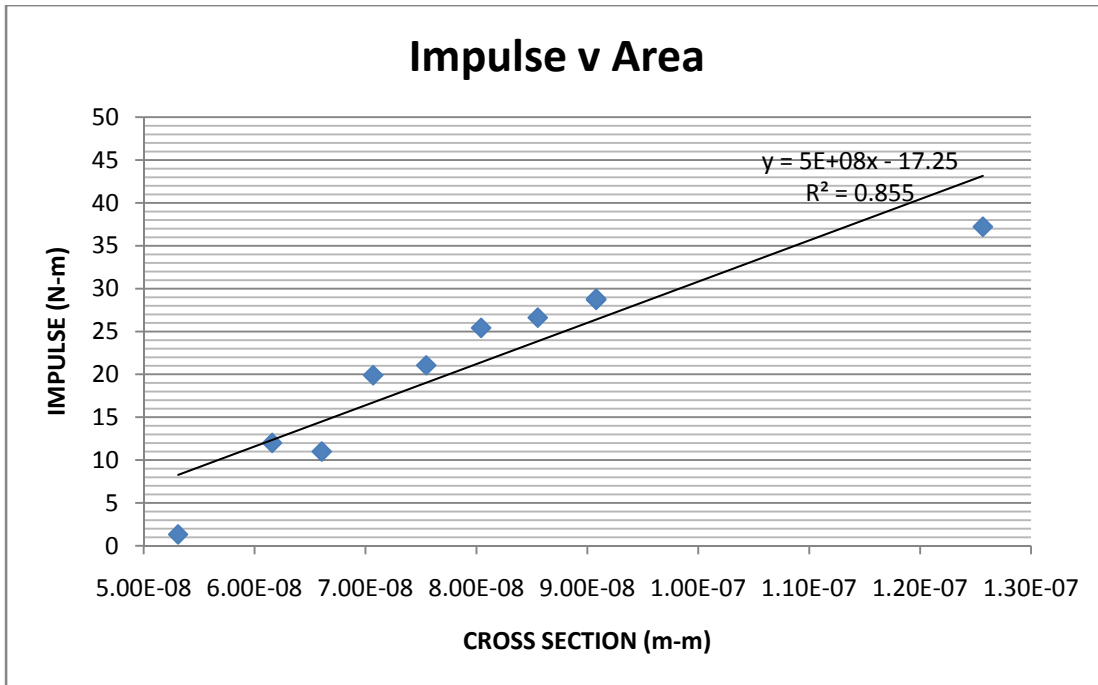


**Figure 6.2:** Graphical representation of test series

Zero Intercept:  $-17.258 \text{ Newton} - \text{Second}$

Slope:  $5.0 \times 10^8 \frac{\text{Newton-Second}}{\text{Meter}^2}$

Non-Linearity: 23.26%

Correlation Coefficient: 0.8557

$C_s$ :  $2.50 \times 10^8 \frac{\text{Newton-Second}}{\text{Meter}^2}$

$\sigma_{C_s} = 9.52 \times 10^7 \frac{\text{Newton-Second}}{\text{Meter}^2}$

$A_f$ :  $0.000317 \text{ meter}$

$\sigma_{A_f} = 3.917 \times 10^{-5} \text{ meter}$

**6.2.2 Results: 1.0 Hz Frequency; 0.5 N Amplitude; 0.5 N Preload**

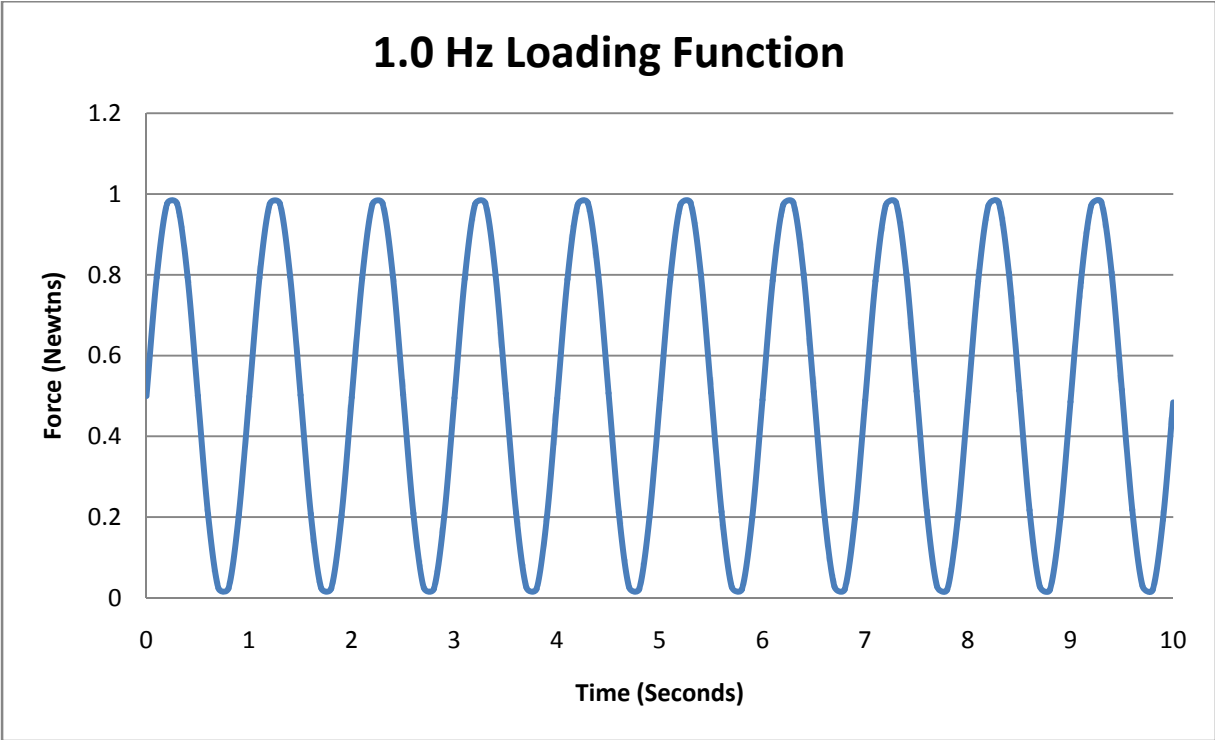


**Figure 6.3:** Example applied loading function (10 cycles)

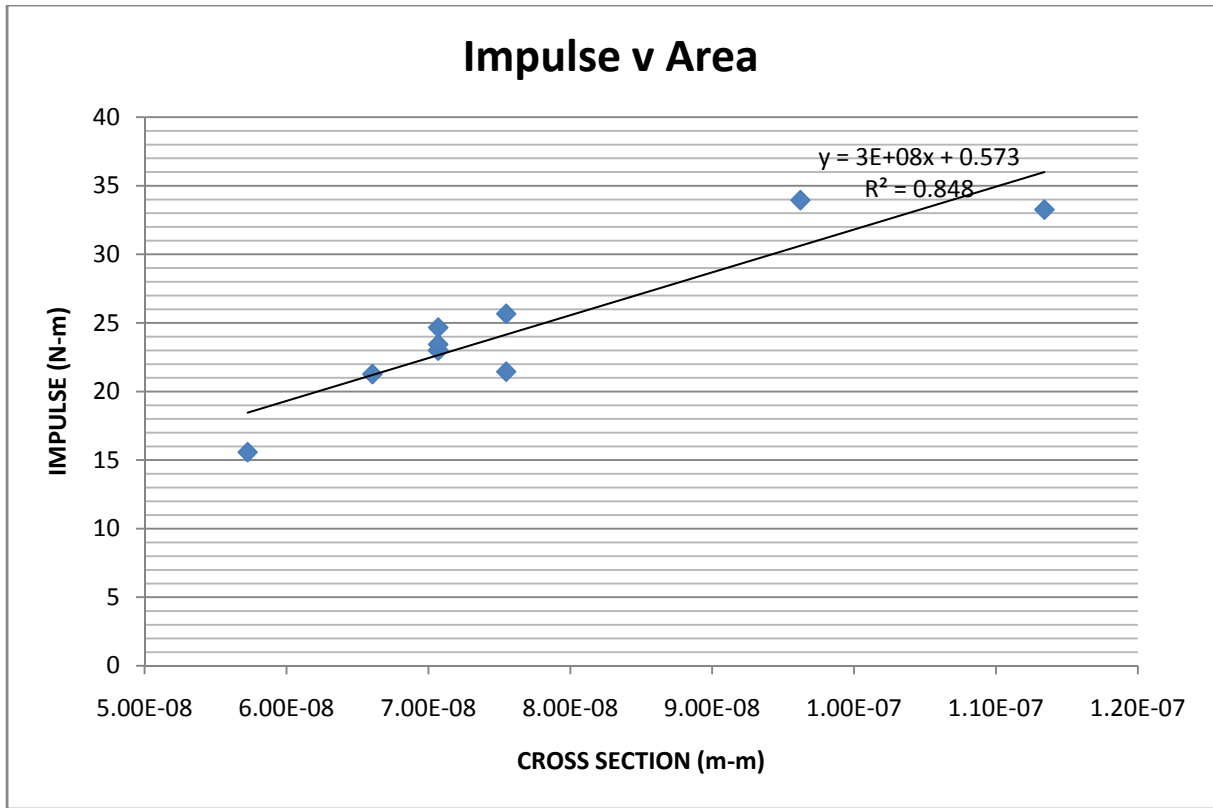


**Figure 6.4:** Graphical representation of test series

Zero Intercept: 0.573 *Newton – Second*

Slope:  $3.0 \times 10^8 \frac{\text{Newton-Second}}{\text{Meter}^2}$

Non-Linearity: 24.55%

Correlation Coefficient: 0.8481

$C_s$ :  $3.20 \times 10^8 \frac{\text{Newton-Second}}{\text{Meter}^2}$

$\sigma_{C_s} = 2.75 \times 10^7 \frac{\text{Newton-Second}}{\text{Meter}^2}$

$A_f$ : 0.000311 *meter*

$\sigma_{A_f} = 3.14 \times 10^{-5} \text{meter}$

**6.2.3 Results: 1.5 Hz Frequency; 0.5 N Amplitude; 0.5 N Preload**

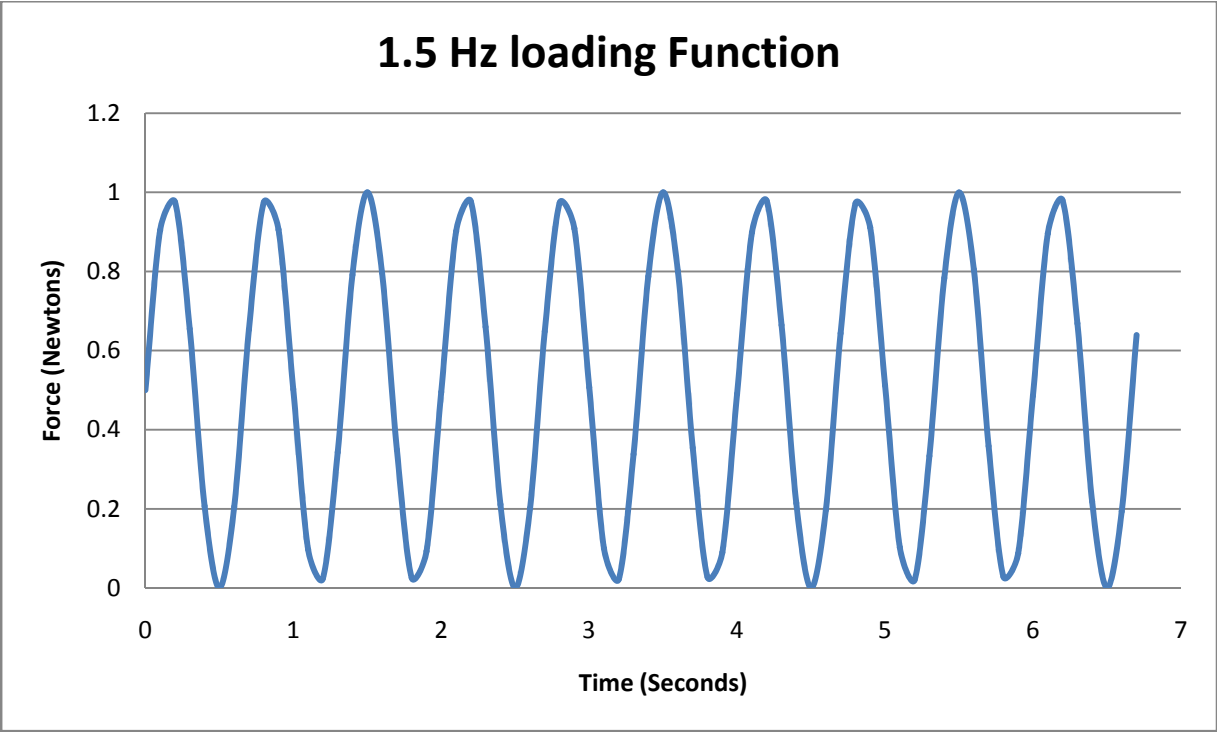


**Figure 6.5:** Example applied loading function (10 cycles)

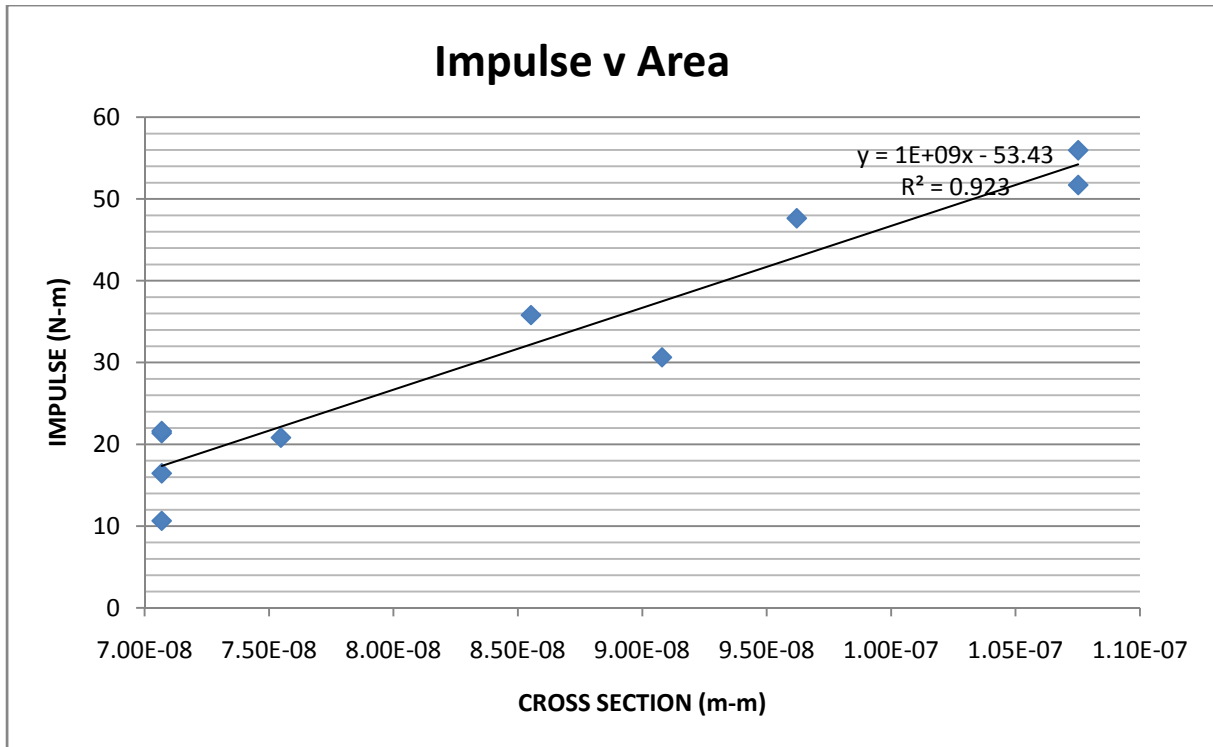


**Figure 6.6:** Graphical representation of test series

Zero Intercept:  $-53.435 \text{ Newton} - \text{Second}$

Slope:  $1.0 \times 10^9 \frac{\text{Newton-Second}}{\text{Meter}^2}$

Non-Linearity: 14.81%

Correlation Coefficient: 0.9234

$C_s$ :  $3.52 \times 10^8 \frac{\text{Newton-Second}}{\text{Meter}^2}$

$\sigma_{C_s} = 1.23 \times 10^8 \frac{\text{Newton-Second}}{\text{Meter}^2}$

$A_f$ :  $0.000327 \text{ meter}$

$\sigma_{A_f} = 2.91 \times 10^{-5} \text{ meter}$

**6.2.4 Results: 2.0 Hz Frequency; 0.5 N Amplitude; 0.5 N Preload**

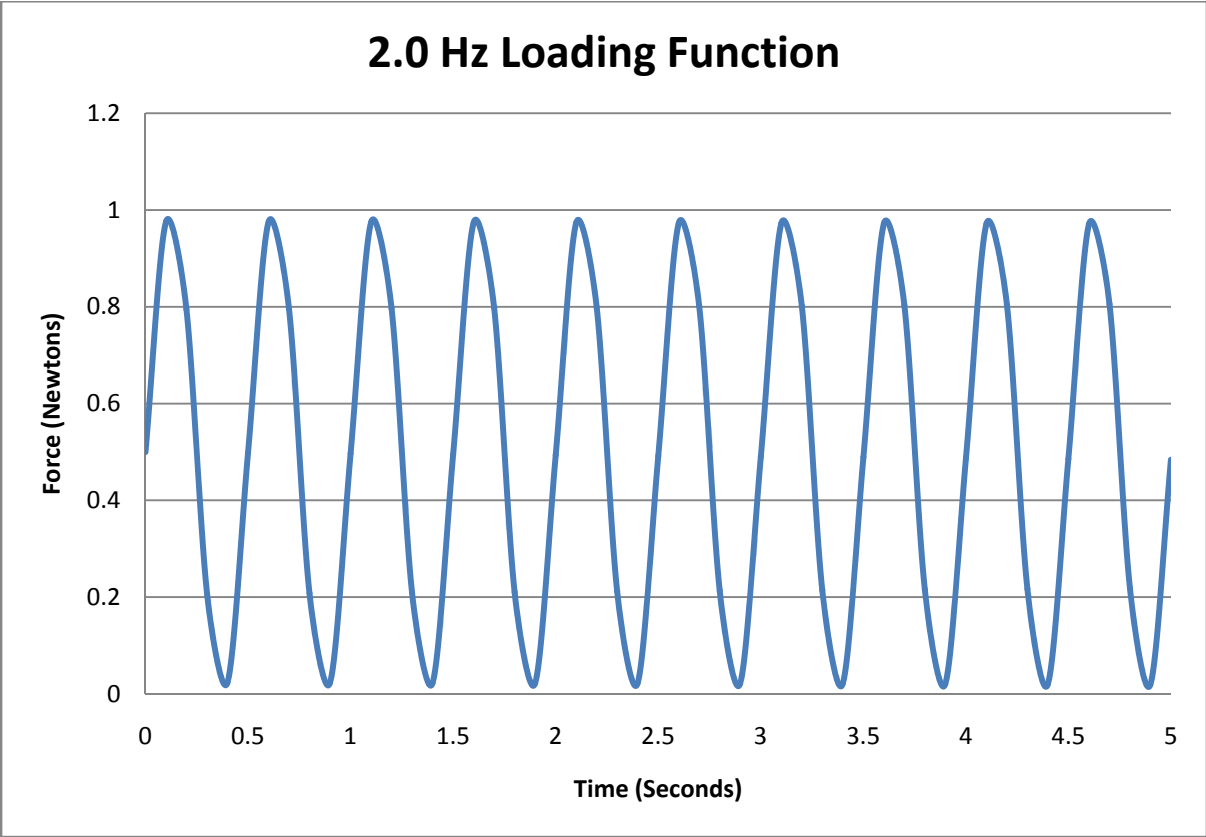


**Figure 6.7:** Example applied loading function (10 cycles)

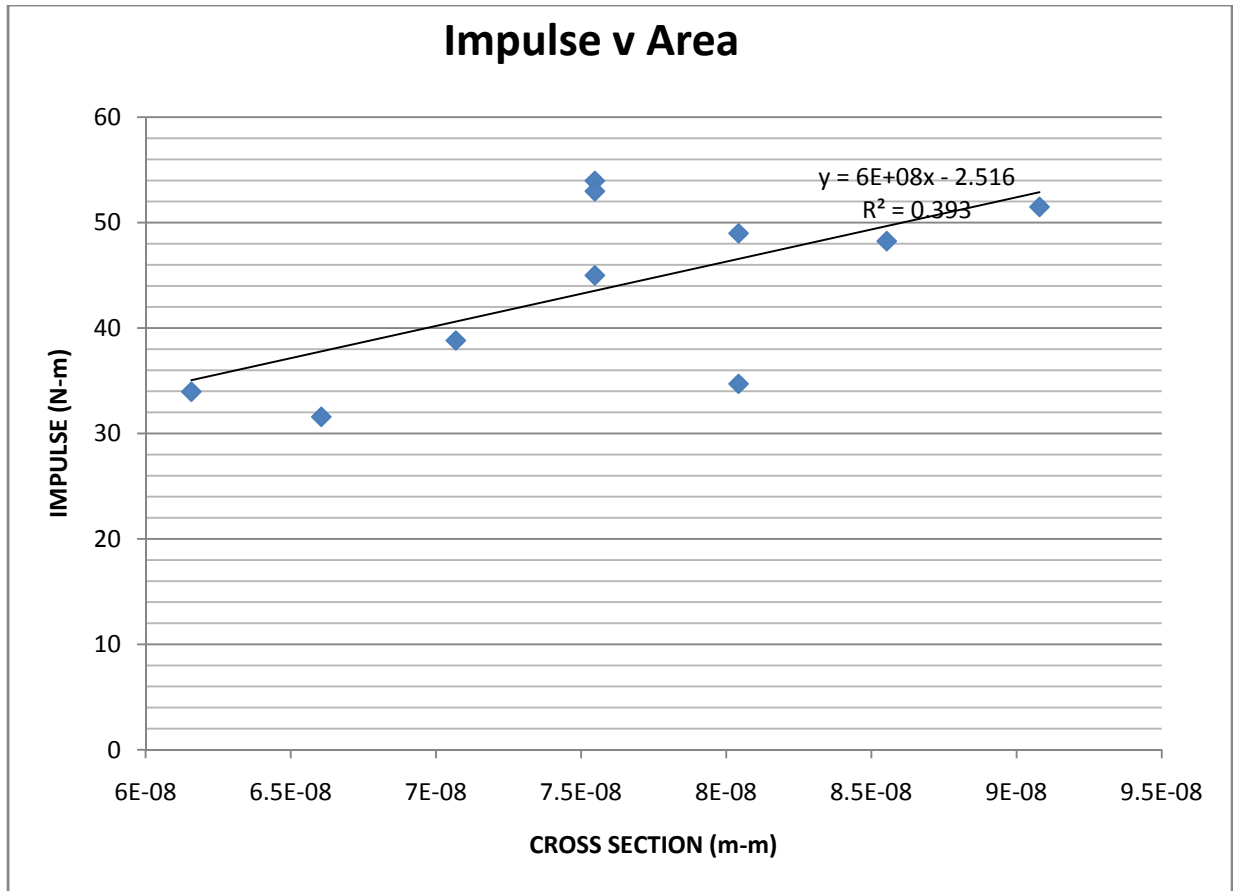


**Figure 6.8:** Graphical representation of test series

Zero Intercept:  $-2.516 \text{ Newton} - \text{Second}$

Slope:  $6.0 \times 10^8 \frac{\text{Newton-Second}}{\text{Meter}^2}$

Non-Linearity: 50.02%

Correlation Coefficient: 0.3934

$C_s$ :  $5.76 \times 10^8 \frac{\text{Newton-Second}}{\text{Meter}^2}$

$\sigma_{C_s} = 8.73 \times 10^7 \frac{\text{Newton-Second}}{\text{Meter}^2}$

$A_f$ :  $0.000311 \text{ meter}$

$\sigma_{A_f} = 1.79 \times 10^{-5} \text{ meter}$

**6.2.5 Results: 2.4 Hz Frequency; 0.5 N Amplitude; 0.5 N Preload**

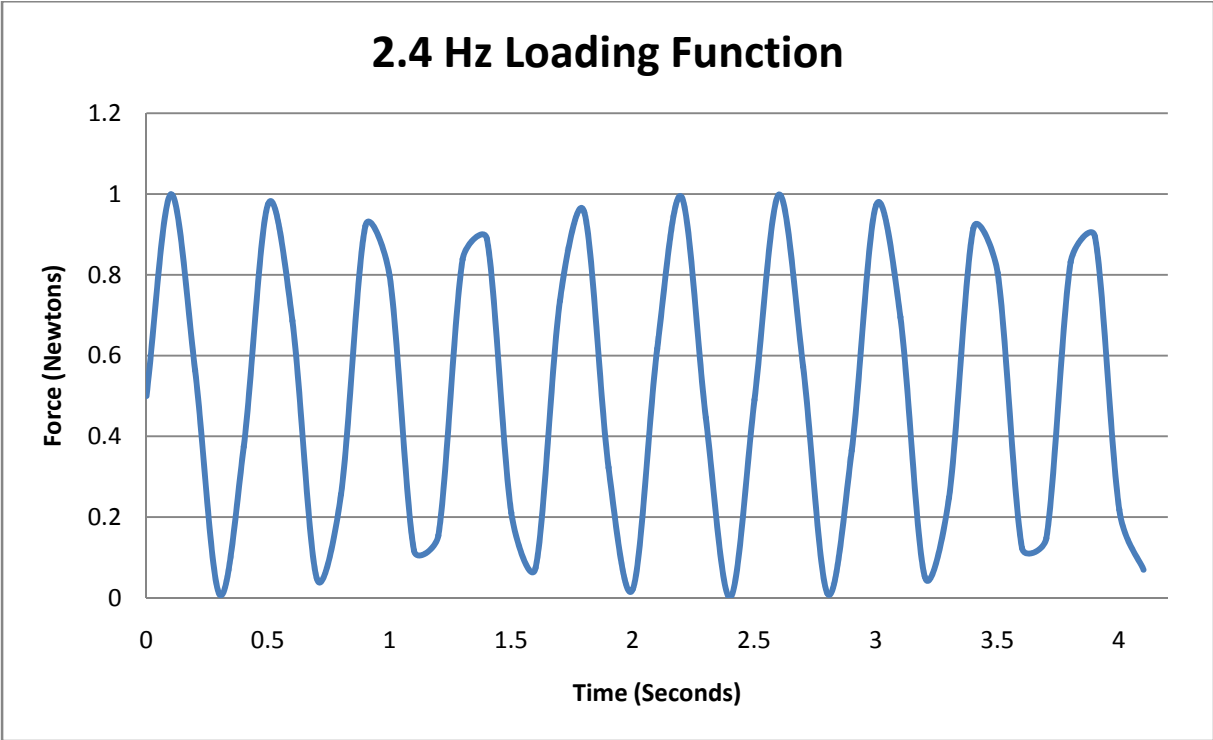


**Figure 6.9:** Example applied loading function (10 cycles) \*Note that the sensed load loses resolution at higher frequencies due to harmonic interaction with the scan rate (10 Hertz)

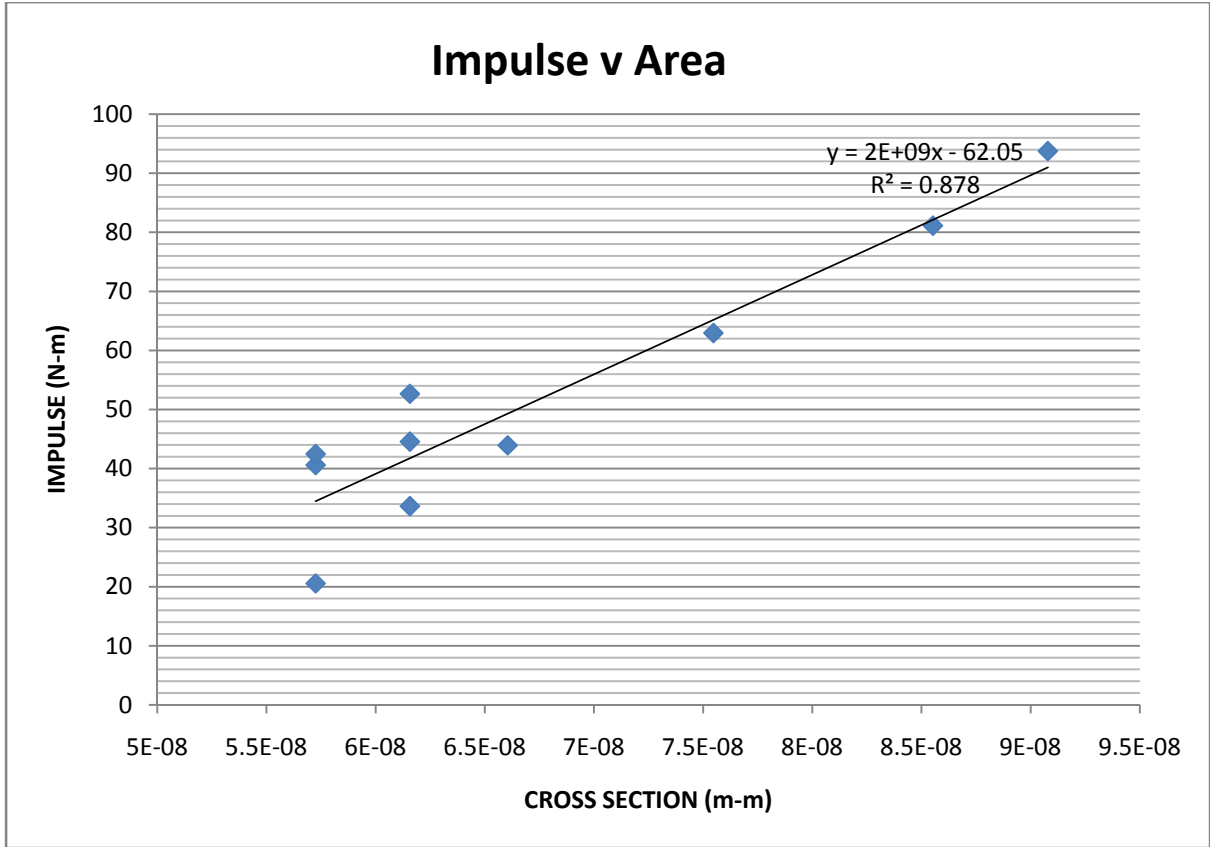


**Figure 6.10:** Graphical representation of test series

Zero Intercept:  $-62.055 \text{ Newton} - \text{Second}$

Slope:  $2.0 \times 10^9 \frac{\text{Newton-Second}}{\text{Meter}^2}$

Non-Linearity: 43.59%

Correlation Coefficient: 0.8789

$C_s$ :  $7.42 \times 10^8 \frac{\text{Newton-Second}}{\text{Meter}^2}$

$\sigma_{C_s} = 1.95 \times 10^8 \frac{\text{Newton-Second}}{\text{Meter}^2}$

$A_f$ :  $0.000292 \text{ meter}$

$\sigma_{A_f} = 2.57 \times 10^{-5} \text{ meter}$

**Table 6.1:** Full set of results tabulated for simplified reference

Frequency	Zero-Intercept	Slope	Non-Linearity	Correlation Coefficient	Average impulse Sustained	Standard Deviation	Average Fascicle Diameter	Standard deviation
0.5 Hz	-17.258	5.00E+08	23.26%	0.8557	2.50E+08	9.52E+07	0.000317	3.92E-05
1.0 Hz	0.573	3.00E+08	24.55%	0.8481	3.20E+08	2.75E+07	0.000311	3.14E-05
1.5 Hz	-53.435	1.00E+09	14.81%	0.9234	3.52E+08	1.23E+08	0.000327	2.91E-05
2.0 Hz	-2.516	6.00E+08	50.02%	0.3934	5.76E+08	8.73E+07	0.000311	1.79E-05
2.4 Hz	-62.055	2.00E+09	43.59%	0.8789	7.42E+08	1.95E+08	0.000292	2.57E-05

## **6.3 Essential Results against Frequency**

### **6.3.1 Basic Data Presentation**

The following plot shows impulse withstood by each sample set as a function of loading frequency. Impulse is taken as the average of the ten values recorded in each test series of the same frequency. As mentioned, the impulse is corrected using division by measured cross-sectional area of each individual fiber. Figure 6.11 gives these basic results.

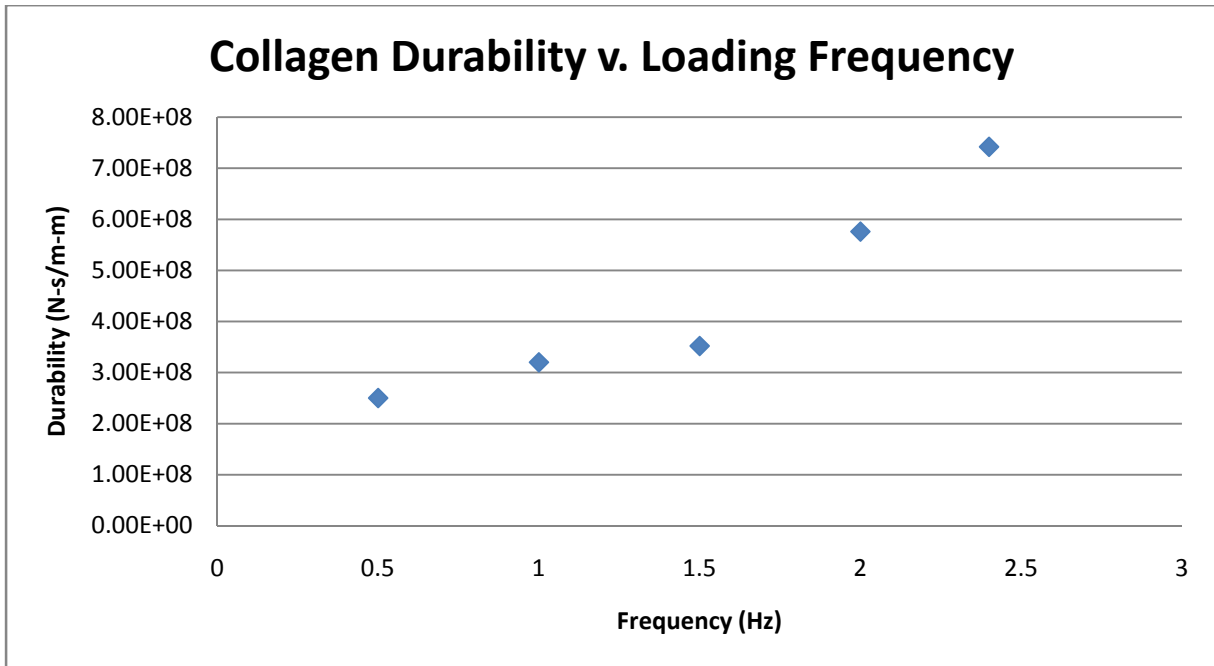


**Figure 6.11:** Graphical representation of basic results

### 6.3.2 Linear Interpretation of Essential Results

Since the interpretation of the present result set emphasizes simplicity in expansion and manipulation of the information, a linear fit is appropriate as long as reasonable correlation is established. Maximum nonlinearity for the data set presented in Figure 6.11 is 34.15% implying that a linear fit is not ideal; however a correlation coefficient of 0.9016 is calculated. For these reasons, the linear interpretation will be given as suitable for general use in calculating susceptibility to tendon damage during training activities where other sources of error overshadow any error introduced by nonlinearity of this data.

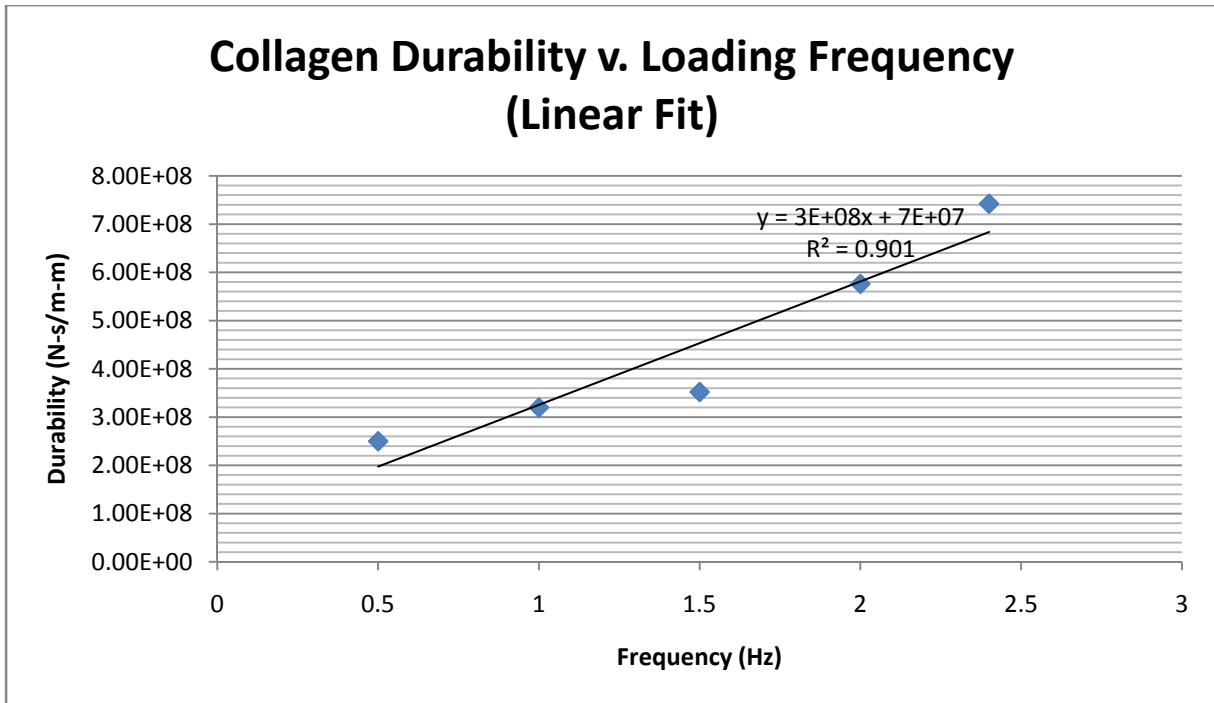


**Figure 6.12:** Linear representation of basic results

Linear regression, as shown in Figure 6.12 yields a best straight line fit corresponding to Equation 6.1:

$$C_S = 3.00 \times 10^8 f_P + 7.00 \times 10^7$$

**Equation 6.1:** Linear approximation to durability

Methodologies described in Chapter 5 propose one possible manner in which this equation can be expanded to yield relevant information on the risk level that a certain training activity presents.

### 6.3.3 Polynomial Fit to Essential Results

A more exact, however not necessarily more appropriate, fit to the data set is a polynomial as previously described in Section 5.8. To improve the accuracy of this analysis, additional partial testing is carried out at 0.3 Hz and 0.7 Hz. These data points allow better characterization of the low frequency region in which the trend is less distinct. Further results of this analysis, demonstrate that correlation is improved very little with polynomial fits above second order, and so only a second order curve fit is presented in Figure 6.13:

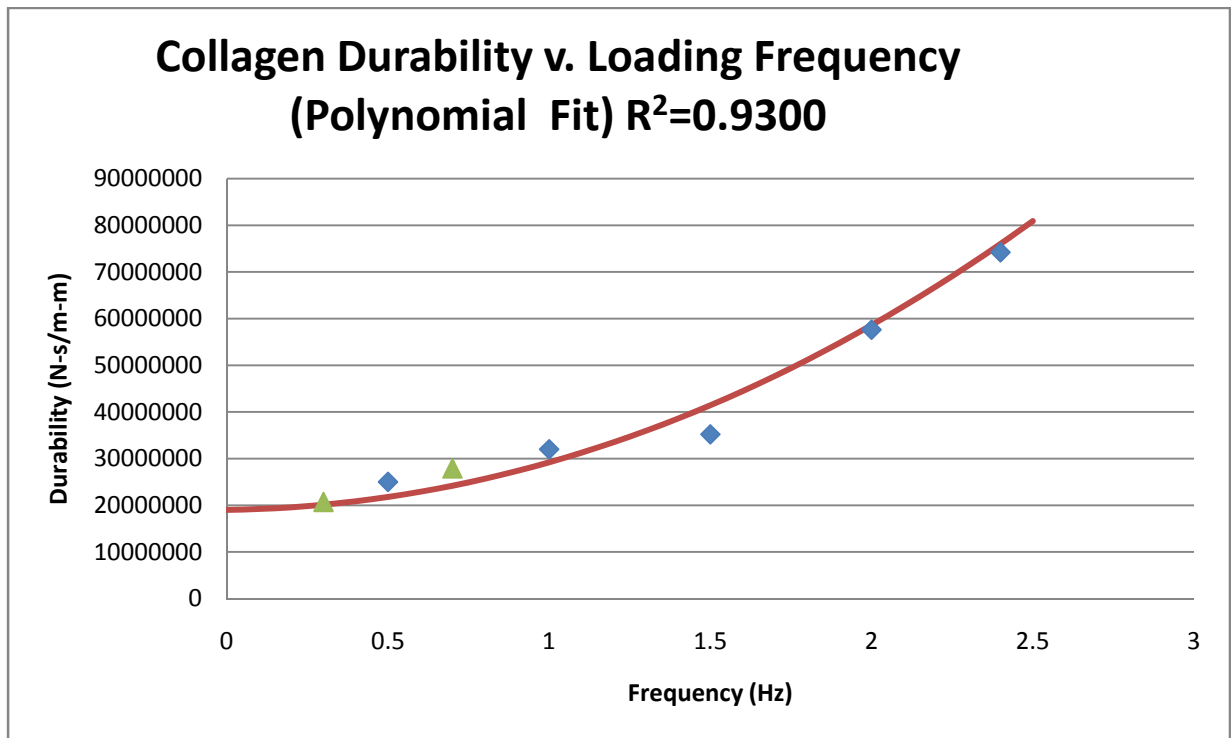


Figure 6.13: Polynomial representation of basic results

Polynomial curve fitting as shown in Figure 6.13 yields a best polynomial fit corresponding to the following second order Equation 6.2:

$$C_S = 1.90x10^8 + 1.00x10^7 f_P + 2.00x10^6 f_P^2$$

**Equation 6.2:** Polynomial fit to durability

While a linear fit is much more practical assuming that these formulae will be used “in the field,” the second order polynomial curve fit shows a much higher correlation. It is recommended that when developing more universal tools from this data, tabular and graphical aids should be produced using the polynomial fit, but any mathematical formulation should be developed as a linear equation.

## **Chapter 7**

### **Advanced Results**

#### **7.1 Overview**

This section will utilize advanced concepts of material science in order to meet the goal set forth in Section 4.8.3 of characterizing individual collagen fascicles with a comprehensive mathematical model, as well as develop a hypothetical mechanistic model based on the specific results and behaviors observed in this project. Various other specific results will also be reported according to procedures that are typically used in testing of viscoelastic materials. Appendix C is provided for a detailed technical review of the concepts that are employed to arrive at the results presented in this chapter.

Note that for results where stress and strain are processed simultaneously, only 0.5 Hz and 1.0 Hz test series are used. Higher frequency tests are eliminated due to adverse effects of harmonic interaction between the data acquisition rate and the mechanical functions as described previously, and due to the general lack of data points per cycle. Future testing at these frequencies is possible using a digital oscilloscope in place of a moderate scan rate data acquisition system. However, the results will be able to be applied only to a small number of cycles suitable only to characterize loss angle and related parameters.

#### **7.2 Dual Response Behaviors**

Analysis of strain verse time plots reveals that the displacement behavior of each test follows one of two distinct patterns. Under close observation, all strains vary harmonically according to the sinusoidal mechanical input to the system as expected. However, at lower frequencies, the strain function is in most cases strictly linear in its increasing trend. To be more precise, the vertical distance between each subsequent peak is uniform for the extent of the test. Any vertical variation between subsequent strain peaks represents a non-recoverable dissipation

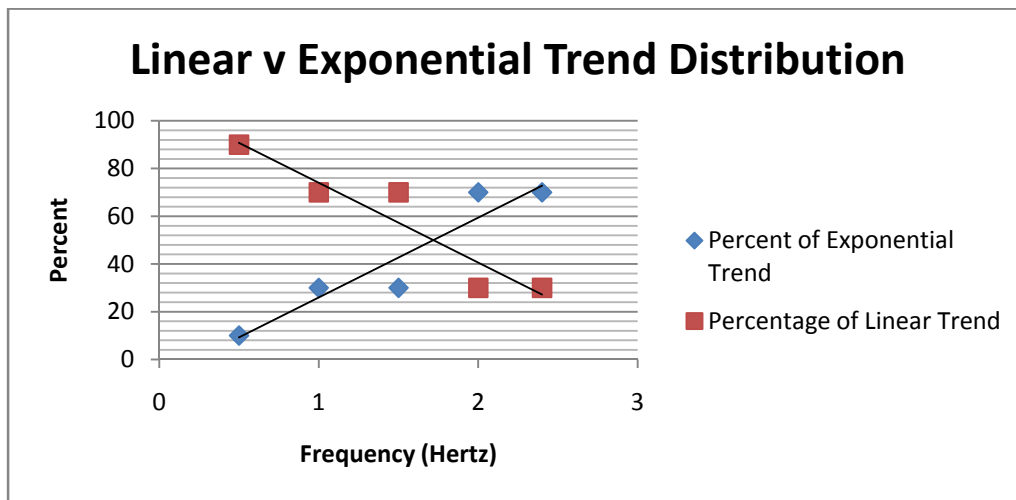
of strain energy by an entropic mechanism of deformation. In other words, the sample dissipates the same amount of strain energy per loading cycle, and the mechanism of deformation is consistent for the length of the test.

A second behavior begins to dominate the material deformation response as frequencies of cycling are increased. Here, a higher order trend is apparent, closely following a behavior described by Equation 7.1:

$$\epsilon_{trend} = 1 - e^{-at}$$

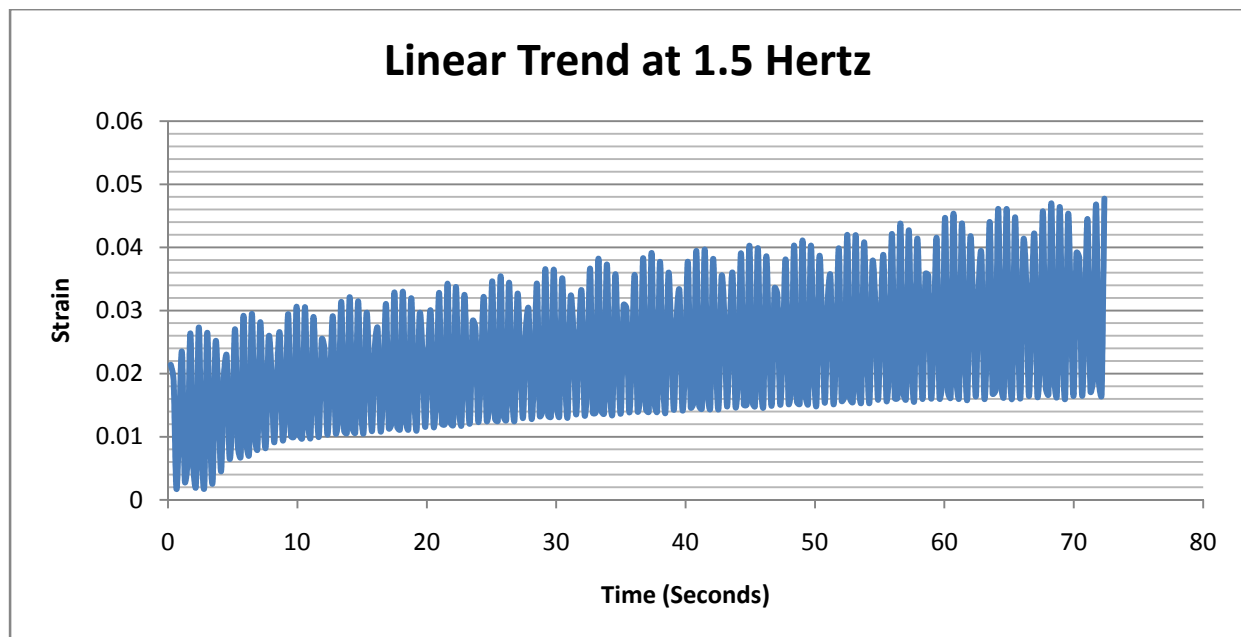
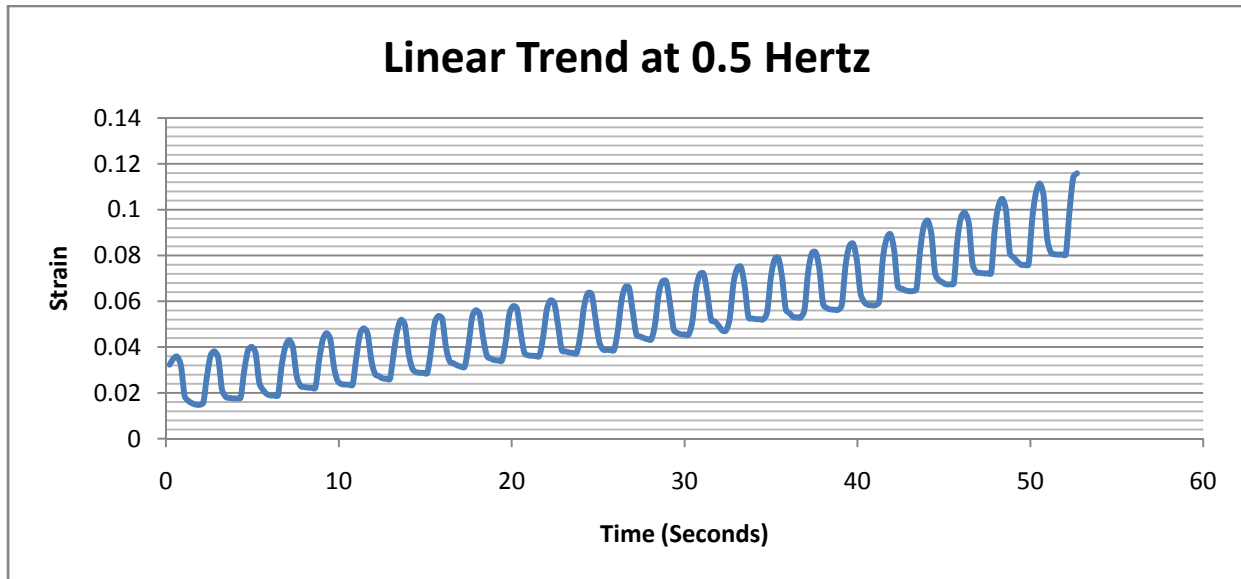
**Equation 7.1:** Model of higher order strain trend

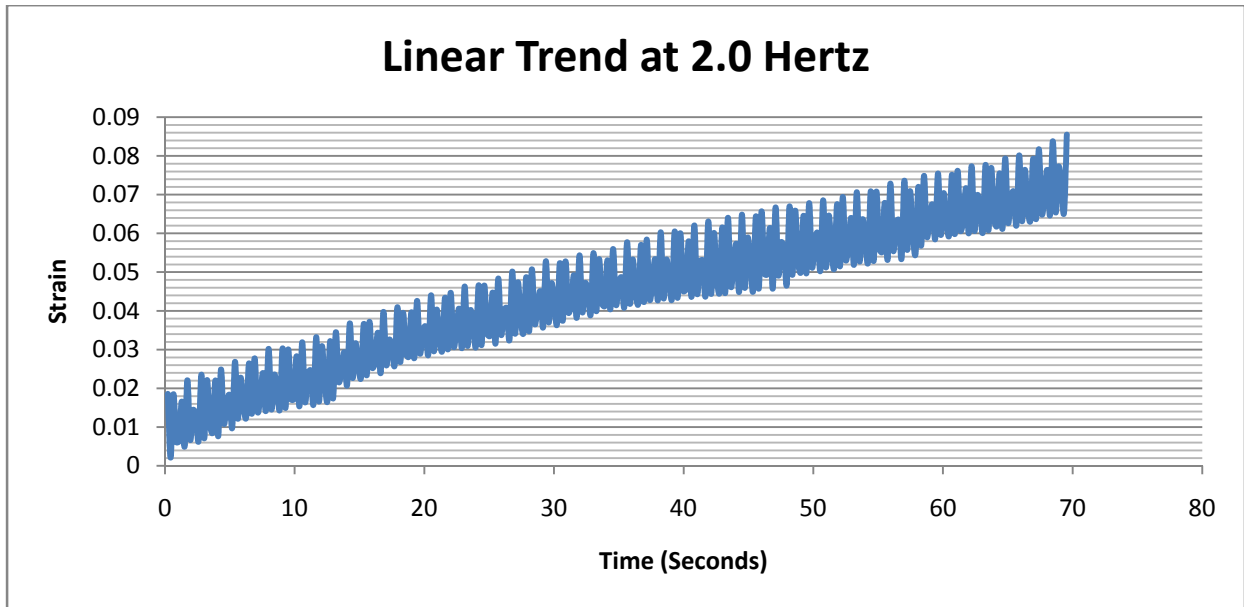
In this case, the vertical distance between subsequent strain peaks decreases as the test progresses indicating that energy dissipation per cycle of the fiber decreases progressively in proportion to Equation 7.1. The trend is toward purely elastic behavior with no hysteric loss per cycle. Noting that 10 tests are completed per frequency, the distribution of observed behaviors is given in Figure 7.1:



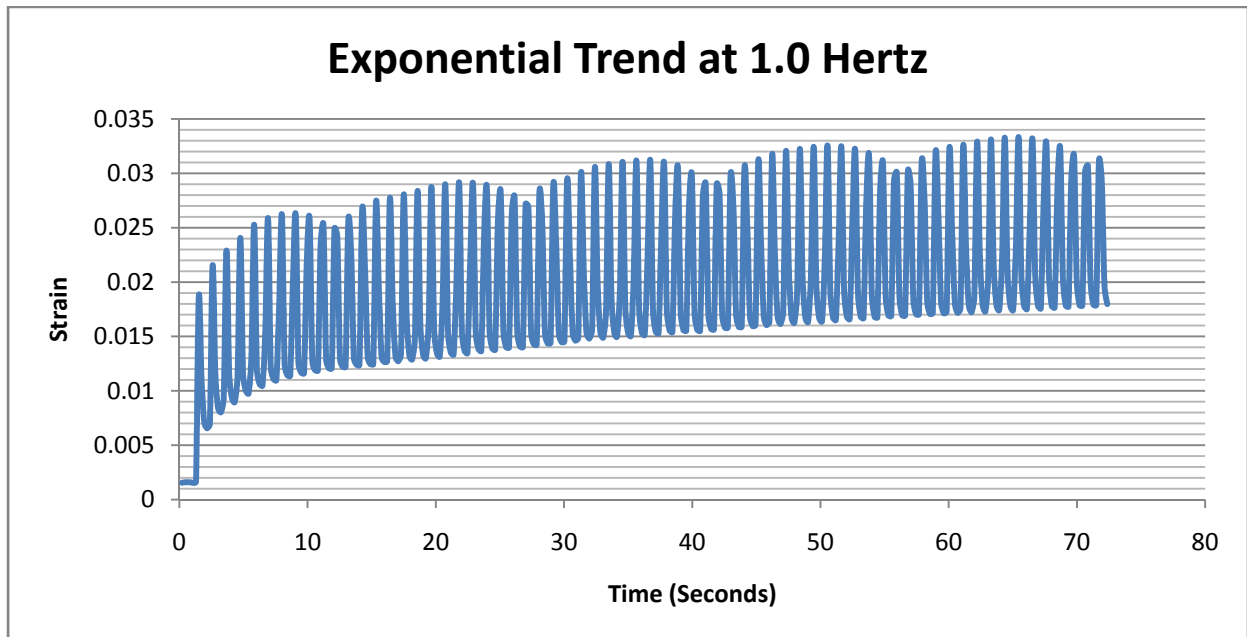
**Figure 7.1:** Trend distribution observed throughout testing

Examples of linear and higher order behavior are shown by actual test results in Figures 7.2 and 7.3 respectively:





**Figure 7.2:** Examples of observed linear strain trend at various loading frequencies



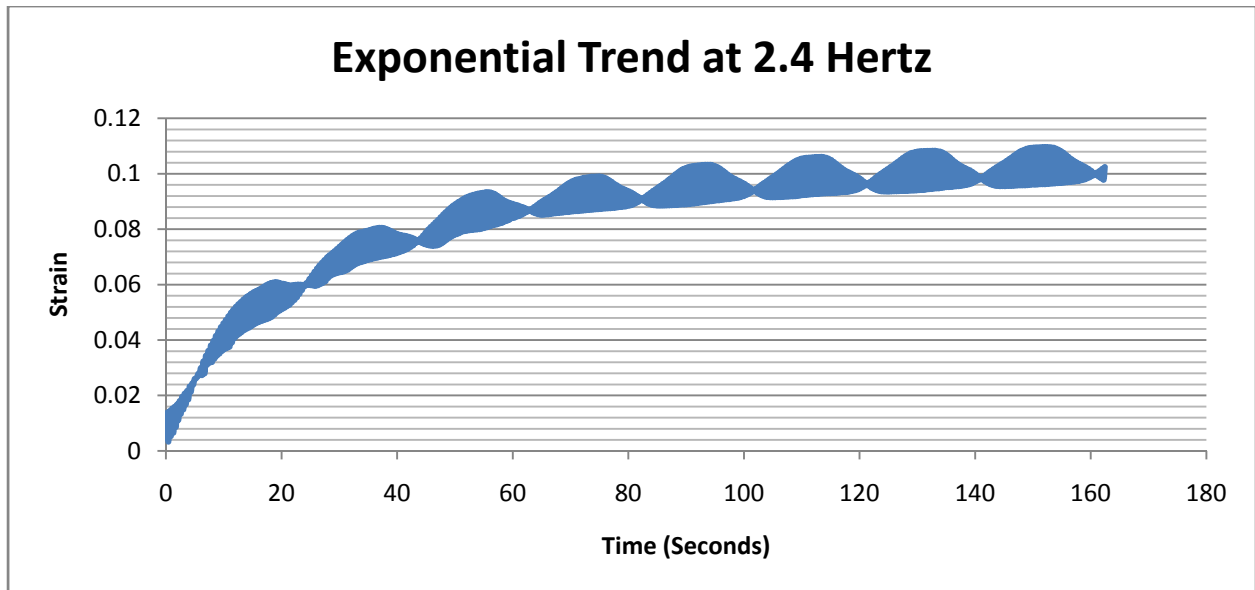
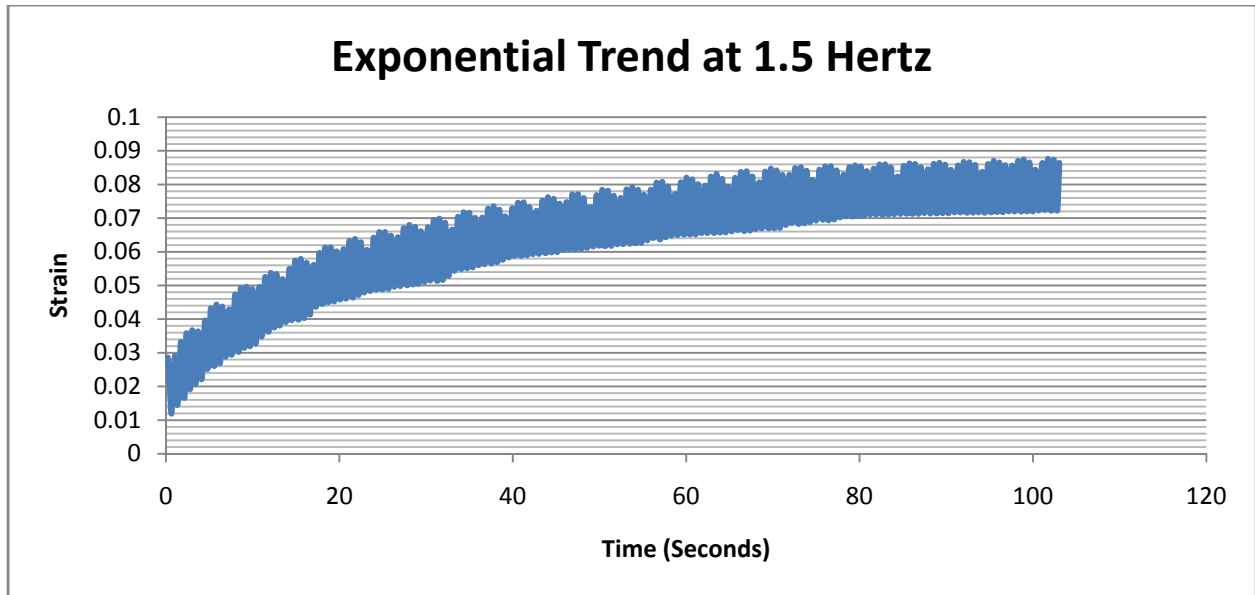


**Figure 7.3:** Examples of observed exponential behavior at various loading frequency

Observation of the linear trend is expected since collagen is known to behave viscoelastically. However, the emergence of a higher order pattern over the test span is a departure from idealized viscoelastic behavior and must be analyzed from the point of view that the properties that control the mechanical behavior of the fiber are changing either due to a time dependent phenomenon or due to the addition of strain energy to the material. Before analyzing

further, it is important to state that the split strain behavior phenomenon is clearly frequency dependent. The higher order behavior is definitively more common at higher loading frequencies and observed much less at lower frequencies. However, it is critical to maintain that linear and higher order behaviors exist at all frequencies tested.

Change of material properties by time dependent mechanisms could be caused by temperature change of the fiber, drying of the sample or change of chemical environment [4, 13, 24, 27, 31]. The observation of a pronounced curved behavior at the beginning of each test found to display higher order behavior negates this conclusion. Higher order behavior as noted in these results implies that the sample behaves more linearly as test time increases. In all cases, test times for observed failure at higher loading frequencies were markedly higher. Therefore, if the above time dependent mechanisms caused the split in behavior, pronounced curved or clearly linear region would be expected to occur uniformly early in each test regardless of frequency, with discrepancies occurring later in each test run. The opposite is observed in the results. Differences in characteristics of mechanical response are prevalent throughout the entire test time. Thus the possibility that time dependent change in the material condition as a cause for the above described split strain behavior is eliminated.

As mentioned in Chapter 4, testing is conducted to characterize dehydration in terms of visual signs that can be confused with visible mechanical damage within the fibril constituents of the fascicle. The results confirm that visual signs of dehydration never arise before four minutes of exposure. While this does not imply that the mechanical properties of the collagen fiber are immune to dehydration where visual signs are not apparent, the effect has already been eliminated as a possibility.

### **7.3 Variation of Instantaneous Strain Rate**

Once the threat of a time dependent effect is eliminated, the remaining possibility is the change of material properties through addition of strain energy. Since this is assumed to be the case, the next step in investigating the causes of the observed split strain behavior is to specify

the exact per cycle parameters that also have a strong correlation to change in frequency of load cycling. Since the strain response is a harmonic function, it can be described by amplitude and frequency alone. Frequency is a controlled parameter and so requires no further analysis. Figure 7.4 shows average observed strain amplitude at each frequency of load variation:

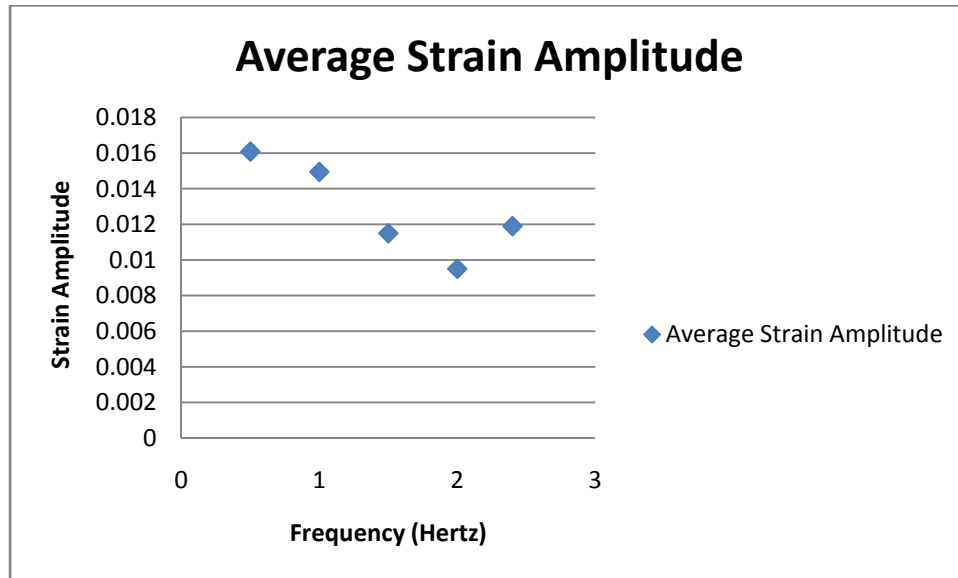


**Figure 7.4:** Observed average strain amplitude plotted against frequency

A strong relationship is not observed from the results. The variation among amplitude is relatively small and further is seen to increase at 2.4 hertz thus breaking the trend of the other four frequency points. No useful result is found in the analysis of frequency and amplitude alone. However, the two parameters are interrelated in that where amplitude is unchanged, increase in frequency results in increased time rate of change of the function or in the case of this work, increase in instantaneous strain rate (steeper slope between peaks) and decrease in the period of time per cycle where strain rate is very low (smaller area near peaks where intermolecular movement is minimal). In an effort to establish the instantaneous strain rate as a viable parameter varying in frequency, Figure 7.5 is presented showing peak strain rate per cycle verse frequency where peak strain rate is given by angular velocity multiplied by amplitude.

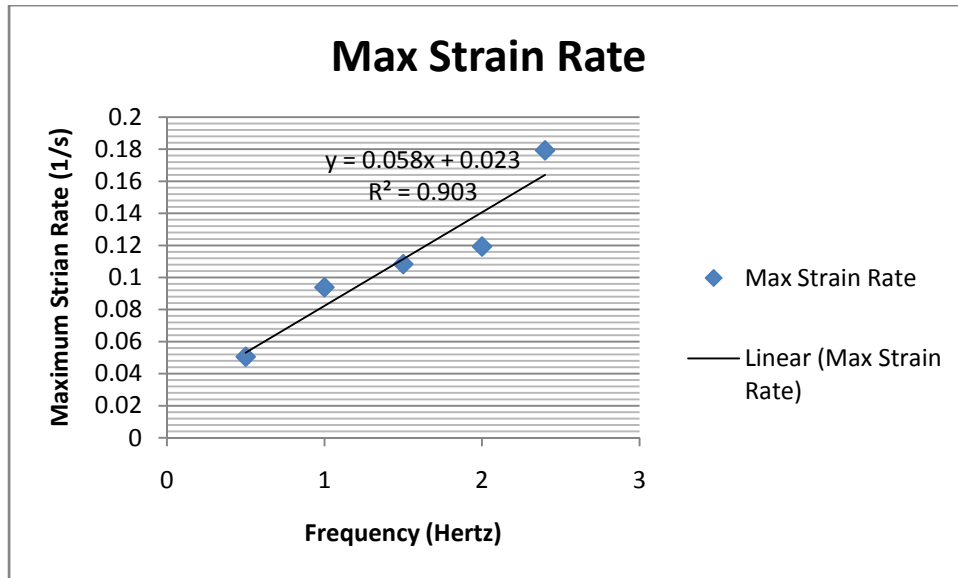


**Figure 7.5:** Maximum observed instantaneous strain rate verse frequency

A strong linear relationship can be observed in this plot. Concepts to take from this analysis are: at higher frequencies relative intermolecular movement occurs at a higher velocity and most importantly, that the period of time per cycle decreases where intermolecular movement is at a minimum in terms of velocity. These ideas will form the basis of the mechanistic model to be proposed subsequently in this work.

## 7.4 Modulus Trends Corresponding to Split Strain Behavior

To further aid in the development of a valid mechanistic model, detailed analysis of the trends in the behavior of the fiber's modulus during purely linear and higher order behavior is carried out. In this analysis, only the 1.0 hertz loading frequency will be scrutinized because of the consistency of the overall results observed in this test series and the best possible number of samples of each type of behavior (7 to 3; linear to higher order) given the results of all data sets. Graphical transient modulus data for two test runs showing higher order behavior are given in

Figure 7.6 for two randomly chosen test runs and in Figure 7.7 for two randomly chosen tests showing linear behavior.

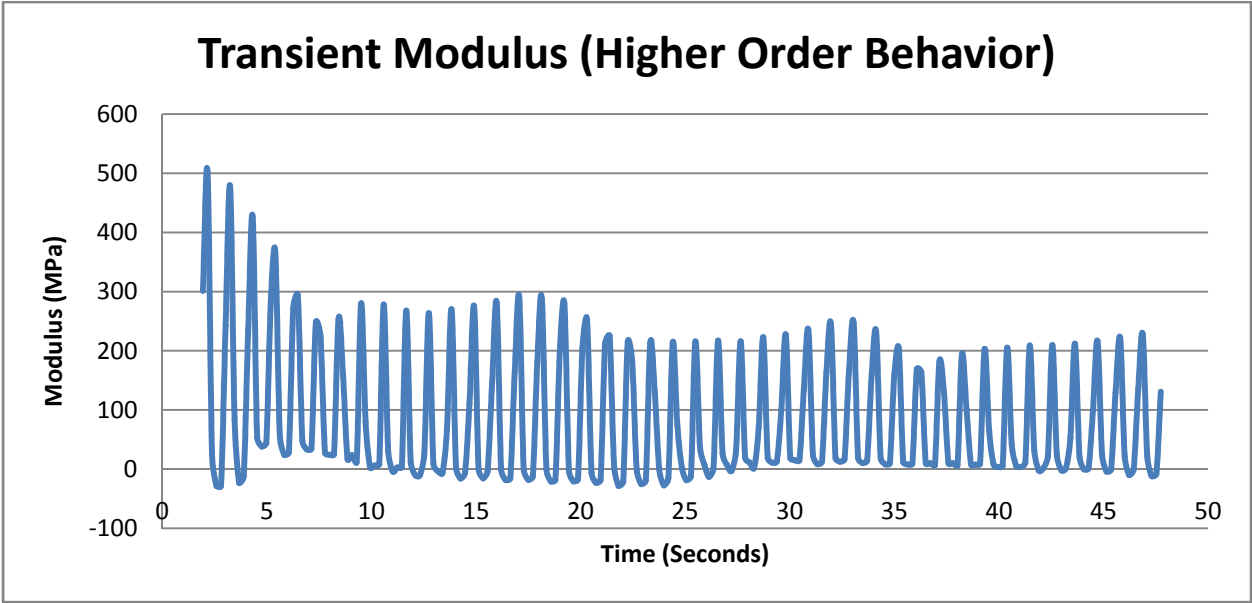
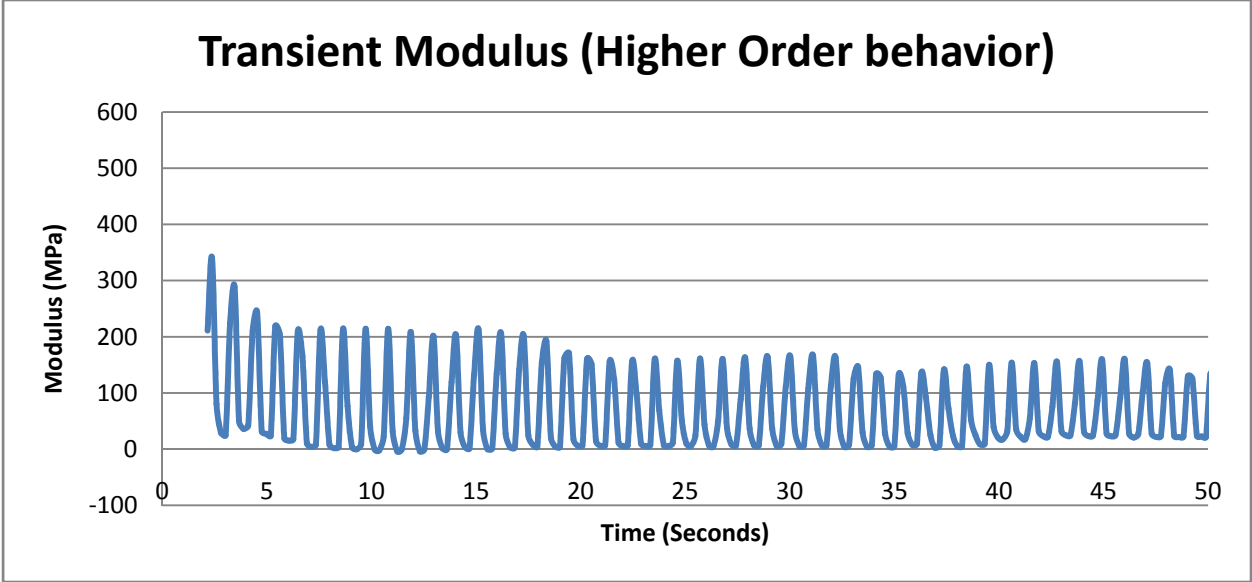


**Figure 7.6:** Graphs showing modulus trend during higher order behavior at 1.0 hertz

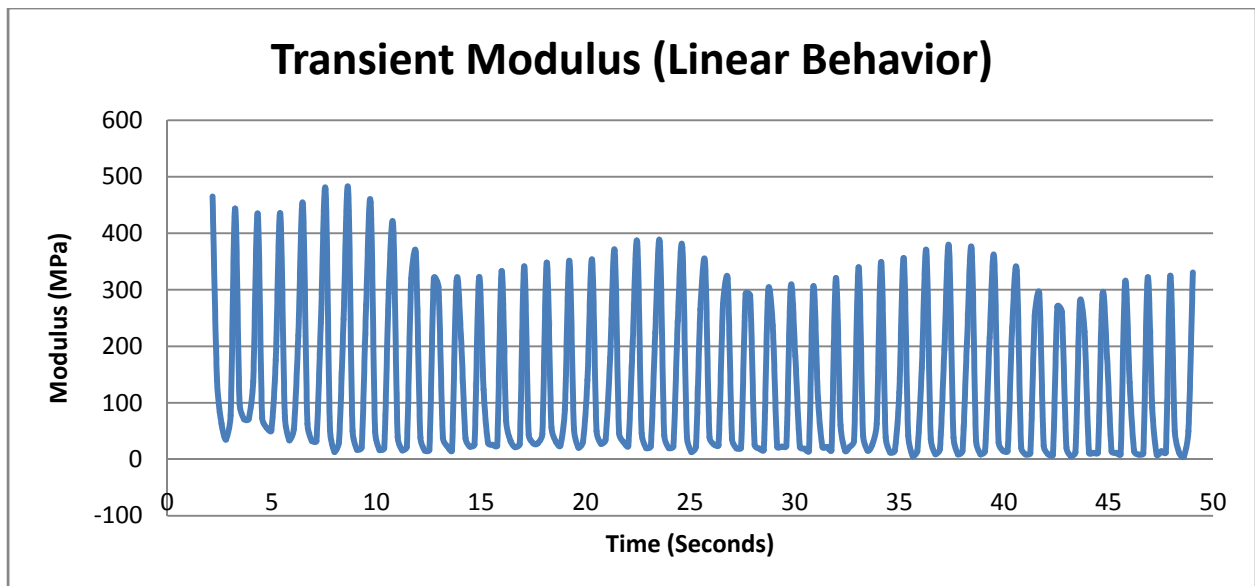
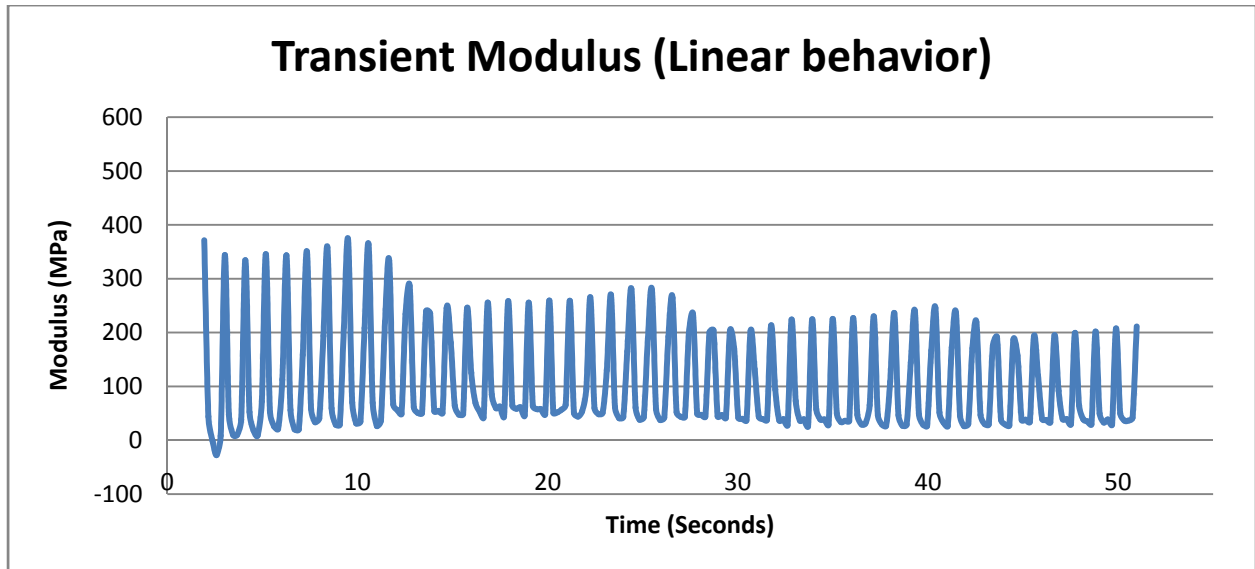


**Figure 7.7:** Graphs showing modulus trend during linear behavior at 1.0 hertz

The main distinction between the modulus behavior in the higher order situation and the modulus behavior in the linear situation is observed in the first 5-10 cycles. Here, it is clearly observed that where higher order behavior was observed, the modulus sharply decreases in each of the first 4 cycles and then more slowly reaches a stable value. In tests where linear behavior is observed, the fiber's modulus is far more stable from the first loading cycle through the entire test.

## 7.5 Discussion of Mechanistic Model

Several important points must be explicitly stated from the experimental observations in order to effectively propose a mechanistic model for the observed behaviors. First, the dual behaviors are completely distinct. Strain graphs as a function of time follow either a clearly curved trend or a completely linear trend (no trend with any degree of curvature is considered linear).

Further, linear behavior dominates the observed results at lower frequencies and curved or higher order behavior is predominantly found at higher frequencies. To this end, complete dominance of neither type of behavior at any frequency is seen. That is, for any series of 10 tests at the same frequency at least one test result shows a behavior that is different from the rest.

To differentiate the behaviors in terms of viscoelasticity and strain energy, the linear strain behavior corresponds to uniform hysteric energy dissipation per cycle that does not vary significantly over the course of a test run or between subsequent cycles. This is evidenced by consistent vertical distances between peaks of the strain verse time plots. Higher order behavior implies that hysteric energy dissipation per cycle lessens over the series of load cycles since the vertical distance between peaks in the strain verse time plot tend toward zero from an initial non-zero value. Transient elastic modulus is observed to decrease uniformly over the duration of a test run that shows a linear strain trend, but transient elastic modulus rapidly decreases before stabilizing during tests that display higher order strain behavior.

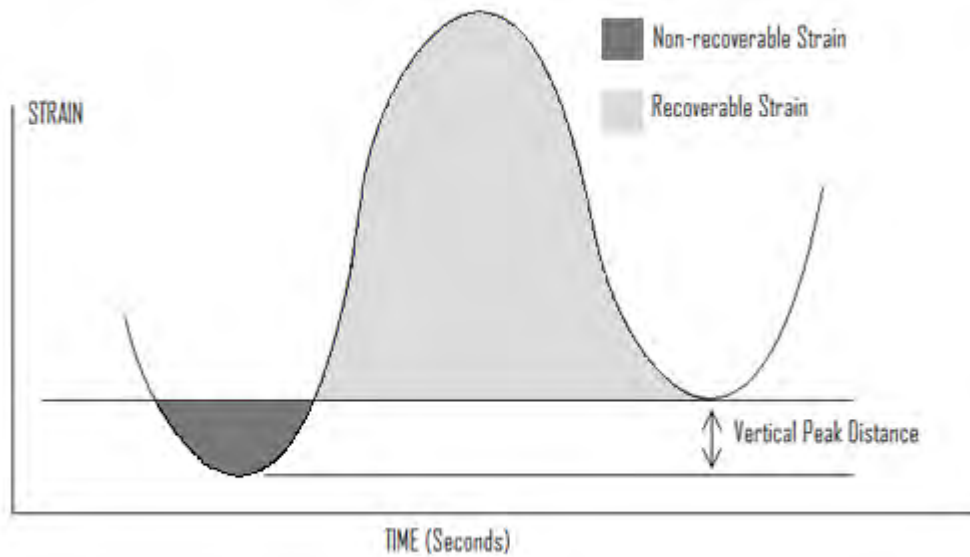


**Figure 7.8:** Dissipated and recoverable portion of strain cycles

Finally, the only non-controlled strain function parameter that shows strong frequency dependence is the maximum instantaneous strain rate measured for the fiber. Note that increased maximum instantaneous strain rate corresponds to higher velocity of sliding between molecules or aligned molecular chains during deformation and decreasing period of minimal relative velocity of adjacent molecules corresponding to the region of the strain peaks and valleys where the strain state of the fiber is not changing rapidly. With this evidence, a detailed mechanistic analysis resulting in the proposal of a suitable deformation mechanism under these conditions can be effectively carried out.

It is hypothesized that hysteric dissipation of strain energy, represented by “non-recoverable strain” in Figure 7.8, is directly related to the number of transverse molecular cross-links broken during the stretching and recovery phases of each loading cycle. Relative movement or sliding of adjacent molecular chains in the load direction during extension and retraction of the repeating molecular structure must be responsible for the destruction of transverse bonds such as cross-links. Therefore, strain that results from the breaking of cross-links is equal to the vertical distance between the strain versus time peaks of subsequent cycles, and strain controlled by stretching of the repeating molecular structure is equal to the recoverable

overlapping vertical distance between subsequent cycles. Further, the ratio of the area of the non-overlapping section of the cycle to the area of the overlapping section presumably gives a measure of the coefficient of restitution for the mechanical process witnessed in that cycle. Figure 7.9 illustrates the 4 phases that occur per cycle during linear behavior:

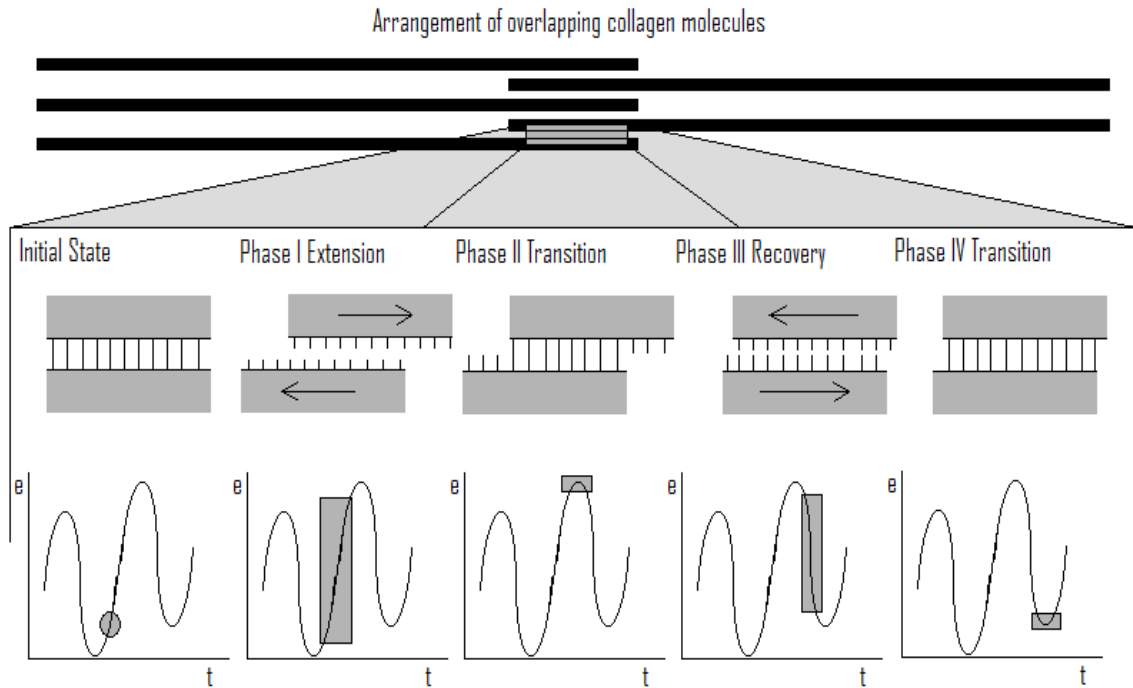


**Figure 7.9:** Mechanistic model cycle for linear behavior

Note that all cross-links are reformed during Phase II and Phase IV, but a residual strain is left in Phase IV since the fiber cannot recover its original position due to a third deformation mechanism related to the friction inherent in the sliding motion. Figure 7.10 relates the same mechanism to higher order behavior:

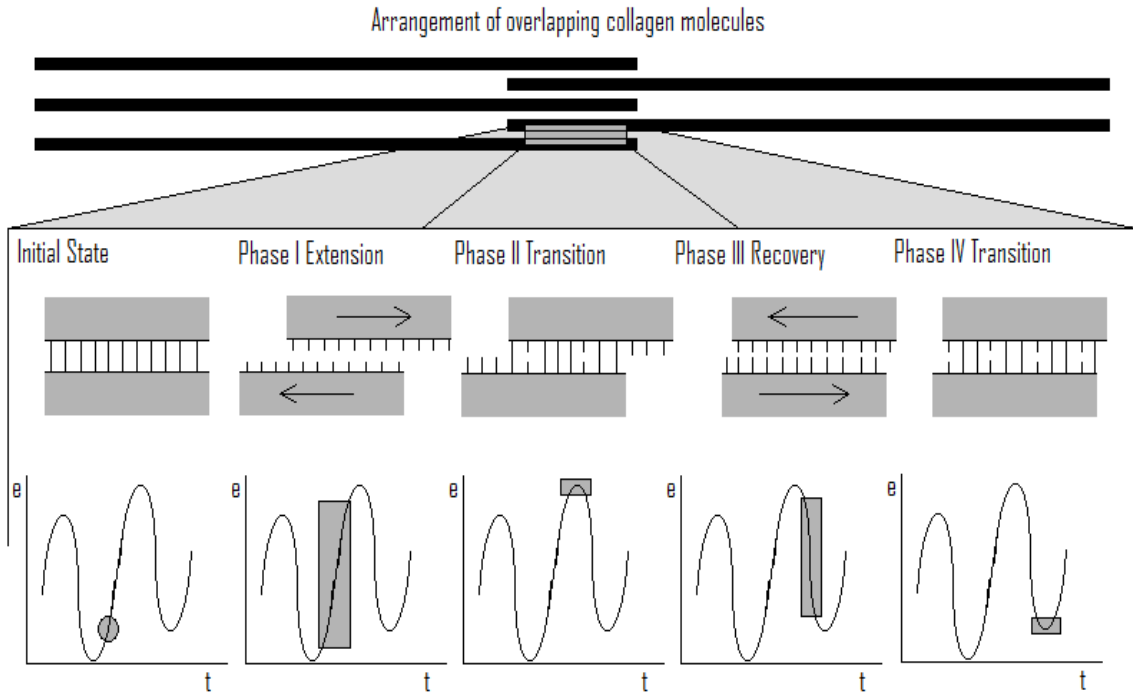


**Figure 7.10:** Mechanistic model cycle for higher order behavior

In the higher order cycle, not all cross-links are reformed in Phase I and Phase II. This occurs because the actual time periods of Phase II and Phase IV are shorter at higher frequencies.

Assuming that approximately the same number or percentage of cross-links is broken for the same amount of strain and same initial cross-link density in the fiber regardless of instantaneous strain rate, a certain amount of time is needed at a minimum instantaneous strain rate to reconstruct the cross-links to the same density. This assumes that the reconstruction of transverse cross-links is a dynamic chemical process that occurs according to some non-zero time constant described conceptually in Figure 7.11. This behavior would result in fewer cross links reforming per cycle at higher load variation frequency where the time at low relative molecular chain velocity per cycle is short.

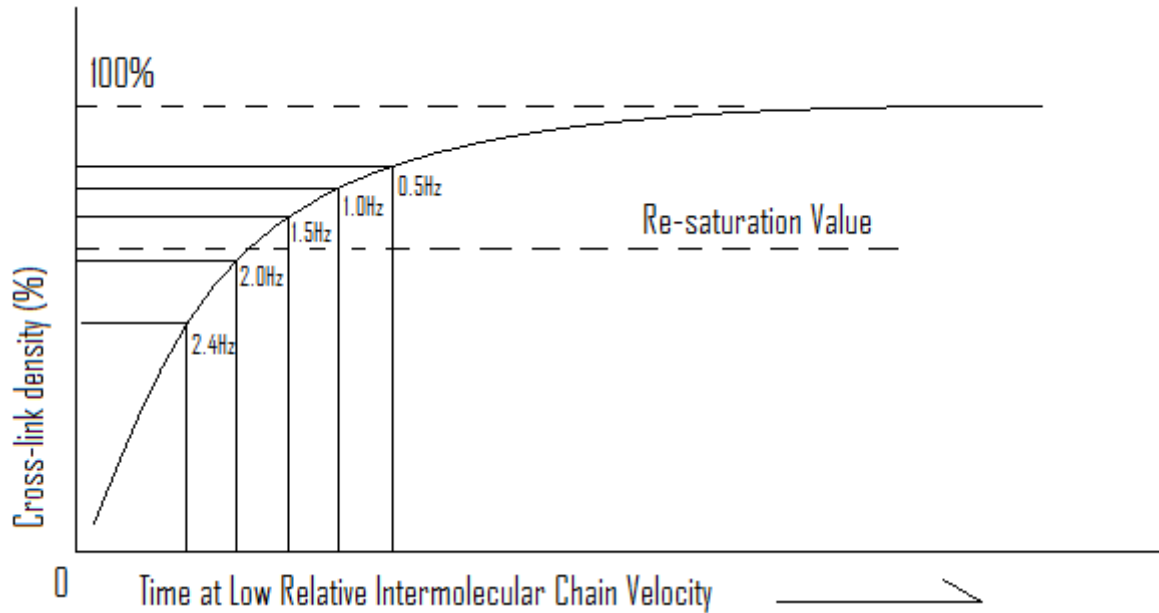


**Figure 7.11:** Assumed behavior of dynamic cross-link reestablishment

It can be inferred therefore that some critical frequency exists in the range studied where re-saturation of cross-links does not occur for that frequency and all higher frequencies. According to this model, inability to re-saturate results in decrease of cross-link density per loading cycle following radioactive type decay evidenced in the rapid loss of transient modulus followed by stabilization shown in tests which display higher order strain behavior.

The overall result is that after each cycle, the collagen fiber has a lower cross-link density tending toward a steady-state condition (an equal number of cross-links are broken and reestablished per cycle). As deformation by cross-link breakage diminishes, the mechanism of deformation by stretching of the repeating molecular structure takes over exhibiting a lower modulus, but also a lower energy loss per cycle. For lower loading frequencies, where the intermolecular chain sliding velocity is sufficiently slow for a sufficient period of time to reestablish full cross-link density, the linear strain verse time trend is observed. In this case, the same number or percentage of cross-links is broken for otherwise equivalent loading cycles. That is, the same number of cross-links is reconstructed, although they are now in more distant locations, during the period of minimal intermolecular chain movement. Finally, the same number of cross-links is broken in the inter-peak phases during the next cycle.

Since the breaking of a cross-link is a highly hysteric mechanism of deformation, the breaking of the same number of cross-links per cycle results in the same energy dissipation per cycle and manifests as uniform vertical distances between the peaks of the strain-time plot. It is also predicted that cross-links are broken during the recovery phase of the fiber because the only requirement for the destruction of cross-links is relative movement or sliding of adjacent molecular chains. The cross-links broken during recovery have the opportunity to reestablish during the low intermolecular velocity transition to the next stretching phase. This double effect is evidenced by the rapid loss of modulus, within the first 5 cycles, observed for higher order strain trends. This validates the proposed model, since many earlier studies conclude that high cross-link density lends to higher fiber modulus [9, 12, 13, 26, 34, 39, 44].

## 7.6 Loss Angle; Loss Tangent; and Dynamic Modulus

Loss angle and loss tangent will be presented for 0.5 and 1.0 hertz test frequencies since they are standard parameters reported for dynamic materials testing. Only low frequencies are used for this analysis since peak to peak distance is the critical parameter to be measured and peak to peak results for higher frequencies are unreliable due to the relatively slow scan rate of data acquisition. Figure 7.12 shows loss angle distribution and loss tangent distribution against the area distribution of samples for both frequencies.

Values were also calculated per frequency. Average loss angle at 0.5 hertz is: 0.303 +/-0.112 radians. Average loss tangent is: 0.316 +/-0.118 (dimensionless). For 1.0 hertz, average loss angle is: 0.905 +/-0.061 radians, and an average loss tangent of: 1.28 +/-0.160 (dimensionless) is calculated.

An example of a material characterization graph used to visually assess the phase shift between input and output signals used in calculation of loss angle and loss tangent is shown in Figure 7.13. Dynamic modulus corresponds directly to the loss tangent as a ratio where:

$$\frac{E''}{E'} = \tan \delta.$$

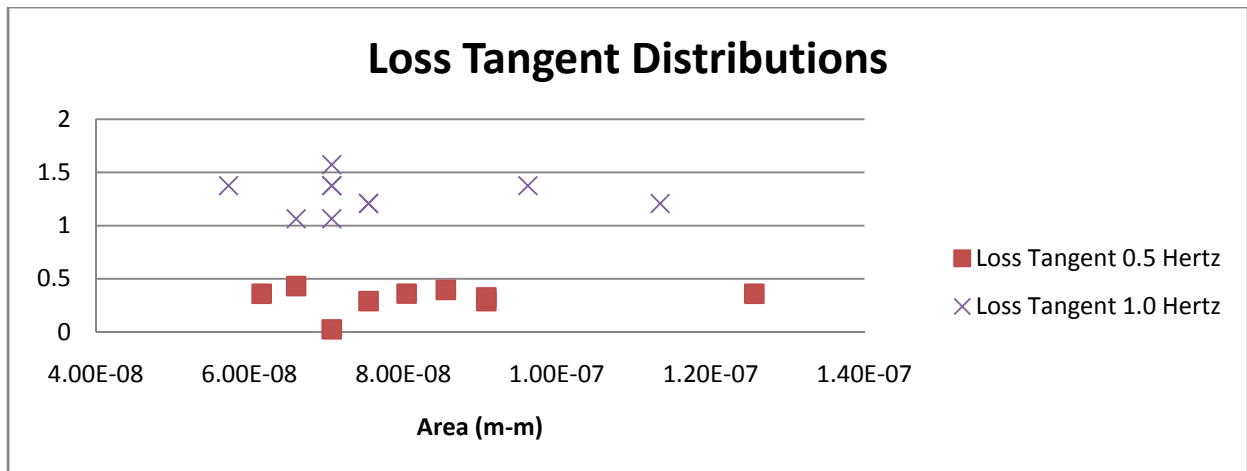
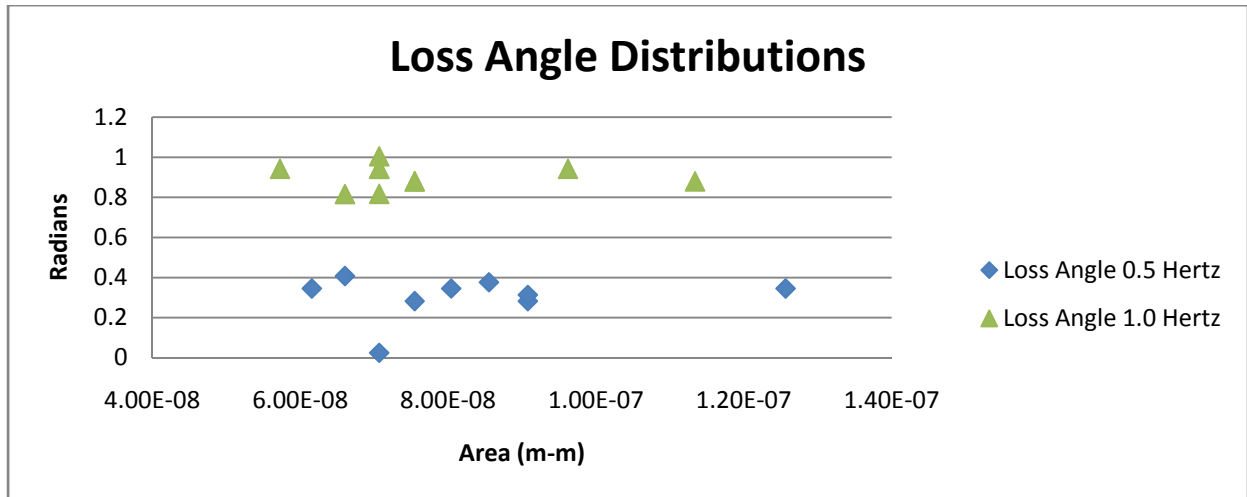


**Figure 7.12:** Distributions of loss angle and loss tangent against sample area

Loss tangent results show no dependence on fiber area, although, as expected they do show strong frequency dependence. Frequency dependency in terms of loss tangent is no more than a dynamic effect, and is not a result of change of material properties induced by change of frequency. These results serve best to bolster the validity of the testing as data scatter is low and frequency dependence is definitively demonstrated as should be expected. Further, the values agree reasonably with those reported in other research on different collagenous structures and by different testing methods (loss tangent 0.3 at 0.5 Hz) [64]. No previous research by reasonably similar methods to those presented here was found in the literature review.

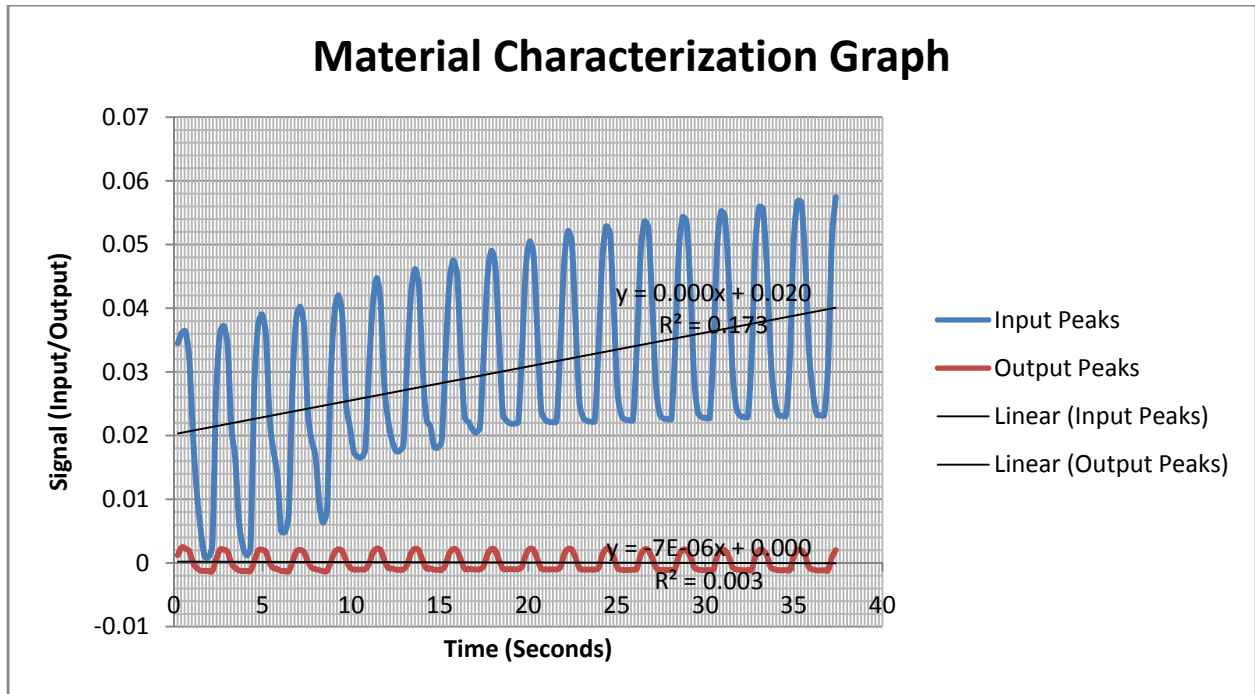


**Figure 7.13:** Example material characterization graph at 0.5 hertz loading frequency

The material characterization graph in Figure 7.13 is used for the peak to peak analysis which yields the phase shift time value from which loss angle, loss tangent and dynamic modulus are determined. Output signals are actually the calculated strain and input signals are load cell voltage. These particular values are used because they are similar in scale which helps to reduce error in the necessary visual interpretation. Individual graphs correspond to individual test runs and are expanded for more accurate visual analysis. Various peak to peak relationships are considered for each graph and values are subsequently averaged to enhance the statistical validity of the presented results.

## 7.7 Proposed Models and Correlation of Solutions

Due to the observation of two distinct time dependent strain behaviors, two mathematical models are proposed. The first model attempts to characterize the action of the fiber showing ideal viscoelastic mechanics in that the increase of strain is linear through the course of a test. An exponential model is used to approximate the non-linear strain per time behavior observed in several tests especially at higher loading frequencies. Again, the cause of the disparity between the two distinct phenomena is not completely clear at the present time.

The nature of the ideal viscoelastic results calls for computational models based on a sinusoidal function added to a linear function equal to the linear regression of the average test run strain output graph according to Equation 7.2:

$$\epsilon(t_1) = A \sin 2\pi f t_1 + a_1 t_1 + a_0$$

**Equation 7.2:** Computational strain template for linearly progressive behavior

Where: A = average amplitude of strain signal for all test frequencies; f = loading frequency;  $t_1$  = time shifted to match output frequency;  $a_1$  = the average slope of the linear regressions of all test frequencies; and  $a_0$  = the average vertical intercept of the linear regressions of all test frequencies, this value is very close to the strain amplitude plus a small strain caused by preloading of the fiber as should be expected. The final proposed linear computational model is given by Equation 7.3:

$$\epsilon(t_1) = 0.0128F_{max} \sin 2\pi f t_1 + 0.007t_1 + 0.019$$

**Equation 7.3:** Proposed computational strain model for linearly progressive behavior

Close correlation to experimental results is shown in graphical results. For example the general model solution for 1.5 hertz in Figure 7.14 is very similar to Figure 7.2 which shows a linear strain signal measured during a test run at the same frequency.

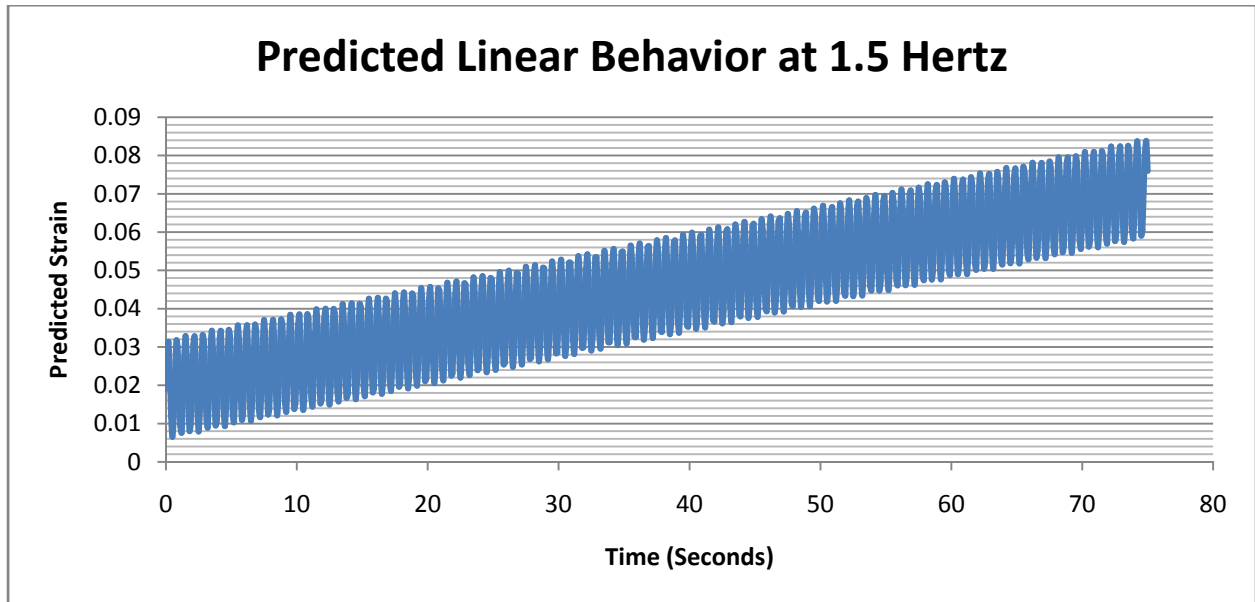


**Figure 7.14:** Predicted linear behavior at 1.5 hertz loading frequency

A similar model is proposed to represent the cases of higher order strain behavior, where an exponential function and associated parameters are substituted for the linear function according to Equation 7.4:

$$\epsilon(t_1) = A \sin 2\pi f t_1 + b_0 \left( 1 - e^{-\frac{t}{b_1}} \right) + b_3$$

**Equation 7.4:** Computational strain template for exponentially progressive behavior

The parameters of the sinusoidal function are the same and  $b_3$  provides a vertical shift of the function, but  $b_0$  and  $b_1$  are exponential parameters determined by extrapolation and averaging, gives the mathematical model for the observed exponential type strain behavior. The final proposed exponential computational model is shown in Equation 7.5:

$$\epsilon(t_1) = 0.01F_{max} \sin 2\pi f t_1 + 0.07 \left( 1 - e^{-\frac{t}{30}} \right) + 0.018$$

**Equation 7.5:** Proposed computational strain model for exponentially progressive behavior

Again, the computational model solution is presented at 1.5 hertz in Figure 7.15 for comparison with example experimental results in Figure 7.3.

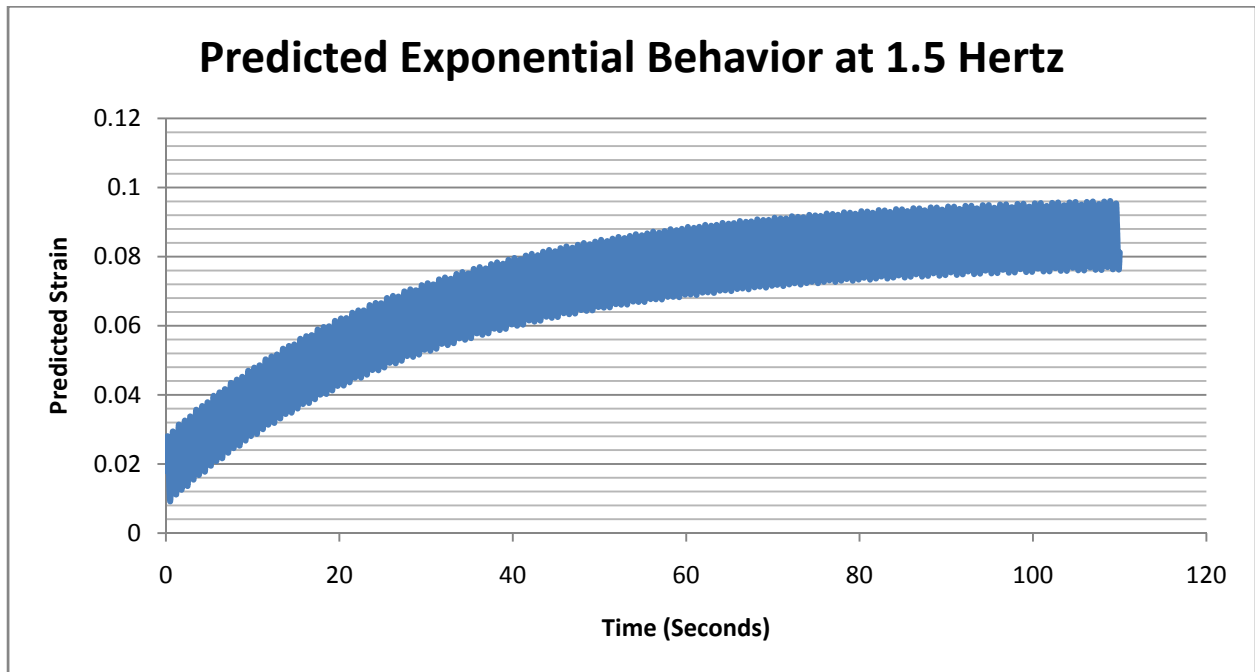


**Figure 7.15:** Predicted exponential behavior at 1.5 hertz loading frequency

## 7.8 Quasi-physical Model

A quasi-physical model including an ideal spring and a hysteric type damper is proposed for characterization of typical collagen fascicle. The best correlation to experimental strain verse time results is seen in a parallel (Kelvin-Voight) arrangement of the spring and damper. Energy methods are used to determine the model solution where input energy is given by Equation 7.6:

$$dE_{input} = F(t)d\epsilon$$

**Equation 7.6:** Kelvin-Voight input energy calculation

Where:  $F(t)$  is the loading function and  $d\epsilon$  is the differential strain element. The output energy equation is then given by Equation 7.7:

$$dE_{output} = \frac{1}{2}K(d\epsilon)^2 + \frac{C_1}{C_2}\omega$$

**Equation 7.7:** Kelvin-Voight output energy calculation

Where:  $K$  is the ideal spring coefficient;  $C_1$  and  $C_2$  are the split damping coefficients which can be expressed as a ratio and act proportionally to angular velocity ( $\omega$ ). Note that when analyzing by energy methods, the differential strain elements are assumed to be equal, thus implying use of the parallel arrangement. Input and output energy formulations can be equated under conservation of energy resulting in the following equation (Equation 7.8):

$$F(t)d\epsilon = \frac{1}{2}K(d\epsilon)^2 + \frac{C_1}{C_2}\omega$$

**Equation 7.8:** Final energy analysis equation for Kelvin-Voight model with hysteric damping

Values of K, and  $C_1 / C_2$  are determined by interpolation, although  $C_1 / C_2$  may be inferred from the loss modulus and storage modulus or the loss tangent. The values of the above parameters are interpolated to be: K = 800 Newtons per meter and  $C_1 / C_2 = 3 \times 10^{-6}$ . Note that in application, an initial sample length must be assumed, for instance, the plot in Figure 7.16 shows a theoretical curve for an initial sample length of 50 millimeters. The strain solution is plotted for loading at 1.5 hertz for comparison to Figure 7.2.

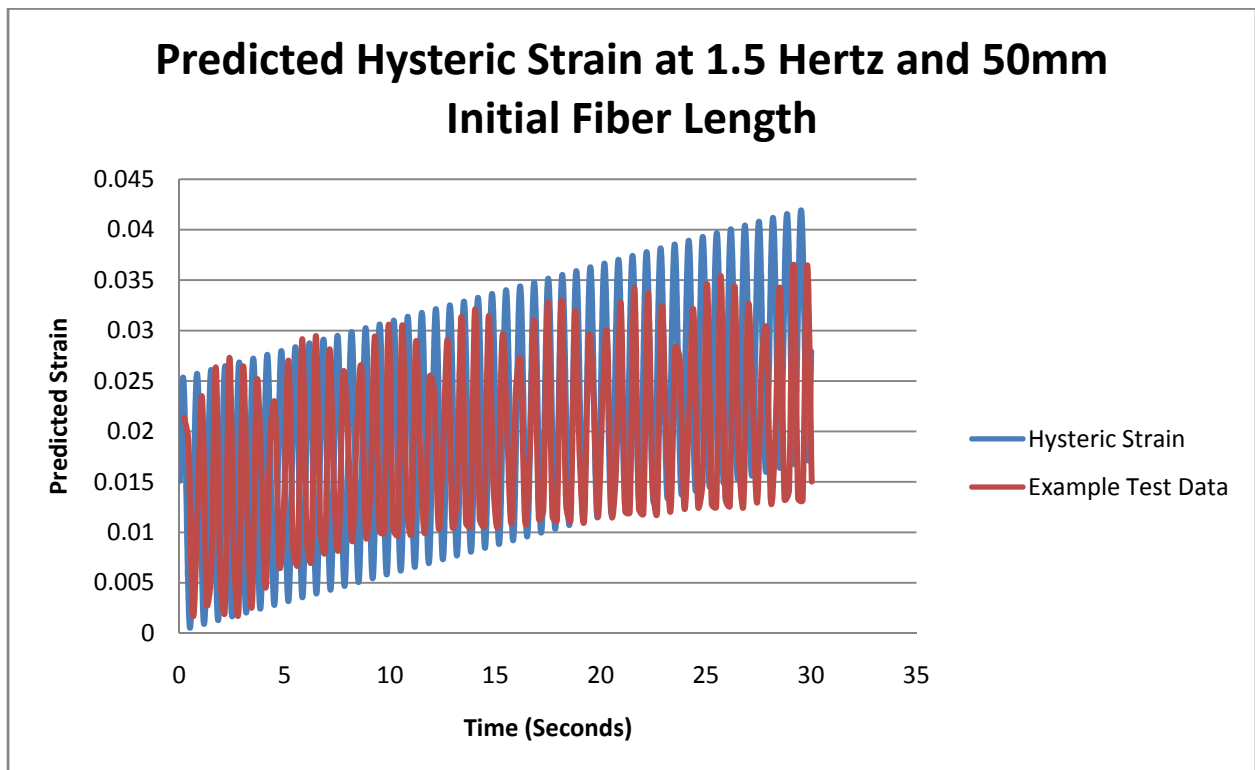


**Figure 7.16:** Strain behavior predicted by Kelvin-Voight model with hysteric damping

\*An example of actual test results is overlaid for comparison

Both computational models and quasi-physical models are successfully applied to characterize the behavior of the collagen fascicle. Referring to Appendix A, model solutions can be compared to the full range of empirically obtained strain data. It is readily seen that all models correlate well to the observed results.

## **Chapter 8**

### **Conclusions and Continuation of Work**

#### **8.1 Overview**

Given the large amount of data analyzed, the various points of view of analysis and the number of phenomena successfully modeled, many conclusions can be drawn for various aspects of this work. Results obtained for impulse to failure can be applied to the training of athletes in a universal sense, although much work must still be completed to properly orient and refine the information presented in this work. Further, the volume of results analyzed under the principals of dynamic mechanical testing of viscoelastic materials yields highly reliable models for predicting the behavior of collagen in any number of other applications. The characterization of collagen as a viscoelastic material in this work adds significantly to the emerging area of dynamic testing of biomaterials.

#### **8.2 Conclusions in Results**

Analysis of the initial result set leads to the definitive conclusion that the durability with respect to impulse of the typical collagen fascicle under dynamic loading increases as the frequency of the applied loading cycle increases. Evidence taken from further analysis involving the observed viscoelastic and advanced results points to the hypothesis that the increased durability may be the result of shift to a strictly axial molecular mechanism of deformation induced by higher instantaneous strain rates eliminating the fiber's ability to reconstruct cross-links during tension cycling. This hypothesis is supported by the higher order strain behavior which is observed to occur predominantly at higher loading frequencies. Both linear and second order polynomial curve fits are applied to characterize the behavior. The characteristic equations are given by Equations 6.1 and 6.2 and can be used to infer practical relations outside of the

laboratory. In all cases, the conclusion drawn for these results is clearly definitive, and further work as described in Chapter 5 can now be undertaken to realize the full intention with which this project originated.

### **8.3 Conclusions in Advanced Results**

Numerous mechanical aspects of Type I collagen are scrutinized in Chapter 7 of this report. Exhaustive strain rate analyses confirm that no definite influence is exerted on the general strain behavior of the sample fiber by frequency change. The most important conclusion that can be drawn is that for otherwise identical overall strain behavior, an increase in frequency dictates an increase in instantaneous strain rates experienced by the fiber, and perhaps more importantly decreases the time period that intermolecular sliding occurs at a minimum velocity. Since the only two independent parameters analyzed showing frequency dependency are fiber durability and instantaneous strain rate, it is highly probable that these properties are interrelated. Non-cyclic durability testing using strain rate as the independent variable is recommended as a future study to more precisely characterize this relationship.

Strain analyses reveal the existence of two distinct types of fiber responses with time. The first, more commonly observed at lower frequencies, demonstrates a uniform linear increase in overall strain corresponding well to behavior displayed by hysterically damped systems. Higher order trend to a stable, no viscous loss, strain state characterizes the second behavior which is found to occur more consistently at higher loading frequencies. It is hypothesized that a consistent degree of cross-link reestablishment is allowed at low load cycle frequencies causing consistent energy dissipation per cycle seen in linear strain-time trends. Conversely, higher instantaneous strain rate and narrow peak width corresponding to small time period of minimal intermolecular velocity associated with higher load cycle frequency reduces the material's ability to reconstruct cross-links. To complete the mechanistic model, it is proposed that deformation by breaking of transverse cross links is more entropic, and dissipates more energy than deformation by elongation of the repeating molecular structure. Since collagen cross-linking is

known to increase the tensile properties of the fiber, the inability to reconstruct cross links causes the fiber to lose modulus very quickly as a series of loading cycles begins.

Results for dynamic modulus and loss tangent serve to standardize observations of this project with values and parameters commonly calculated in dynamic testing. It was found that the loss tangent calculated from the present results corresponds well to values reported in other similar projects (in the region of 0.3 loss tangent for 0.5 hertz load variation frequency) although different methods and collagen structures were utilized.

Computational and quasi-physical models were developed and proposed to characterize the behaviors observed. The best fitting computational model for uniform linear strain behavior is a sinusoid added to a first order linear function given by Equation 7.2. A similar function is proposed for higher order trends where the linear function is replaced by an exponential function subtracted from one. The exponential computational model is given by Equation 7.4. Quasi-physical modeling is often applied to viscoelastic materials. For the results in this work, a parallel arrangement Kelvin-Voight model with an ideal spring and hysteric damper is proposed. The model is solved using energy analysis and characteristic coefficients are interpolated with results displayed in Figure 7.16.

## **8.4 Future Collagen Testing**

A large number of variations to the testing presented in this work can be developed based on the apparatus that has been constructed. Some examples to be considered are given, but many more are possible. Testing of ultimate strength can be undertaken with various modifications to standard quasi-static testing. For instance, an initial function can be applied to the fiber followed by a quasi-static ultimate strength test. High speed non-cyclic dynamic testing is also possible to the point of fibril damage or ultimate fascicle failure. More extreme loading frequencies may be tested helping to further validate the viscoelastic characterization presented here.

## **8.5 Testing of Fibers in General**

Many other thin fibers whether biological or otherwise can be tested with this equipment. Applications in continuous fiber composites are obvious possibilities. The main limiting factor is the ability of the linear motor to produce a detectable strain in the fiber, and therefore, high modulus fibers, such as carbon fiber, may not be candidates for testing with this equipment.

Other biological structures of similar form and dimension to the collagen fascicle can also be tested since the machine is designed to operate in in-vitro type conditions. Some possibilities include, but are not limited to: blood vessels, ligament, skin etc. Perhaps with some modification, testing of the mechanical properties of neural tissue may even be possible.

## References

- [1] Shigley, J., Mischke, C., Budynas, R., *Mechanical Engineering Design Seventh Edition*, McGraw Hill, New York, 2003.
- [2] ASTM D4762-08 “Standard Guide for Testing Polymer Matrix Composite Materials,” ASTM International, West Conshohocken, PA, 2008, DOI: 10.1520/D4762-08.
- [3] Fung, Y.C., *Biomechanics: Mechanical Properties of Living Tissues*, Springer, San Diego, 1993.
- [4] Lin, H.C., Chang, J. H., Jain Sandeep, G., Eric E., Kure, T., Kato, T., Fukai, N., Azar, D. T., “Matrilysin Cleavage of Corneal Collagen Type XVIII NC1 Domain and Generation of a 28-kDa Fragment,” *Investigative Ophthalmology and Visual Science*, Vol. 42.11, 2001, pp. 2517-2524.
- [5] Lavagnino, M., Arnoczky, S. P., Egerbacher, M., Gardner, K. L., Burns, M. E., “Isolated Fibrillar Damage in Tendons Stimulates Local Collagenase mRNA Expression and Protein Synthesis” Michigan State University, 2005.
- [6] Kenakin, T. P., *A Pharmacology Primer Second Edition*, Academic Press, Burlington, 2006.
- [7] Castellani, P.P., Morocutti, M., Franchi, M. Ruggeri, M., Bigi, A., Roveri, N., “Arrangement of Microfibrils in Collagen Fibrils of Tendons in the Rat Tail,” *Cell and Tissue Research*, Vol. 234.3, 1983, pp. 735-743.
- [8] Goodsell, D. S., “Molecule of the Month,” Protein Data Bank, April, 2000.
- [9] Buehler, M. J., Wong, S. Y., “Entropic Elasticity Controls Nanomechanics of Single Tropocollagen Molecules,” *Biophysical Journal*, Vol. 93.1, 2007, pp. 37-43.
- [10] Freeman, J. W., “Collagen Molecular Modeling Type I Collagen,” Musculoskeletal Tissue Regeneration Laboratory, Virginia Tech University, 2007.
- [11] Kubo, K., Kanehisa, H., Kawakami, Y., Fukunaga, T., “Influence of Static Stretching on Viscoelastic Properties of Human Tendon Structures in vivo,” *Journal of Applied Physiology*, Vol. 90.2, 2001, pp. 520-527.

- [12] Siegel, R.C., "Collagen Cross-linking Synthesis of Collagen Cross-links in vitro with Highly Purified Lysyl Oxidase," *Journal of Biological Chemistry*, Vol. 251.18, 1976, pp. 5786-5792.
- [13] Jørgensen, P. H., Oxlund, H., "Growth hormone increases the biomechanical strength and collagen deposition rate during the early phase of skin wound healing," *Wound Repair and Regeneration*, Vol. 4.1, 2002, pp. 40-47.
- [14] Shen, Z. L., Dodge, M. R., Kahn, H., Ballarini, R., Eppell, S. J., "Stress Strain Experiments on Individual Collagen Fibrils," *The Biophysical Society*, Vol. 95.8, 2008, 3956-1963.
- [15] Gutschmann, T., Hassenkam, T., Cutroni, J. A., Hansma, P. K., "Sacrificial Bonds in Polymer Brushes from Rat Tail Tendon Functioning as Nanoscale Velcro" University of California, 2005.
- [16] Eriksen H., A., Sharp, C. A., Robins, S. P., Sassia, M.L., Ristelia, L., Risteliad, J., "Differently Cross-linked and Uncross-linked Carboxy-terminal Telopeptides of Type I Collagen in Human Mineralised Bone," *Bone*, Vol. 34.4, 2004, pp. 720-727.
- [17] Kantor, L., Hsrding, H. P., Ron, D., Schiffmann, R., Aneski, C. R., Kimball, S. R., Elroy-Stein, O., "Heightened Stress Response in Primary Fibroblasts Expressing Mutant eIF2B Genes from CACH/VWM Leukodystrophy Patients," *Human Genetics*, Vol. 118.1, 2005, pp. 99-106.
- [18] ASTM F2212-08e1 "Standard Guide for Characterization of Type I Collagen as Starting Material for Surgical Implants and Substrates for Tissue Engineered Medical Products," ASTM International, West Conshohocken, PA, 2008, DOI: 10.1520/F2212-08E01.
- [19] Lodish, Berk, Zipursky, Matsudaira, Baltimore, Darnell, *Molecular Cell Biology*, W H Freeman, 2000.
- [20] Kastelic, J., Galeski, A., Baer, E., "The Multicomposite Structure of Tendon," *Connective Tissue*, Vol. 6, 1978, pp. 11-23.
- [21] Riley, G., "Molecular Composition of Tendon Extracellular Matrix," *Expert Reviews in Molecular Medicine*, Vol. 7.5, 2005.
- [22] Crago, P. E., Houk, J. C., Rymer, W. Z., "Influence of Motor Unit Recruitment on Tendon Organ Discharge," *Neuroscience Abstracts*, 1, 1975, p. 280.

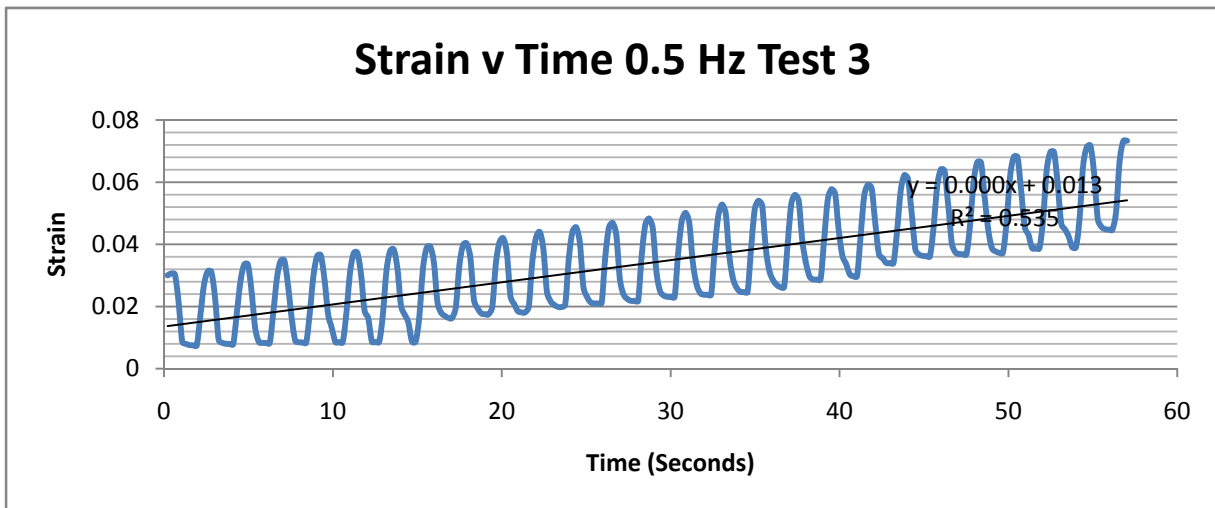
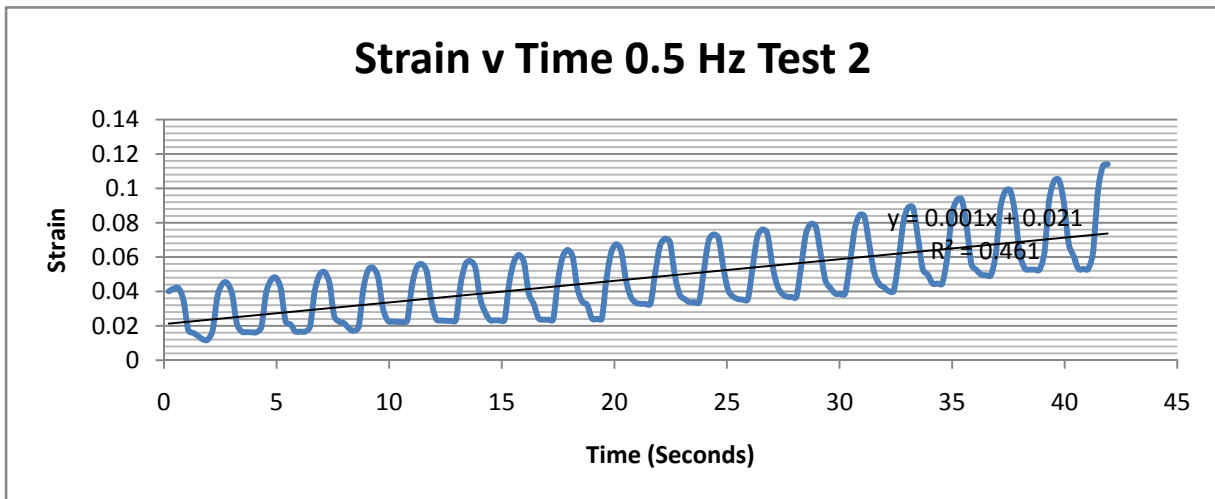
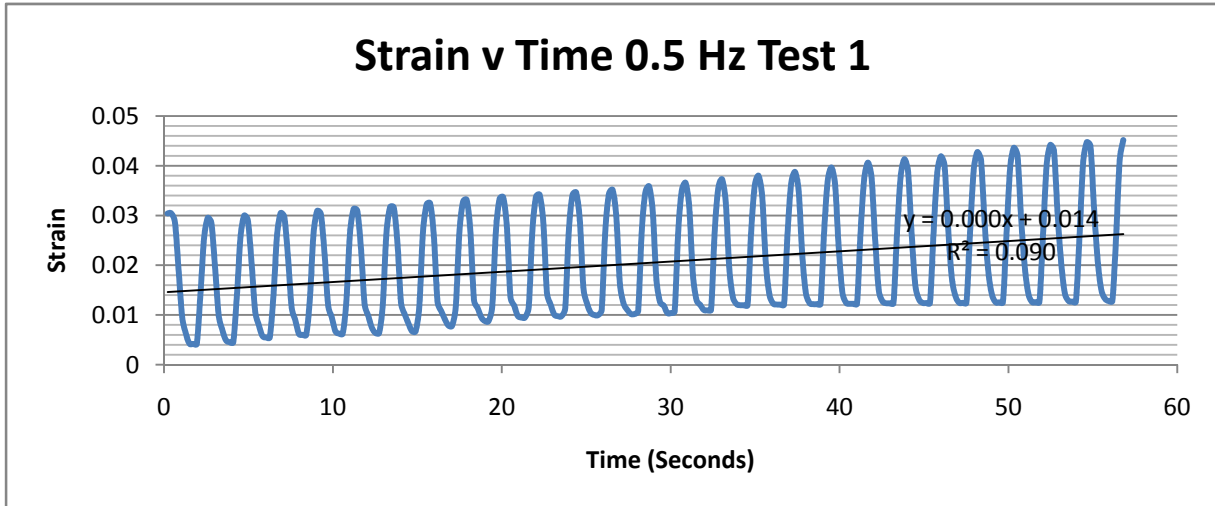
- [23] Stvrtnova, V., Jakubovsky, J., Hulin, I., *Pathophysiology Principles of Disease*, Academic Press, Burlington, 1995.
- [24] Hirano, Y., Fukunaga, T., Muramatsu, T., Murakoa, T., Takeshita, D., Kawakami, Y., “Mechanical Properties of Tendon and Aponeurosis of human Gastrocnemius Muscle in vivo,” *Journal of Applied Physiology*, Vol. 90, 2001, pp. 1671-1678.
- [25] Lees, S., Heeley, J. D., Ahern, J. M., Oravec, M. G., “Axial Phase Velocity in Rat Tail Tendon Fibers at 100 MHz by Ultrasonic Microscopy” *Ultrasonics Symposium*, 1982, pp. 638-639.
- [26] Brinckerhoff, C. E., Benoit, M. C., Culp, W. J., “Autoregulation of Collagenase Production by a Protein Synthesized and Secreted by Synovial Fibroblasts: Cellular Mechanism for Control of Collagen Degradation,” *PNAS*, Vol. 82.7, 1985, pp. 1916-1920.
- [27] Ray, R., Cabal-Manzano, R., Moser, A. R., Waldman, T., Zipper, L. M., Aigner, A., Byers, S. W., Riegel, A. T., Wellstein, A., “Up-Regulation of Fibroblast Growth Factor-Binding Protein, by  $\beta$ -Catenin during Colon Carcinogenesis,” *Cancer Research*, Vol. 63, 2003, pp. 8085-8089.
- [28] Worthington Biochemical Corporation, “Collagenase,” *Worthington Enzyme Manual*, Lakewood, 2009.
- [29] Lavelle, P., “The Trouble with Anti-inflammatories,” *ABC Health and Wellbeing*, 15 June 2005.
- [30] Couzin, J., “Safety of Anti-inflammatories gets a Closer Look,” *ScienceNOW Daily News*, 14 December 2005.
- [31] Rigby, B. J., Hirai, N., Spikes, J. D., Eyring, H., “The Mechanical Properties of Rat Tail Tendon,” *The Journal of General Physiology*, 1958.
- [32] Cavalcante, F. S. A., Ito, S., Brewer, K., Sakai, H., Alencar, A. M., Almeida, M. P., Andrade Jr., J. S., Majumdar, A., Ingenito, E. P., Suki, B., “Mechanical Interactions between Collagen and Proteoglycans: Implications for the Stability of Lung Tissue,” *Journal of Applied Physiology*, Vol. 98, 2005, pp. 672-679.
- [33] Nagatomi, J., Gloeckner, C., D., Chancellor, M., B., Sacks, M. S., “Passive-state Viscoelastic Properties of Normal vs. Neurogenic Bladder Wall Tissue,” *Summer Bioengineering Conference*, 2003.

- [34] Stella, J. A., Sacks, M. S., "On the Biaxial Mechanical Properties of the Layers of the Aortic Valve Leaflet," *Journal of Biomechanical Engineering*, Vol. 129.5, 2007, pp. 757-767.
- [35] Untaroiu, C., Darvish, K., Crandall, J., Deng, B., Wang, J.T., "Identification of Viscoelastic Properties of Human Medial Colateral Ligament using Finite Element Optimization," ISB 20<sup>th</sup> Conference, 2008.
- [36] Screen, H. R. C., Bader, D. L., Lee, D. A., Shelton, J. C., "Local Strain Measurement within Tendon," *Strain*, Vol. 40.4, 2004, pp. 157-163.
- [37] Kulin, R. M., Jiang, F., Vecchio, K. S., "Aging and Loading Rate Effects on the Mechanical Behavior of Equine Bone," *JOM*, Vol. 60.66, 2008, pp. 39-44.
- [38] Burgin, L. V., Aspden, R. M., "Impact Testing to Determine the Mechanical Properties of Articular Cartilage in Isolation and on Bone," *Journal of Material Science*, Vol. 703.11, 2007, p. 10.
- [39] Kobs, R. W., Muvarak, N. E., Eickhoff, J. C., Chesler, N. C., "Linked Mechanical and Biological Aspects of Remodeling in Mouse Pulmonary Arteries with Hypoxia-induced Hypertension," *American Journal of Physiology*, Vol. 288, 2005, pp. 1209-1217.
- [40] Donnelly, E., Williams, R. M., Downs, S. A., Dickinson, M. E., Baker, S. P., van der Meulen, M. C. H., "Quasistatic and Dynamic Nanomechanical Properties of Cancellous Bone Tissue Relate to Collagen Content and Organization," *Journal of Materials Research*, Vol. 21.8, 2006, pp. 2106-2117.
- [41] Chaudhry B. A. H., Muhamed A, Yost, M, Bull, S, Frankel, D, "Nanoscale Viscoelastic Properties of an Aligned Collagen Scaffold," *Material Science*, Vol. 20.1, 2009, pp. 257-263.
- [42] Wenger, M. P. E., Horton, M. A., Mesquida, P., "Nanoscale Scraping and Dissection of Collagen Fibrils," *Nanotechnology*, Vol. 19, 2008, p. 11.
- [43] Wenger, M. P. E., Bozec, L., Horton, M. A., Mesquida, P., "Mechanical properties of Collagen Fibrils," *Biophysical Journal*, Vol. 93.4, 2007, pp. 1255-1263.
- [44] Blank, R. D. Baldini, T. H., Kaufman, M., Bailey, S., Gupta, R., Yershov, Y., Boskey, A. L., Coppersmith, S. N., Demant, P., Paschalis, E. P., "Spectroscopically Determined Collagen Pyr/deH-DHLNL Cross-Link Ratio and Crystallinity Indices Differ Markedly in Recombinant Congenic Mice with Divergent Calculated Bone Tissue Strength," *Connective Tissue Research*, Vol. 44.3-4, 2003, pp. 134-142.

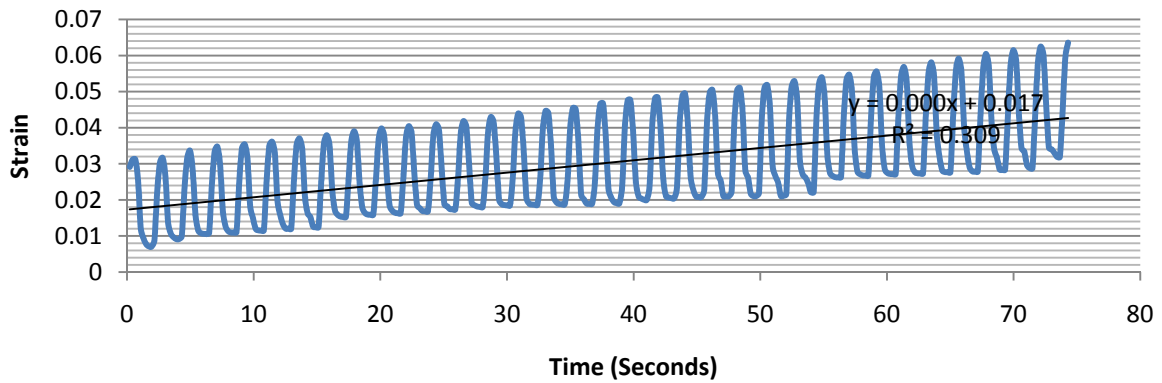
- [45] Cheema, U., Chuol, C.B., Sarathchandra, P., Nazhat, S. N., Brown, R.A., “Mechanical Loading Determines Collagen Fibril Diameter Independent of Cell Activity,” *European Cells and Materials*, Vol. 11.3, 2006, p. 32.
- [46] Foutz, T. L., Griffin, A. K., Halper, J. T., Rowland, G. N., “Effects of Activity on Avian Gastrocnemius Tendon,” *Poultry Science*, Vol. 86, 2007, pp. 211-218.
- [47] Williams, R. M., Zipfel, W. R., Webb, W. W., “Interpreting Second-Harmonic Generation Images of Collagen I Fibrils,” *Biophysical Journal*, Vol. 88.2, 2005, pp. 1377-1386.
- [48] Vader, D., Kabla, A., Weitz, D. A., Mahadevan, L., “Strain-induced Alignment in Elastic Collagen Gels,” *Engineering for the Life Sciences*, University of Cambridge, 2007.
- [49] Gentleman, E., Lay, A. N., Dickerson, D. A., Nauman, E. A., Livesay, G. A., Dee, K. C., “Mechanical Characterization of Collagen Fibers and Scaffolds for Tissue Engineering,” *Biomaterials*, Vol. 24, 2003, pp. 3805-3813.
- [50] Agarwal, G., “Oligomerization and Interaction of DDR1 with Collagen: an AFM and FRET Microscopy Study,” *Biophysical Journal*, Vol. 96.3, 2009, p. 209a.
- [51] Goranova, V., Vizza, E., Motta, P. M., “Collagen Fibrillar Network in Estrous and hCG Stimulated Rabbit Uterus: A SEM Study after NaOH Maceration,” *Archives of Histology and Cytology*, Vol. 56.3, 1993, pp. 231-241.
- [52] Medscape Today, “Clinical Gait Analysis and its Role in Treatment Decision Making,” *Medscape General Medicine*, Vol. 1.1, 1999.
- [53] Trochim, W. M. K., “Internal Validity,” *Research Methods Knowledge Base*, 2006.
- [54] Trochim, W. M. K., “The T-Test,” *Research Methods Knowledge Base*, 2006.
- [55] Katsnelson, A., “Lab Rat Genome Sequenced,” *Scientific American*, April, 2004.
- [56] Hansen, D. C., “Metal Corrosion in the Human Body: The Ultimate Biocorrosion Scenario,” *The Electrochemical Society Interface*, Summer, 2008, pp. 31-34.
- [57] Globalspec, “ABEC Rating,” *Ball Bearing Specifications*, 2009.
- [58] Sambrook, F., *Molecular Cloning: A Laboratory Manual Second Edition*, Cold Spring Harbor Laboratory Press, New York, 1989.
- [59] Crowell, B., *Newtonian Physics*, [www.lightandmatter.com](http://www.lightandmatter.com), 2006.

- [60] Pang, B. S. F., Ying, M., “Sonographic Measurements of Achilles Tendons in Asymptomatic Subjects,” *Journal of Ultrasound Medicine*, Vol. 25, pp. 1291-1296.
- [61] Singh, S. K., “Composition of Harmonic Motions,” [www.cnx.org](http://www.cnx.org), 2007.
- [62] O’Haver, T., “Curve Fitting A: Linear Least Squares,” *Intro to Signal Processing*, University of Maryland at College Park, 2008.
- [63] Beard, J. R., Galea, S., Vlahov, D., “Longitudinal Population-based Studies of Affective Disorders: Where to from Here?,” *BMC Psychiatry*, Vol. 8.83, 2008.
- [64] Ng, K. W., Kugler, B. S., Doty, S. B., Ateshian, G.A., Hung, C. T., “Scaffold Degradation Elevates the Collagen Content and Dynamic Compressive Modulus in Engineered Articular Cartilage,” *Osteoarthritis and Cartilage*, Vol. 17.2, 2009, pp. 220-227.
- [65] Eisenberg, A., Reich, S., “The Dynamic Viscoelastic Properties of Some Non-crystalline Metals,” McGill University, 1970.
- [66] Duffie, N. A., “Spring Mass Damper Systems,” University of Wisconsin, Madison, 2004.
- [67] Kubik, J., “The Reciprocity Theorem in Coupled Problems of Viscoelastic Thermodiffusion,” *Acta Mechanica*, Vol. 50, 1984, pp. 285-290.
- [68] Lakes, R., “Viscoelastic Phenomena,” *Viscoelastic Solids*, University of Wisconsin, 2008.
- [69] Li, L., “Dynamic Mechanical Analysis (DMA) Basics and Beyond,” Perkin Elmer Instruments, 2000.

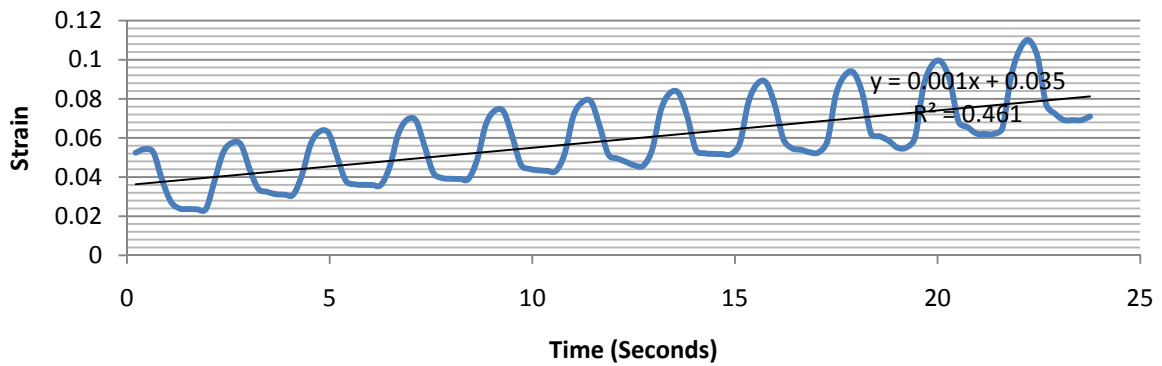
## Appendix A: Complete Strain per Time Results



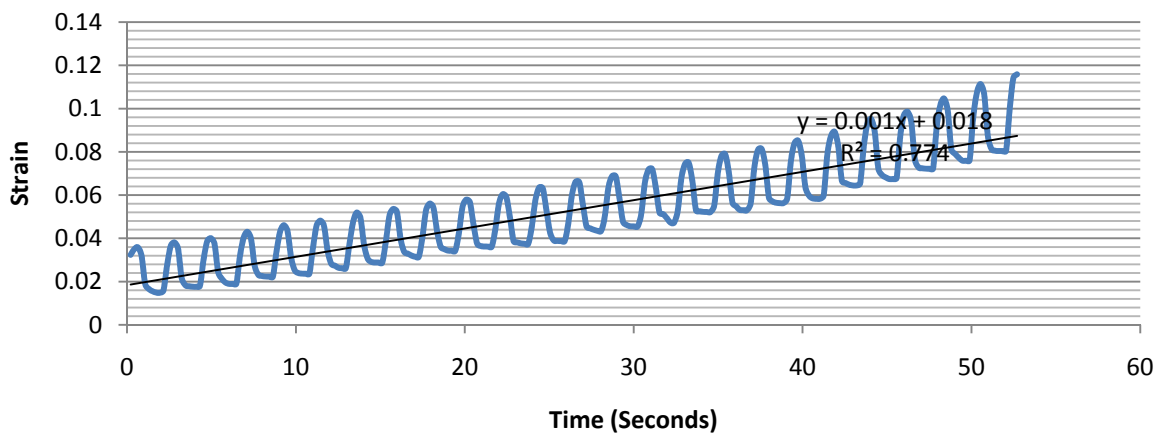
### Strain v Time 0.5 Hz Test 4

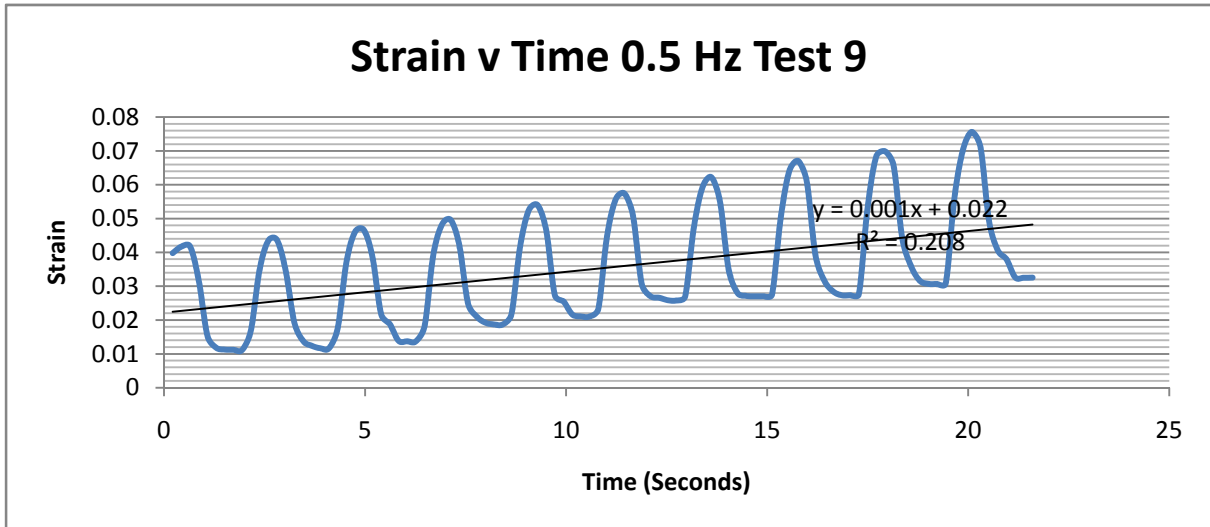
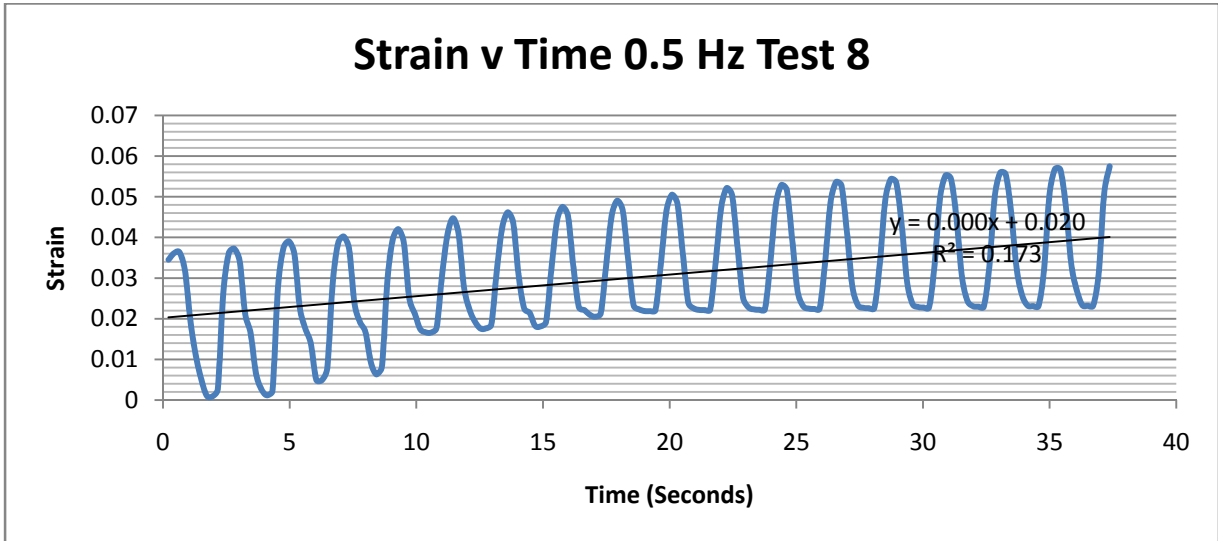
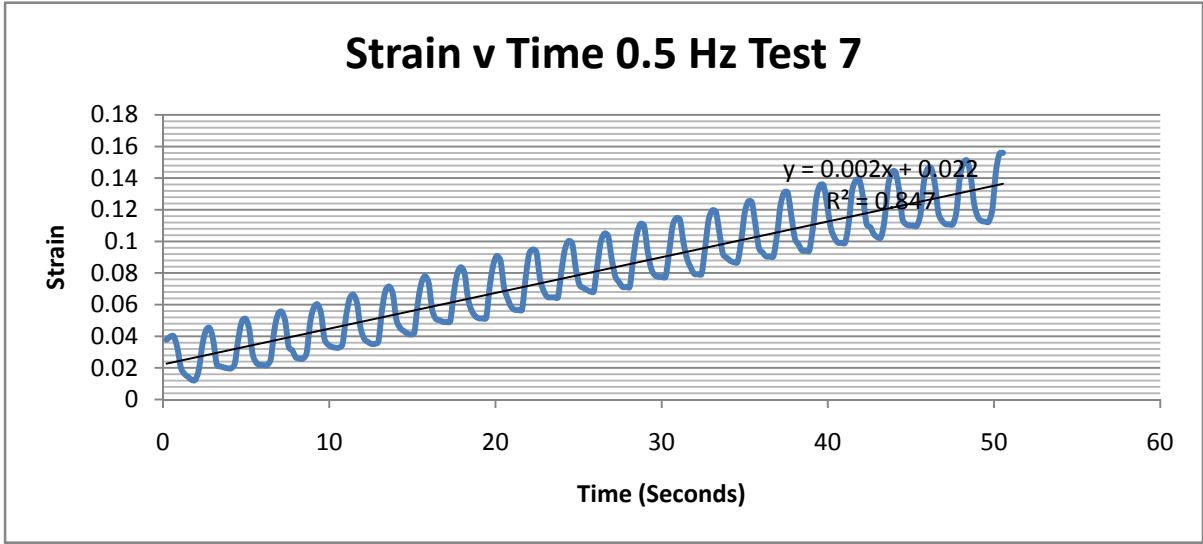


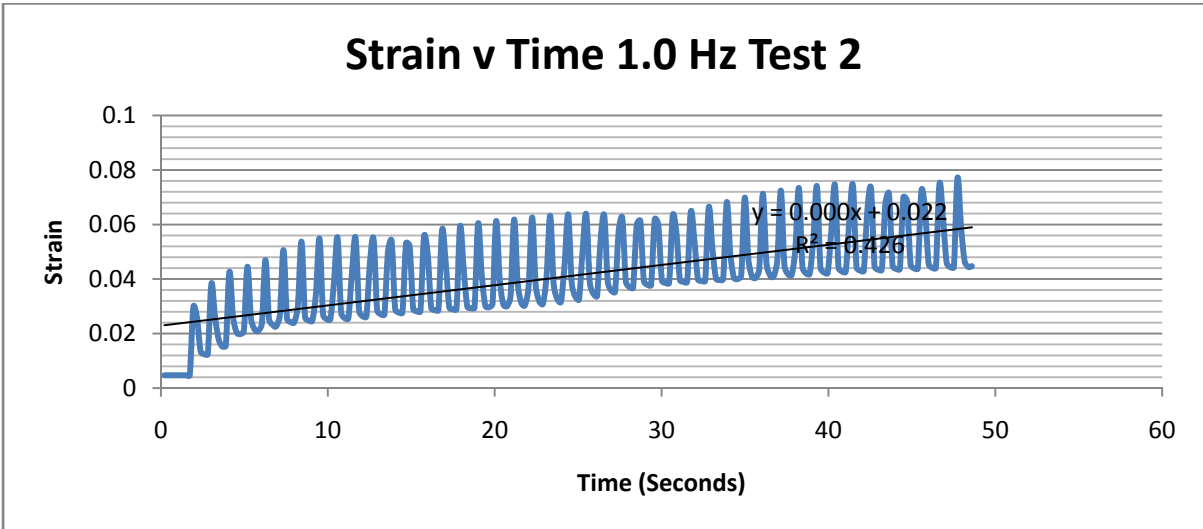
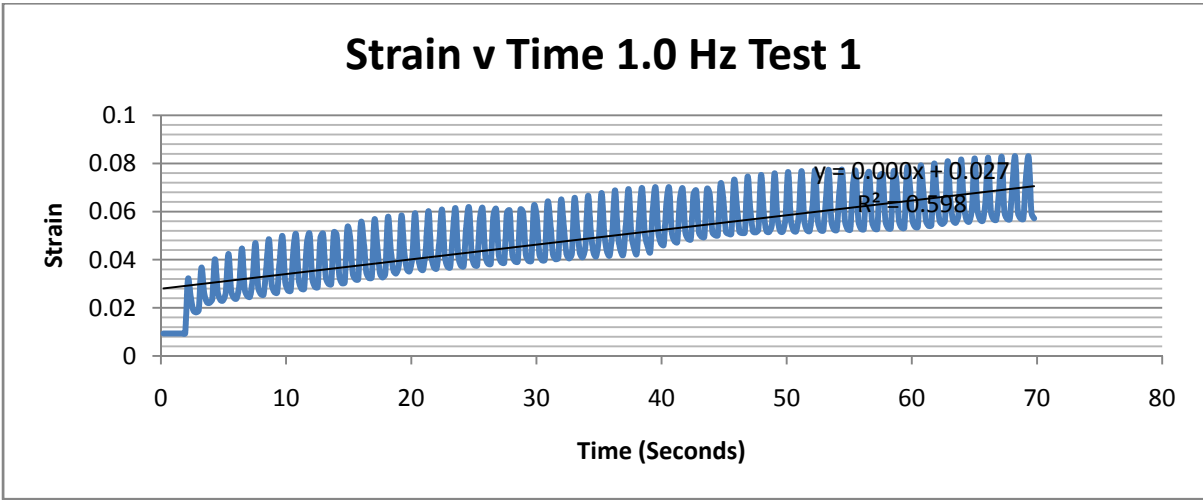
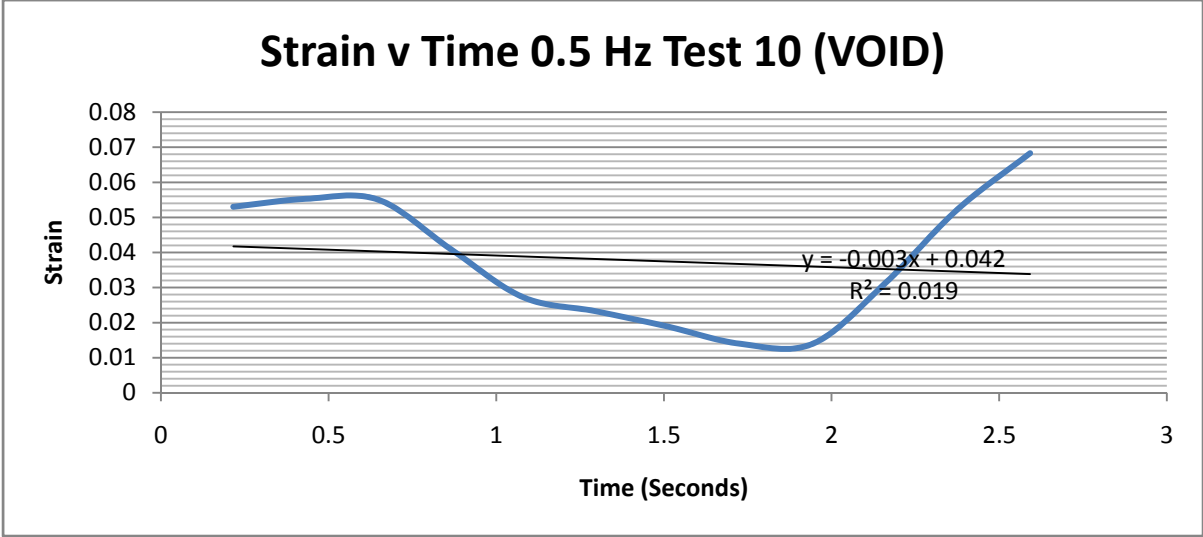
### Strain v Time 0.5 Hz Test 5

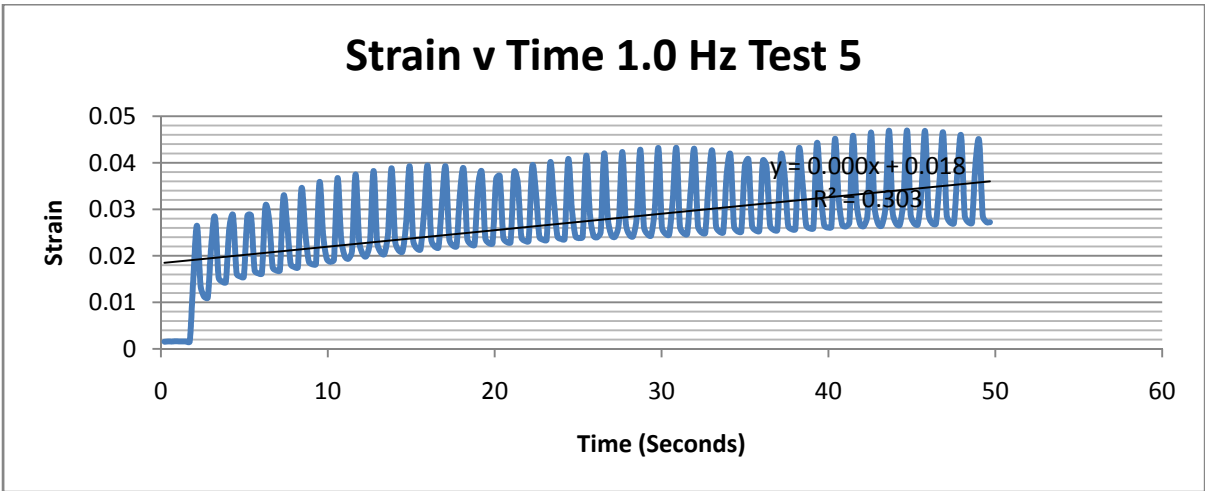
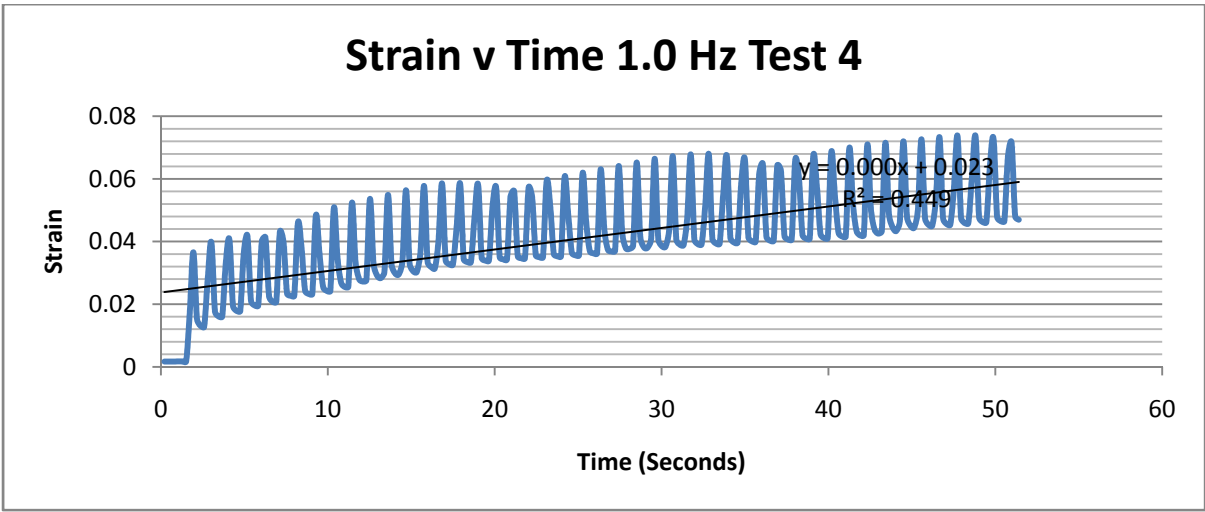
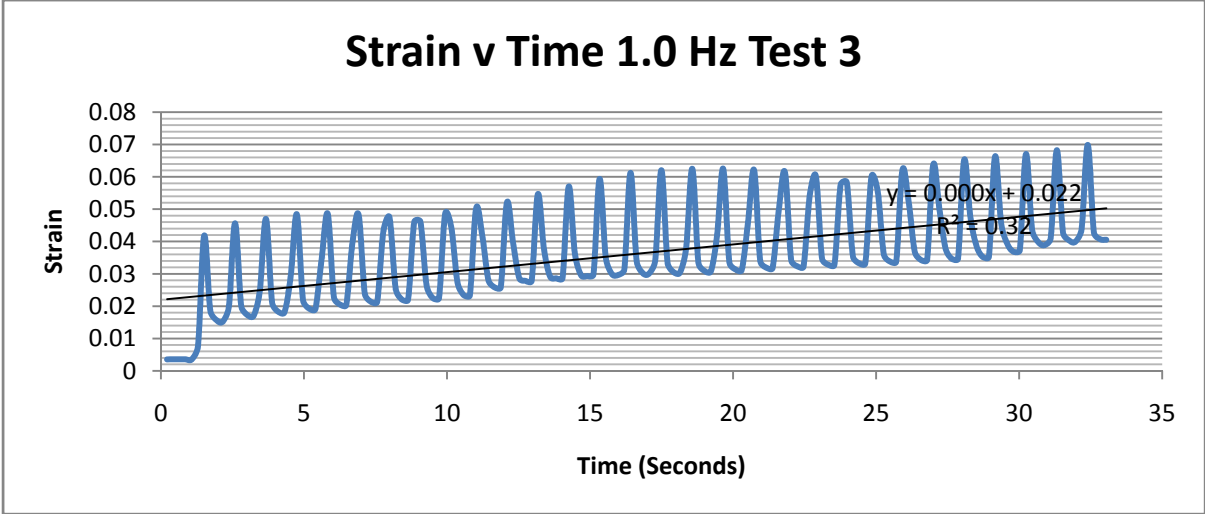


### Strain v Time 0.5 Hz Test 6

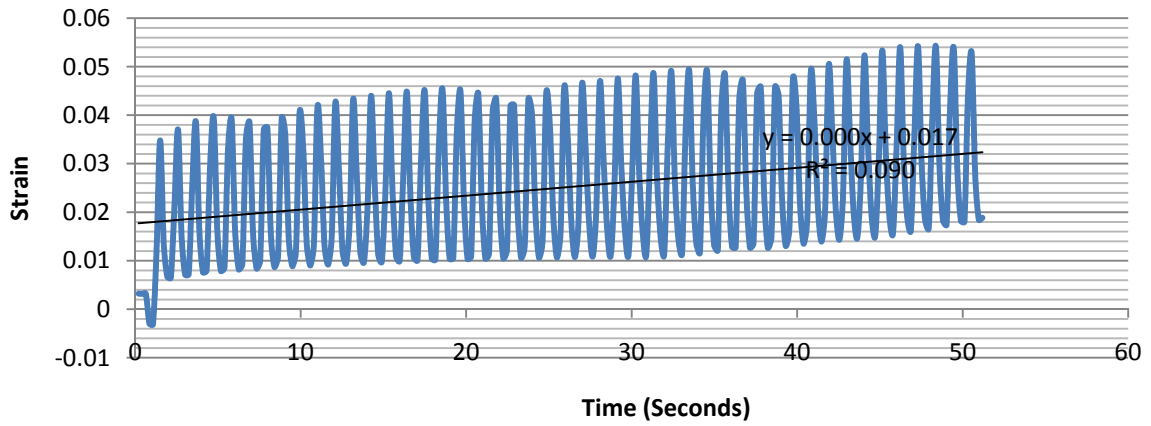




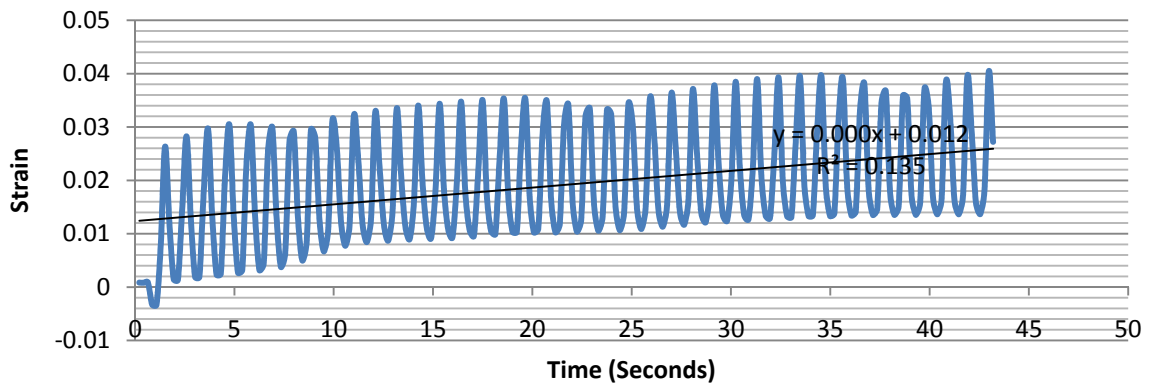




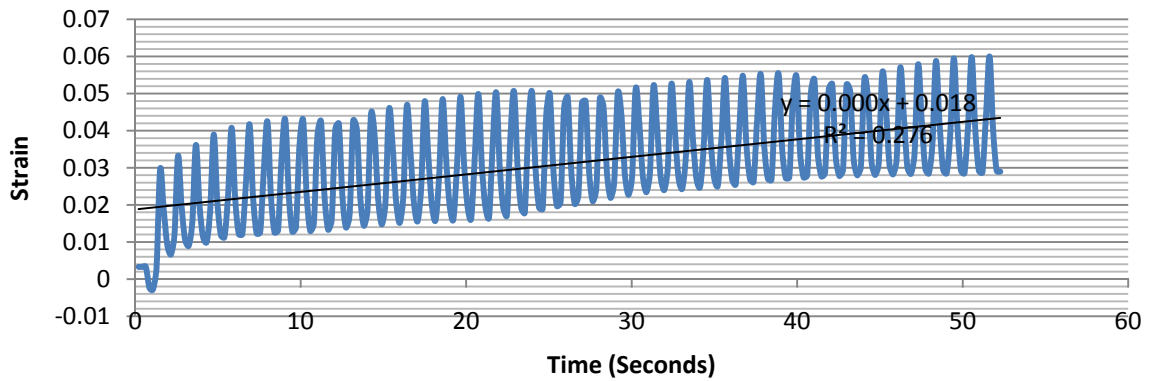
### Strain v Time 1.0 Hz Test 6

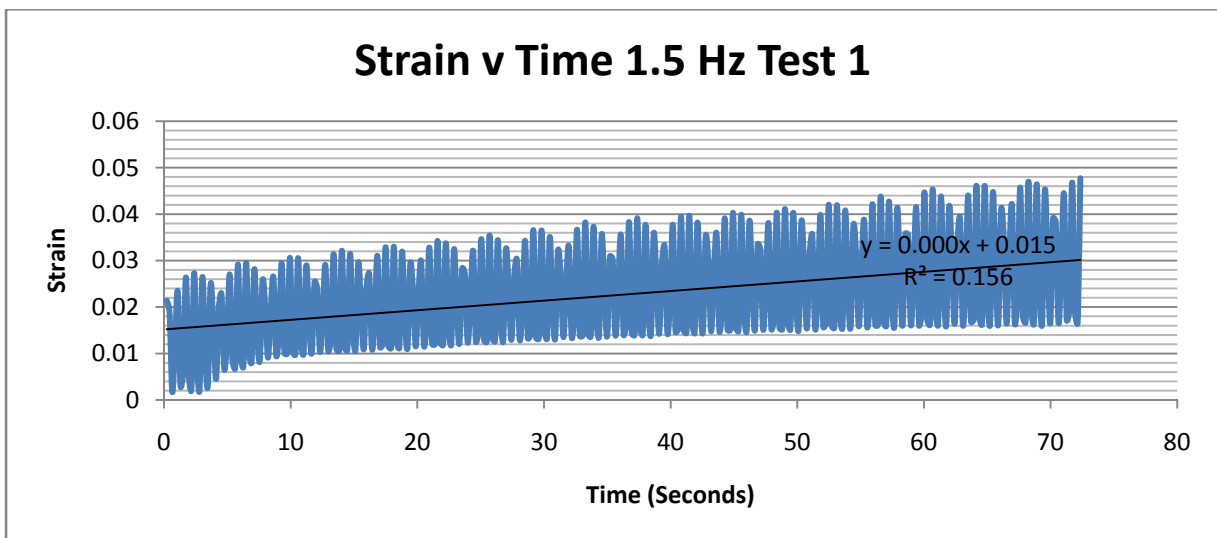
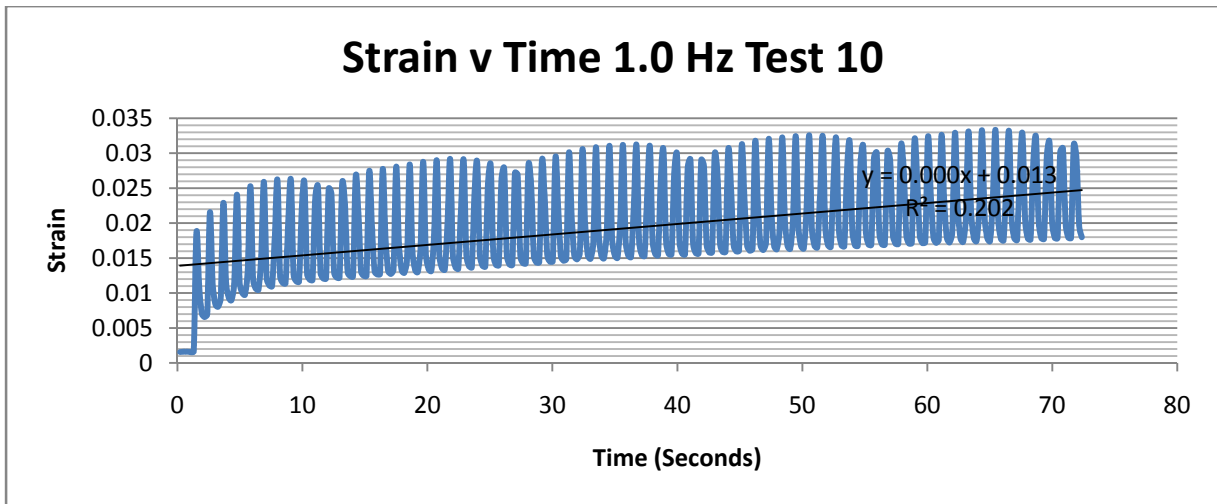
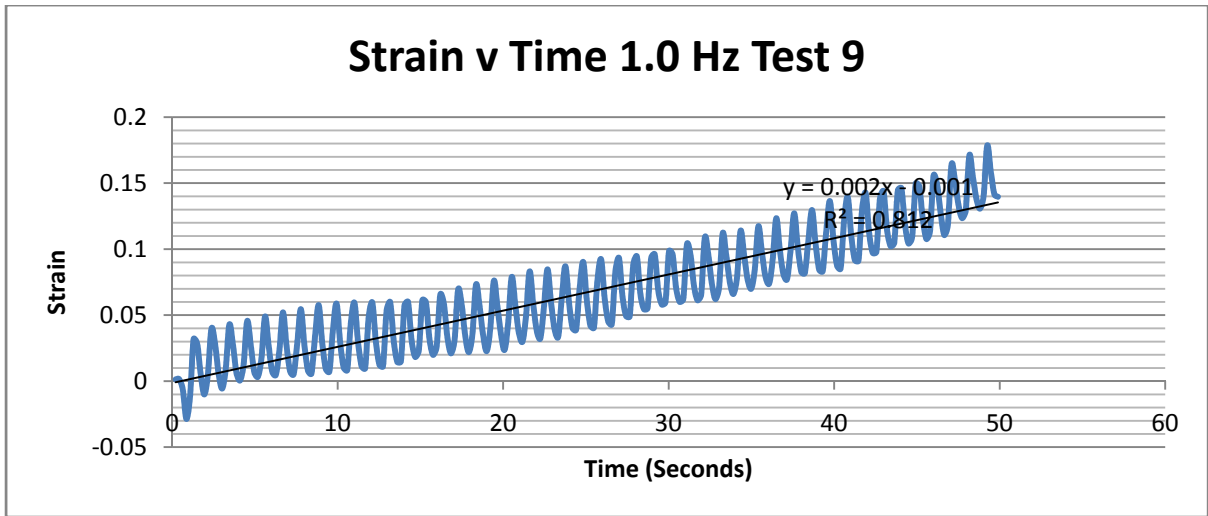


### Strain v Time 1.0 Hz Test 7

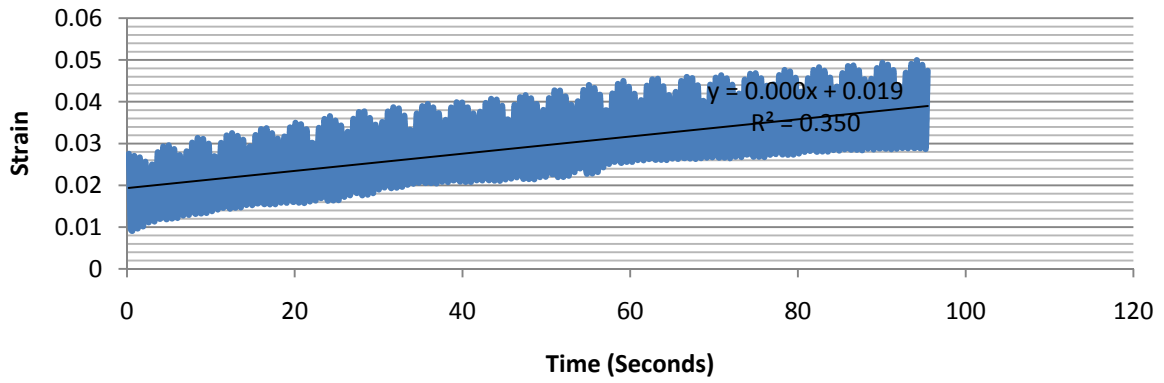


### Strain v Time 1.0 Hz Test 8

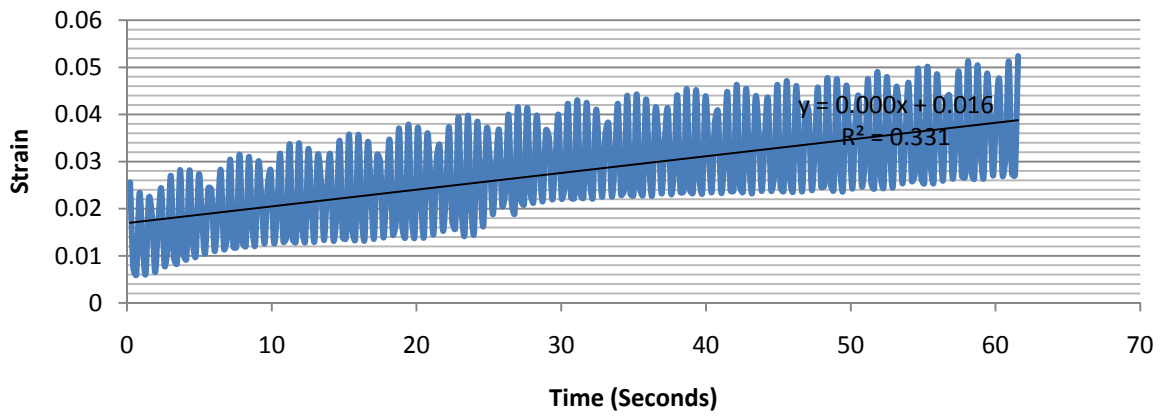




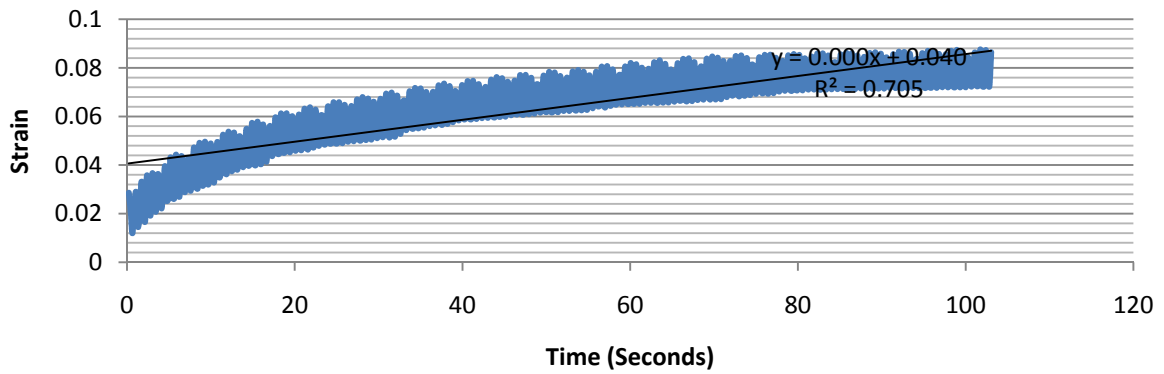
### Strain v Time 1.5 Hz Test 2



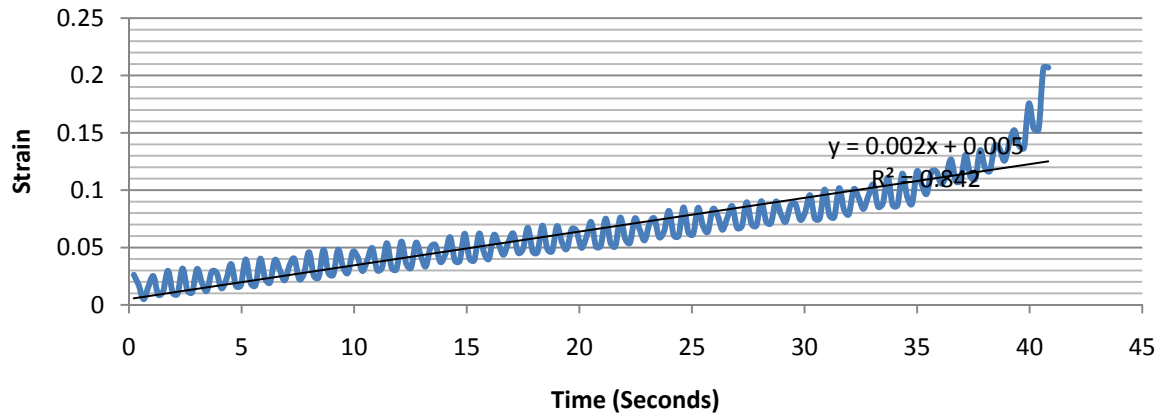
### Strain v Time 1.5 Hz Test 3



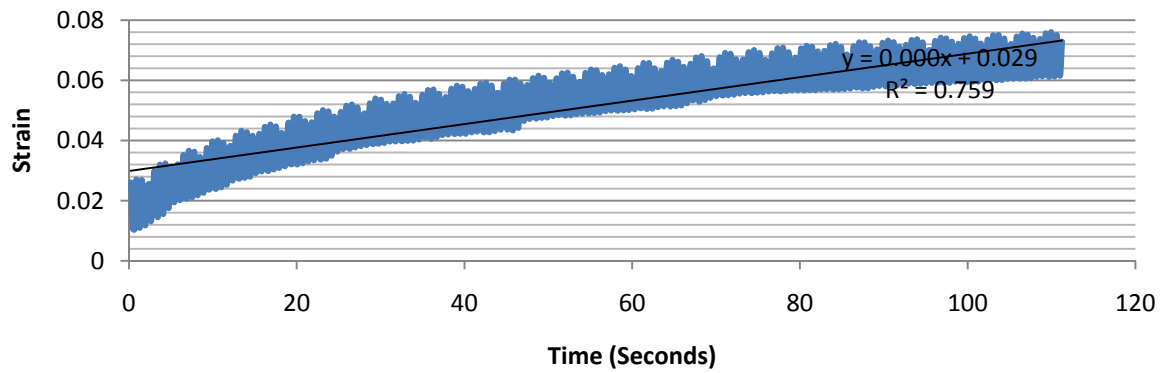
### Strain v Time 1.5 Hz Test 4



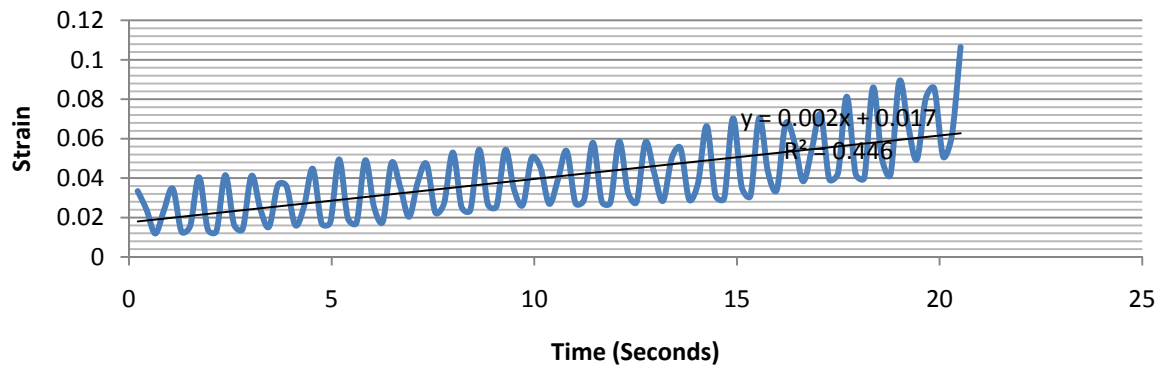
### Strain v Time 1.5 Hz Test 5



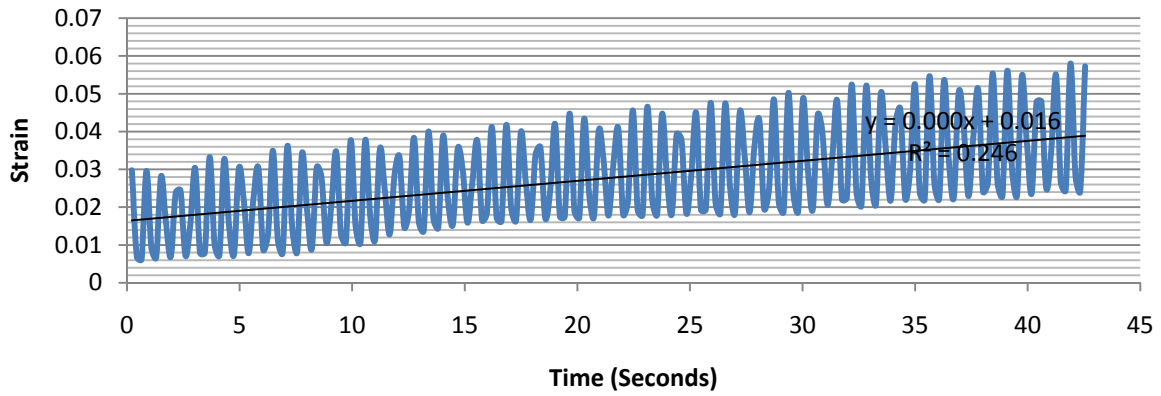
### Strain v Time 1.5 Hz Test 6



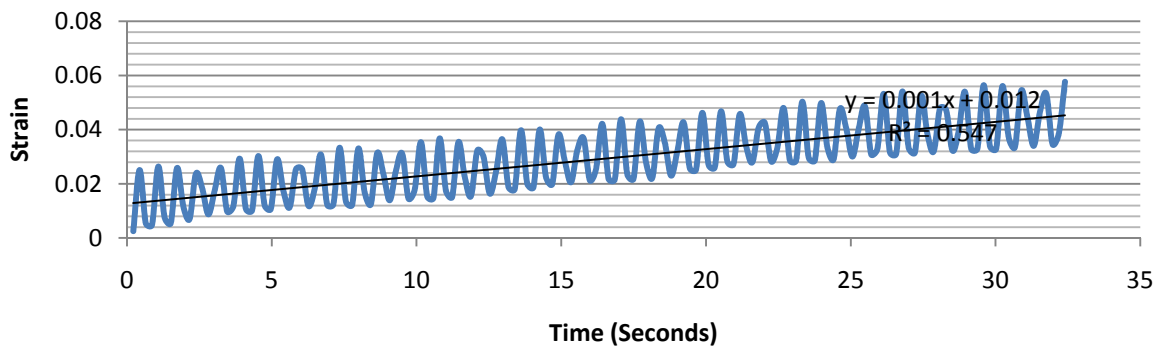
### Strain v Time 1.5 Hz Test 7



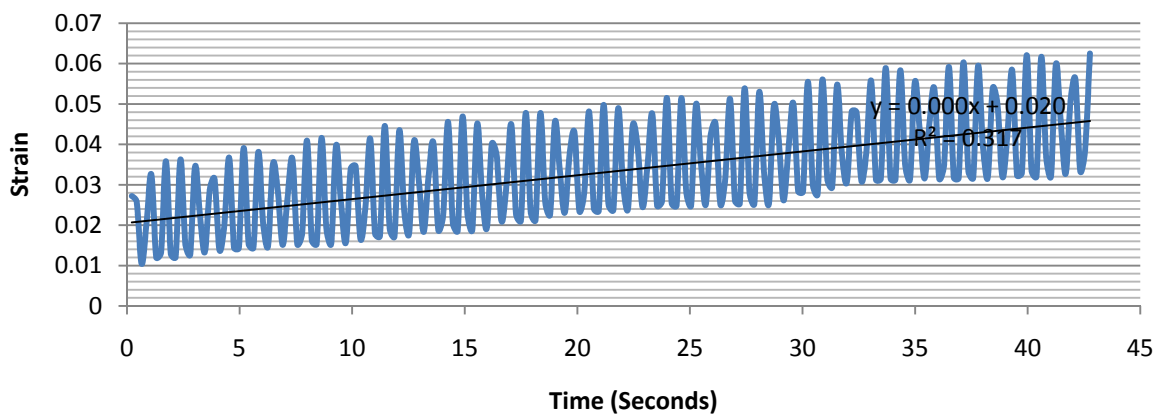
### Strain v Time 1.5 Hz Test 8



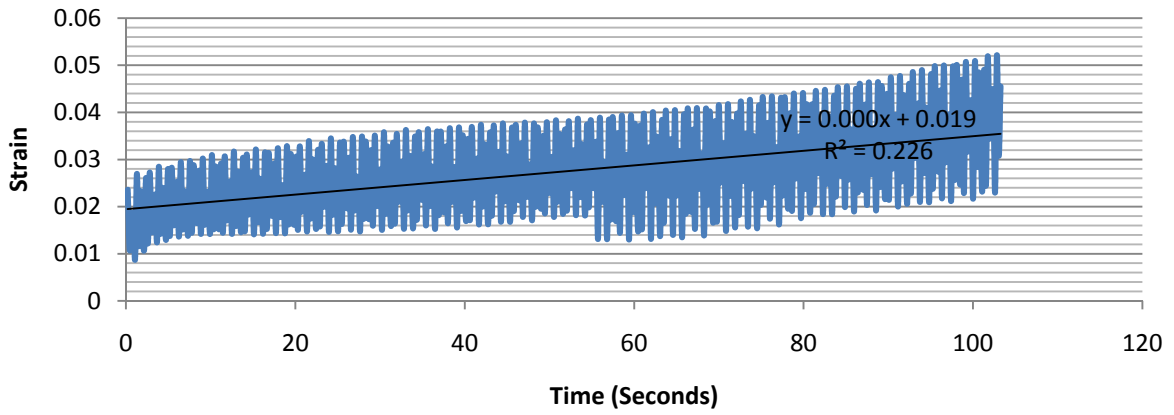
### Strain v Time 1.5 Hz Test 9



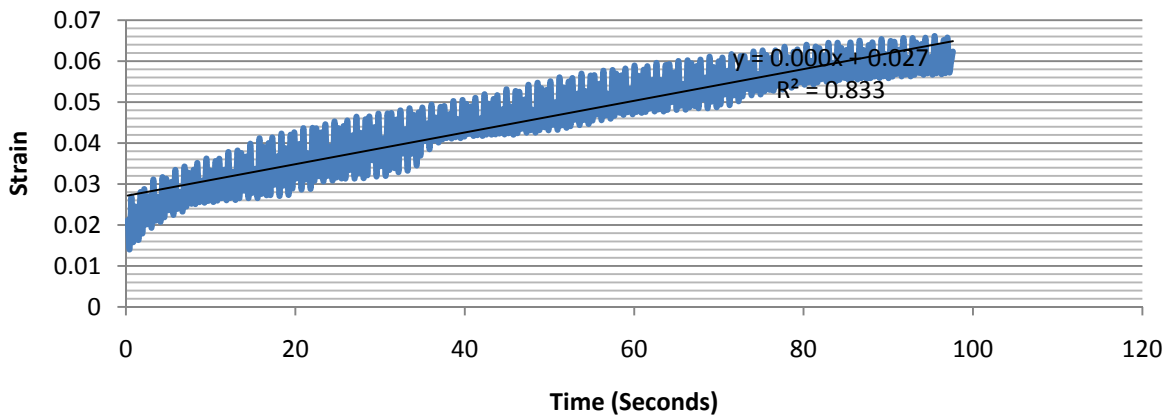
### Strain v Time 1.5 Hz Test 10



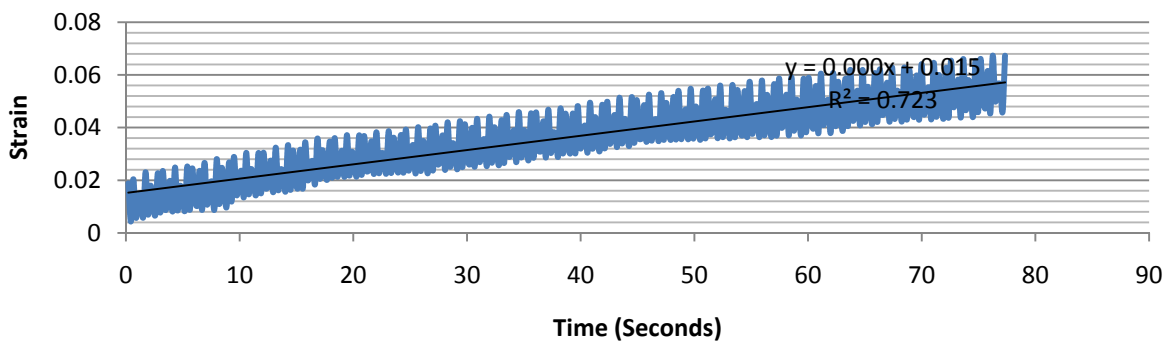
### Strain v Time 2.0 Hz Test 1



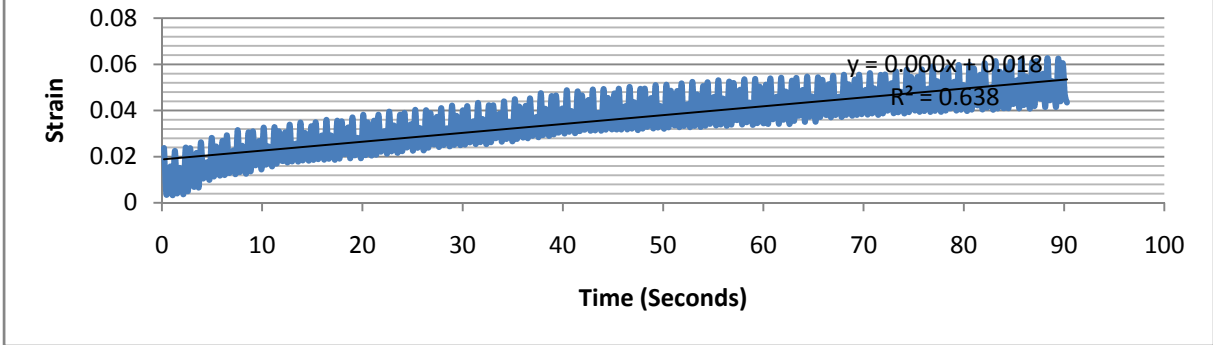
### Strain v Time 2.0 Hz Test 2



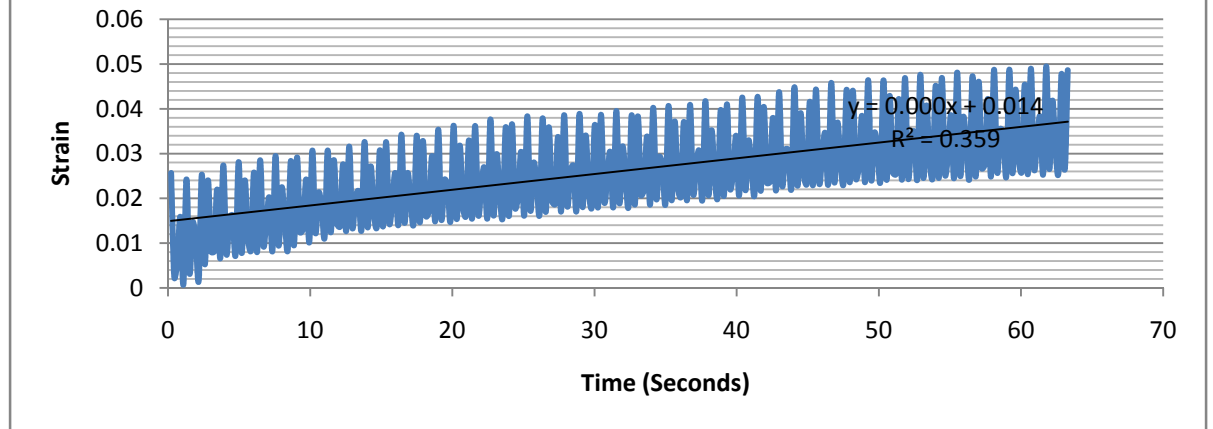
### Strain v Time 2.0 Hz Test 3



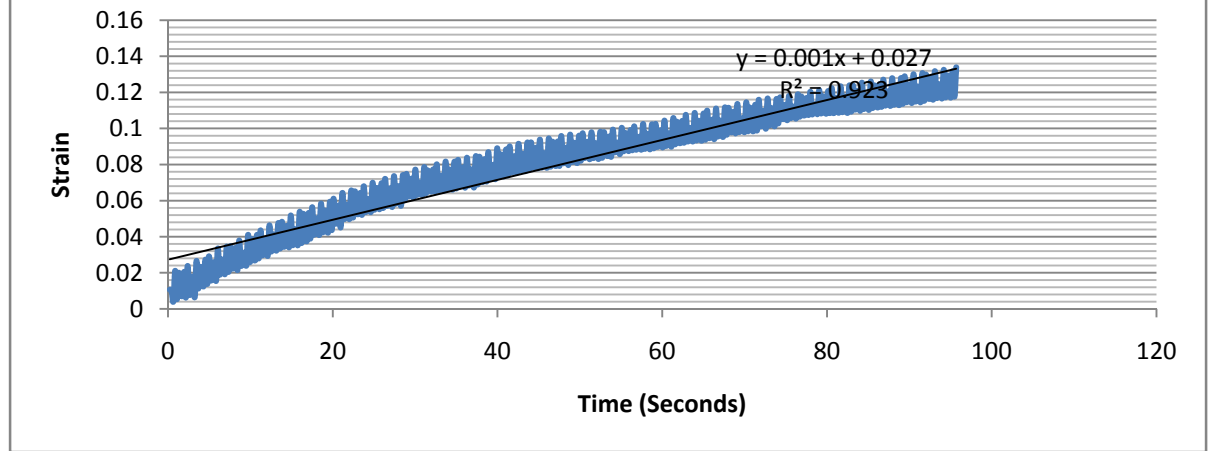
### Strain v Time 2.0 Hz Test 4



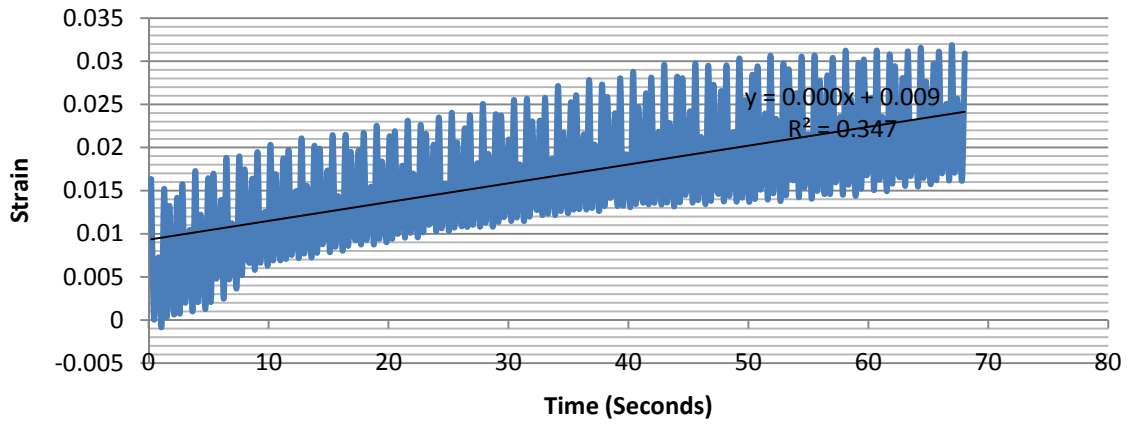
### Strain v Time 2.0 Hz Test 5



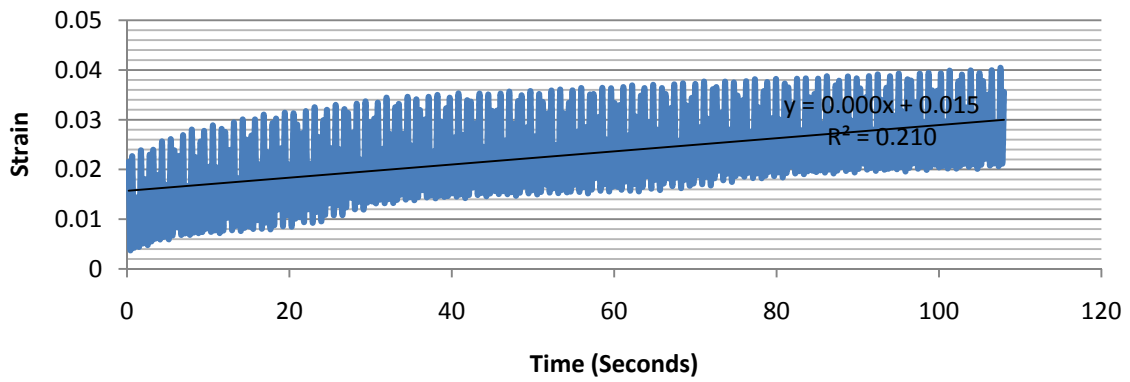
### Strain v Time 2.0 Hz Test 6



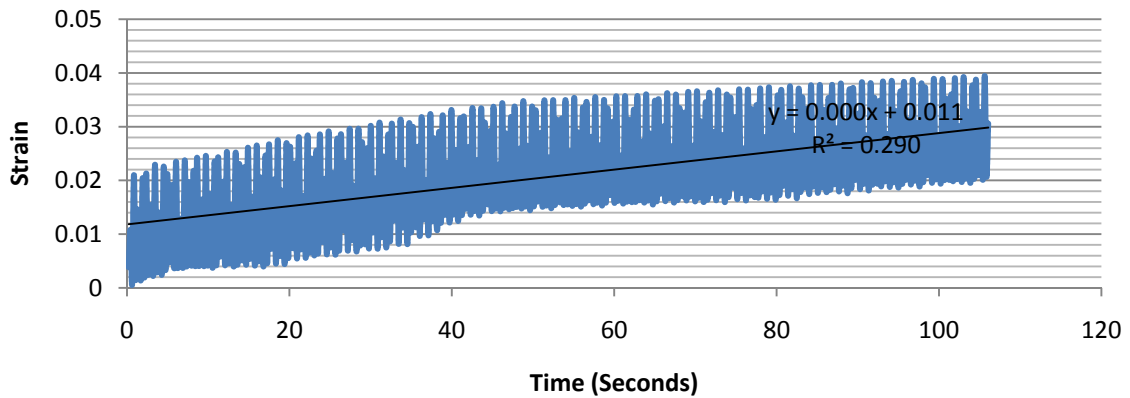
### Strain v Time 2.0 Hz Test 7



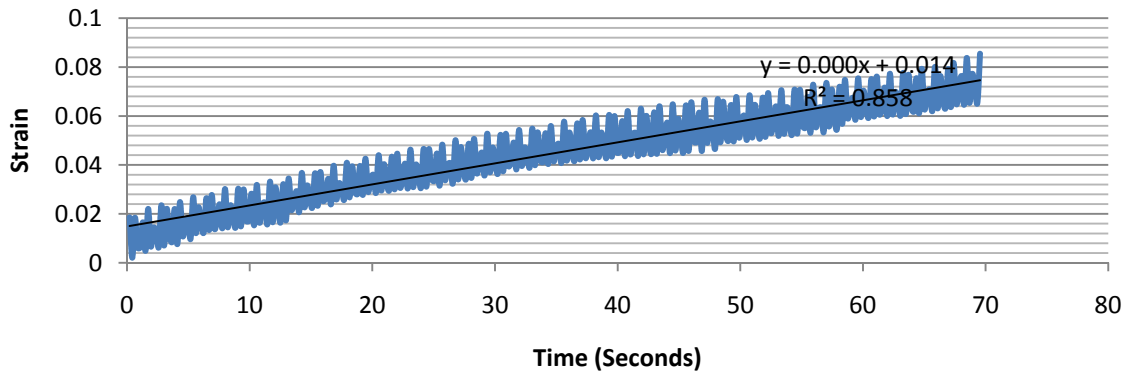
### Strain v Time 2.0 Hz Test 8



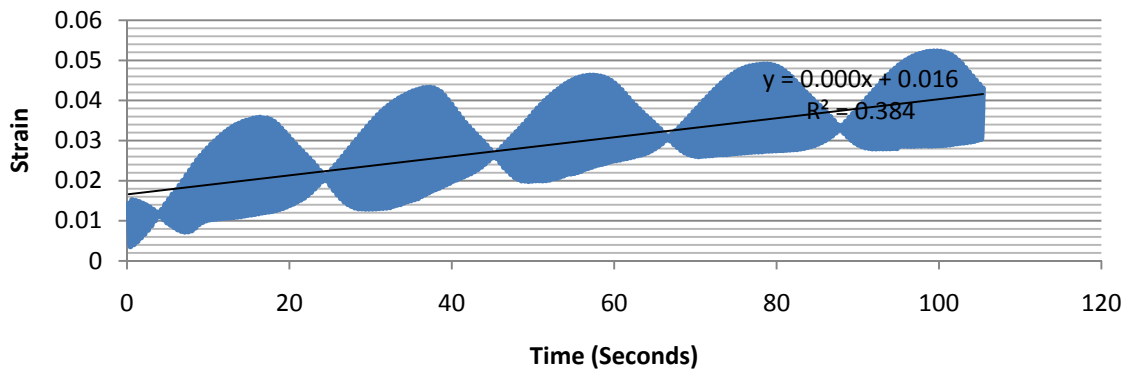
### Strain v Time 2.0 Hz Test 9



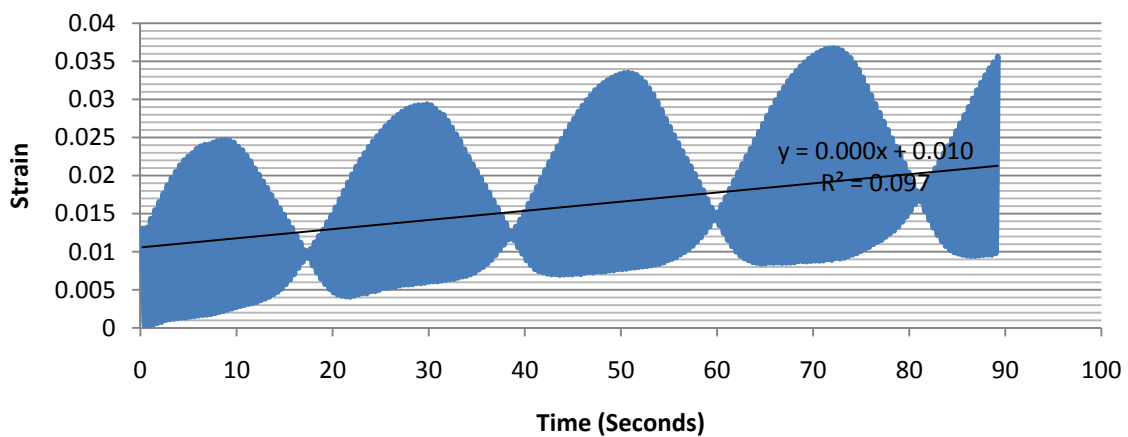
### Strain v Time 2.0 Hz Test 10

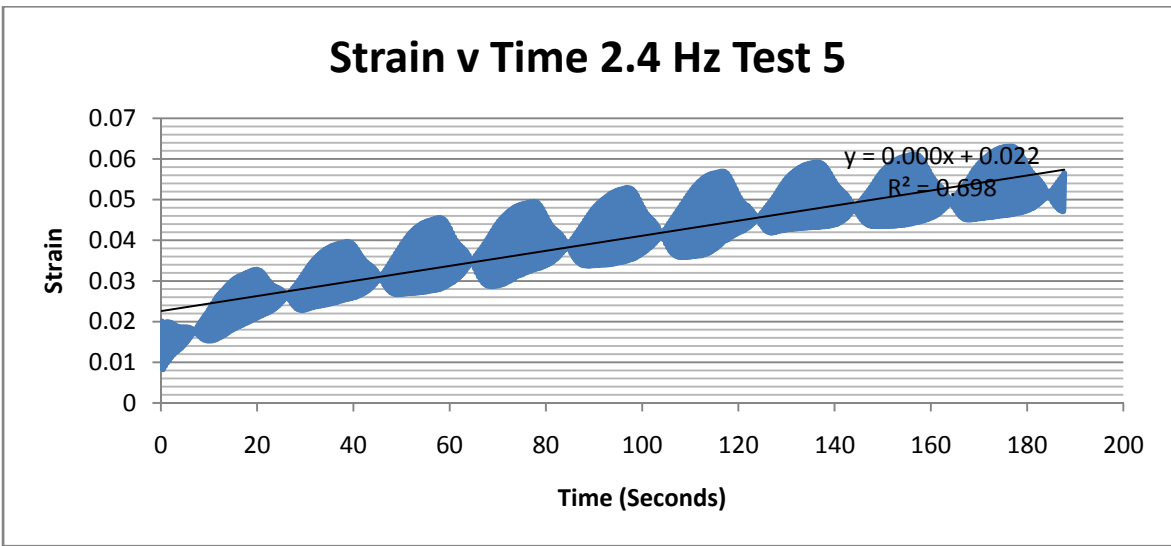
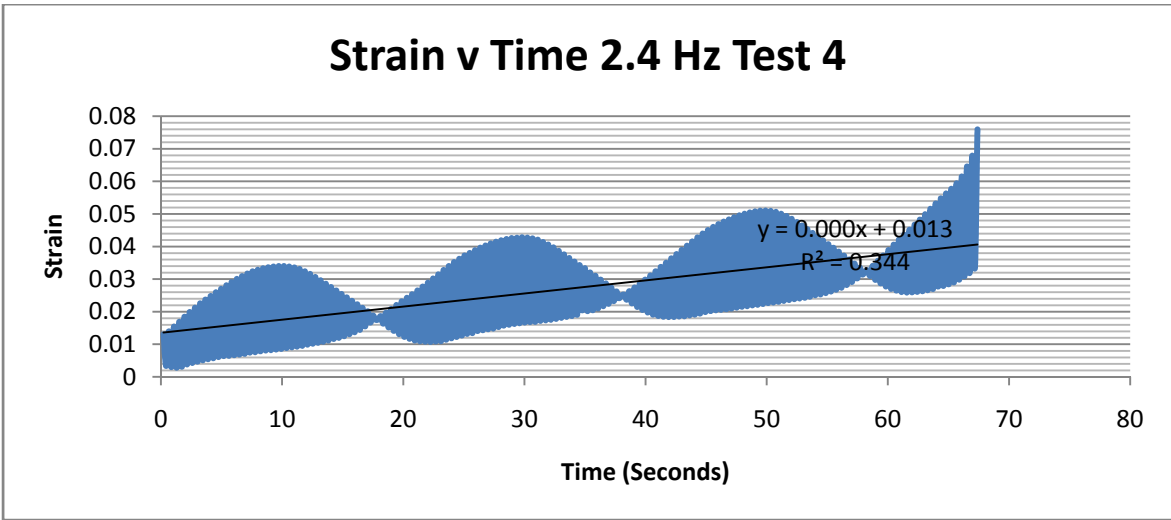
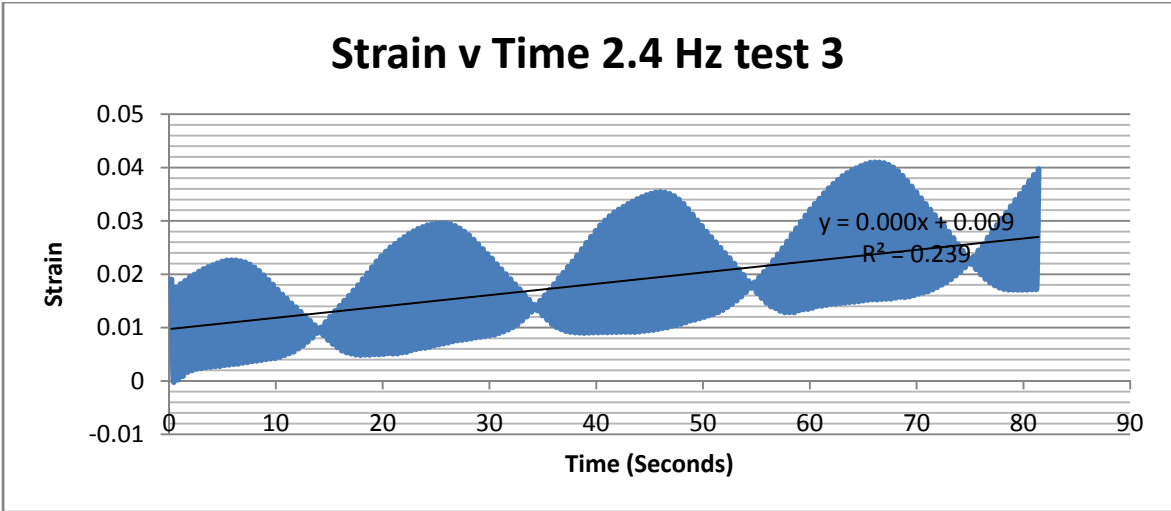


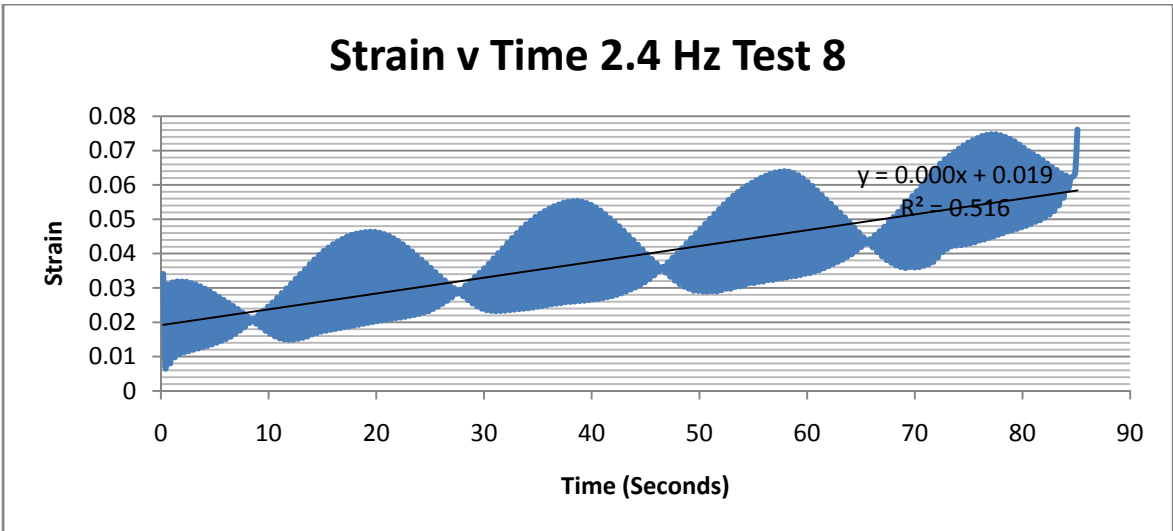
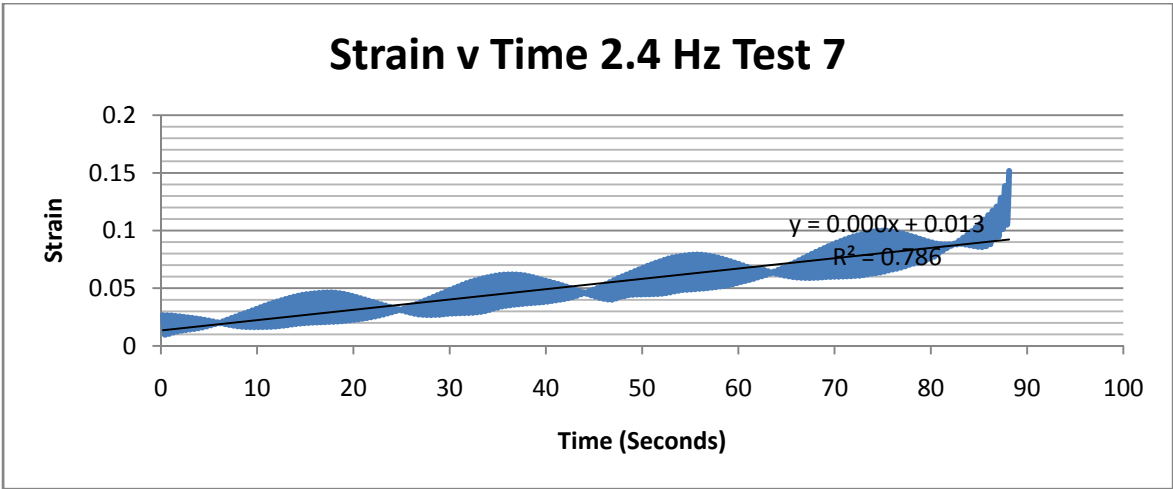
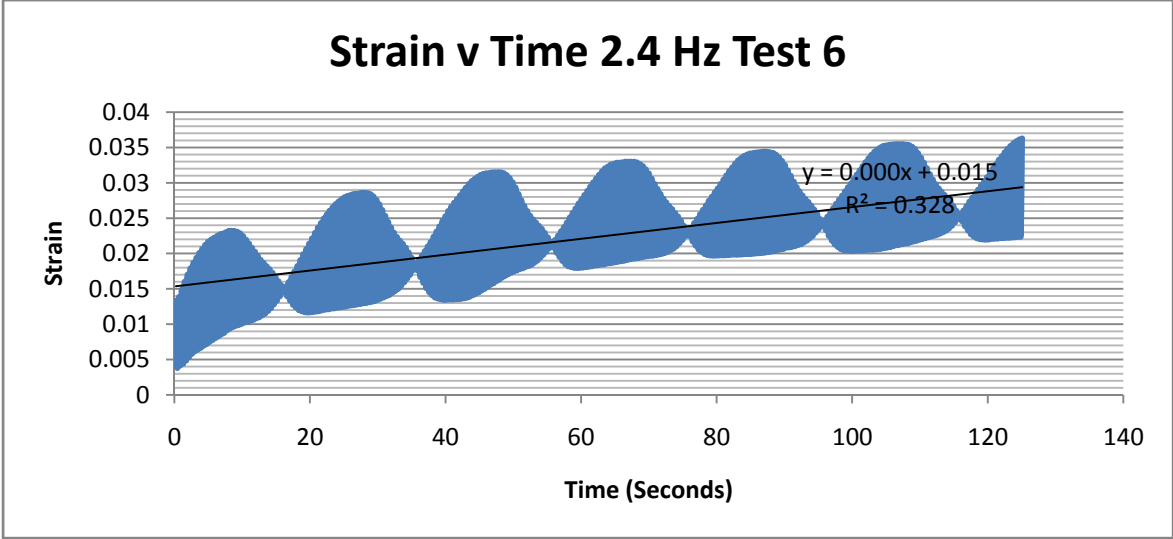
### Strain v Time 2.4 Hz Test 1



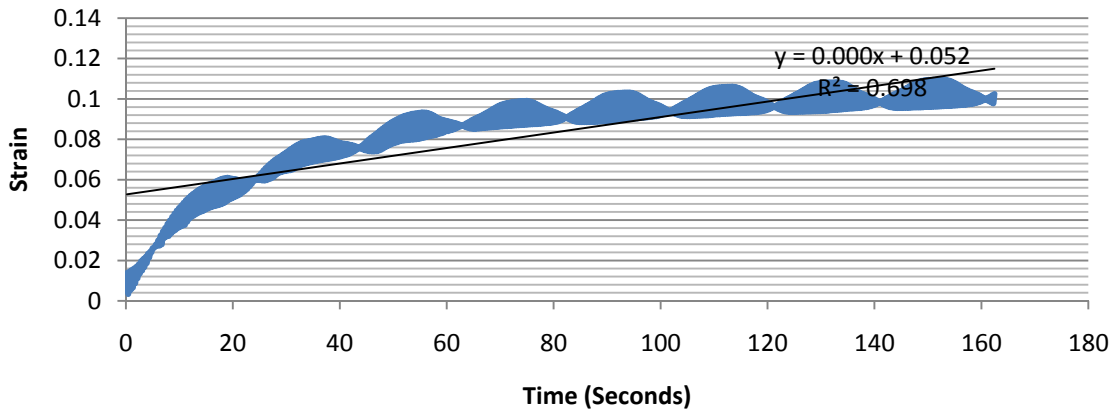
### Strain v Time 2.4 Hz Test 2



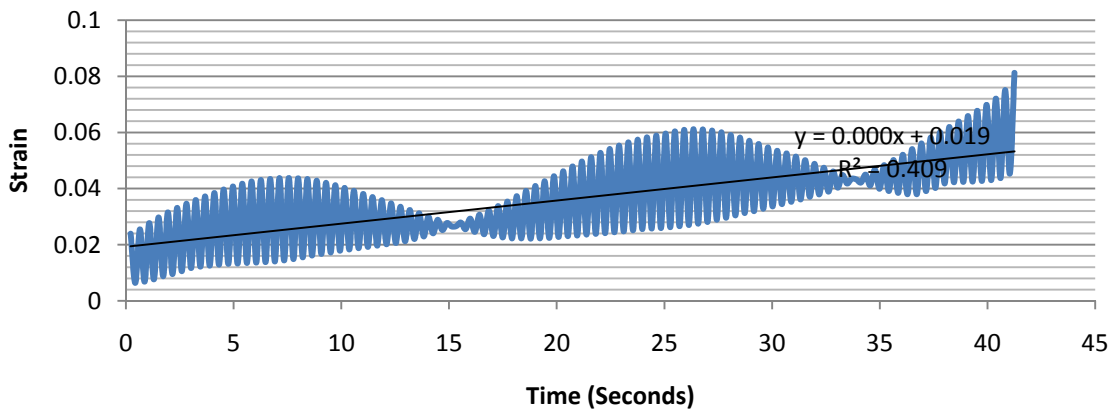




### Strain v Time 2.4 Hz Test 9



### Strain v Time 2.4 Hz Test 10



## Appendix B: Photographs



The above photographs show fascicles under zero applied tension. The characteristic crimp or wave pattern can be observed from two different perspectives. The top picture shows the pattern from above as indicated by the regular transverse proliferation. Waves can be seen from the side in the second photograph where an alternating transverse proliferation is observed.



As tension is applied to the sample, the crimp pattern disappears and the sample is viewed as above under the microscope. Only slight tension is applied to the pictured sample to demonstrate the visual representation of the fiber's initial undamaged condition. Note a complete lack of dark pronounced transverse features that indicate damage.

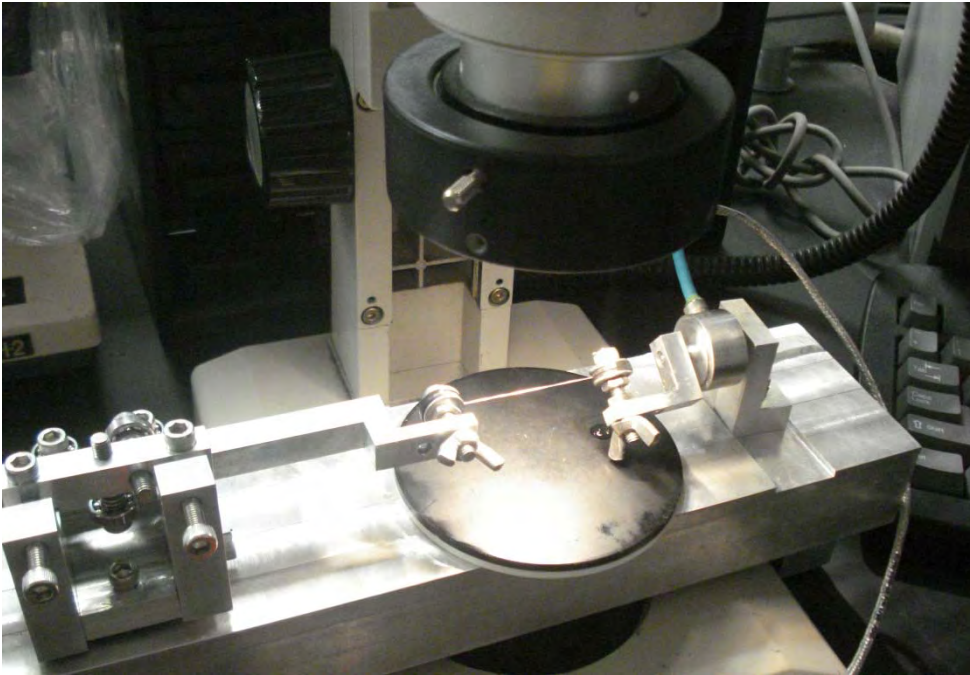
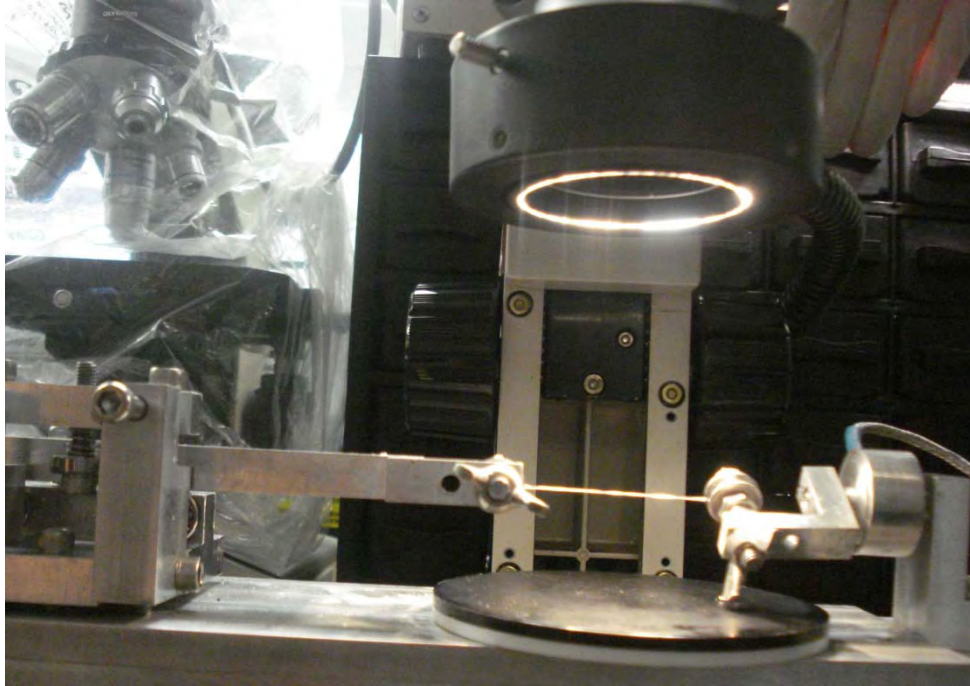




The above four photographs show examples of damaged fascicles viewed under magnification. White arrows indicate distinct points that indicate definitive damage on the fibrillar level.



The complete experimental setup is shown above. Equipment and functional role from left to right is as follows: Laptop set acquiring data directly into Excel spreadsheet; Sensor power supplies and data acquisition module collecting voltage signals from sensors in contact with the fiber; Petri dish containing untested collagen; Test apparatus showing voice coil motor, LVDT, linear bearing, test area with fiber and load cell; Computer monitor with magnified real-time image of sample under varying tension; Linear power supply and function generator connected to voice coil motor. This photograph was taken during a 2.0 hertz test run.



A closer view of the fiber under tension is presented above. Note linear bearing at the left; precision guide rod connecting the voice coil motor to the sample; Annular light source; Sample clamps and sample fiber; Load cell with connection to DC power and data acquisition.

## Appendix C

### Review of Viscoelasticity

#### C.1 Overview

Having established a mathematical model to fit the essential data set which can subsequently be used to draw many further conclusions, the advanced result set will now be presented. To preface these results, a review of the methods, mechanics, models and mathematics pertaining to highly viscoelastic materials is appropriate.

Type I collagen is a unique fibrous polymer with a highly ordered directional structure, and so its analysis as such differs from other polymers in the mechanics that yield the viscoelastic effect. However, Type I collagen's unidirectional action greatly simplifies the tensor analysis. In this review chapter, the molecular level mechanics of Type I collagen viscoelasticity will be ignored, and the macro-mechanics will be the focus.

Testing of general structural engineering materials often disregards viscoelasticity to any significant extent. This omission is acceptable in the majority of cases since most metals and composites exhibit only nominal viscous behavior in typical engineering situations [65]. When dealing with materials that have more pronounced viscoelasticity, however, numerous additional considerations must be accounted for when developing testing methods. At the same time various innovative techniques become available to quantify viscoelastic behavior.

Since viscoelastic materials demonstrate a combination of pure elasticity and pure viscosity, quasi-physical models are typically created using various combinations of different numbers of ideal springs and ideal dampers in arrangements of series and/or parallel connections [66, 67]. Several standard models are already established, but any new arrangement can be prescribed to fit newly discovered behaviors, modes and materials.

Along with the mathematical solutions to the quasi-physical models, viscoelastic behavior is often modeled through Volterra integral equations. General tensor analysis calls for two coupled equations to fully define the interdependent effects of elasticity and viscosity in

such materials [66, 67]. Moving forward from the general mathematical models, many simplifications and assumptions are made before reaching a conclusive set of equations.

### C.2 Macro-mechanics of Viscoelastic Materials

In basic terms, viscoelasticity manifests as two distinct but completely related phenomena: creep and stress relaxation. Creep is the non-zero rate of strain observed in a material under a constant state of stress, see Figure C.1. Stress relaxation, the inverse behavior, is the rate of change of stress observed in a material under an unchanging strain state, see Figure C.2.

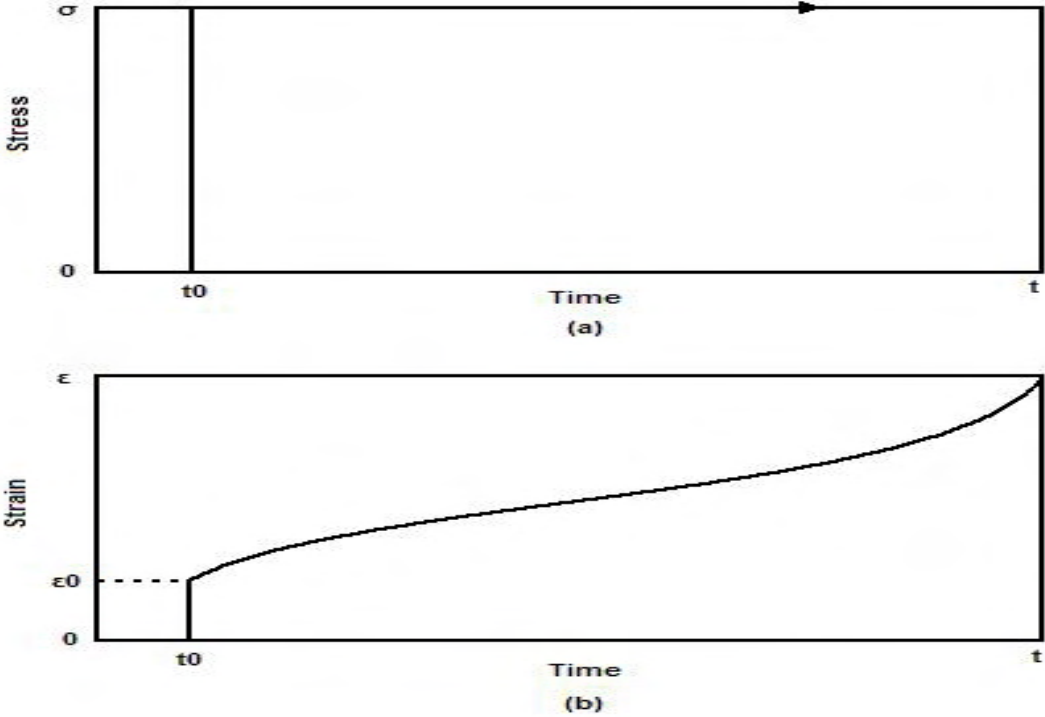
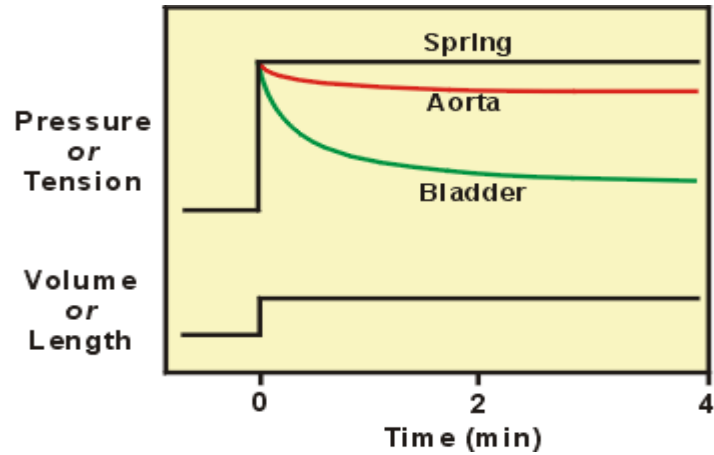
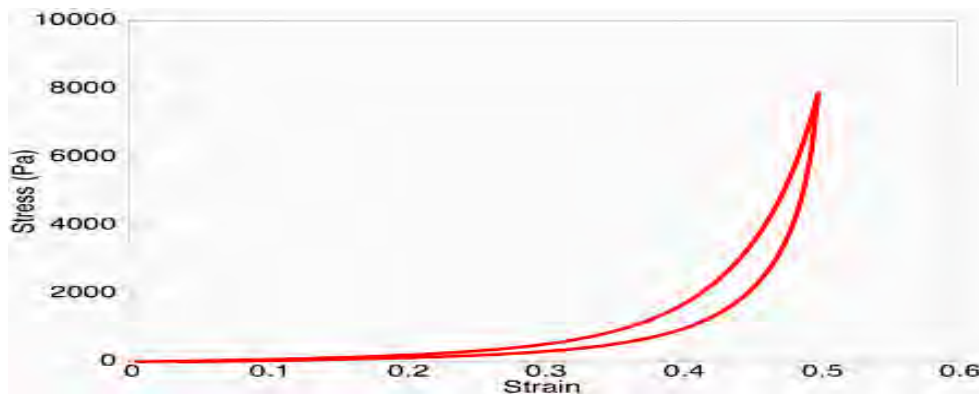


Figure C.1: Graphs demonstrating viscoelastic creep



**Figure C.2:** Graph demonstrating viscoelastic stress relaxation on selected biomaterials

While a material exhibits one or both of the above described behaviors, part or all of the purely viscous deformation is lost as unrecoverable energy. The portion of returned energy, in general, is termed the coefficient of restitution, and so the same concept and vocabulary can be used for describing interactions of viscoelastic materials. For instance, natural collagen has a coefficient of restitution around 95%. Lost energy of deformation, often termed mechanical hysteresis, can be observed or quantified in several ways. In single cycle loading, the unrecoverable energy is equal to the area of the hysteresis loop found between the loading and unloading curves of the stress/strain plot as in Figure C.3 for example.



**Figure C.3:** Generic representation of a viscoelastic hysteresis loop

Repeated cyclic loading will result in a pronounced phase shift angle between the mechanical input and output as noted in Figure C.4A. The phase shift angle for an interaction of 100% coefficient of restitution will be zero while where the coefficient of restitution is 0%, the phase shift angle will be 90 degrees. The relationship between the coefficient of restitution and the phase angle is linearly proportional. This phase shift angle is equal to that often seen in dynamic analysis of engineering mechanisms, the only difference being that the viscous damping comes from internal molecular mechanisms, and not from a separate mechanical entity.

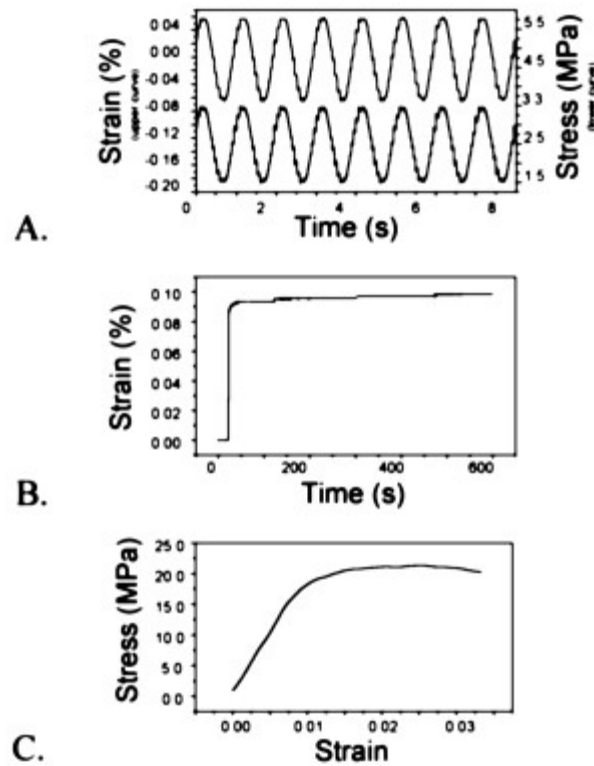


**Figure C.4:** Cyclic test with controlled strain state demonstrating phase shift

Further, whereas elastic deformation per time is ideally instantaneous, viscous deformation may take a completely linear (Newtonian) form or various nonlinear forms as seen cursorily in Figure C.5. Nonlinear viscosity is synonymous with non-Newtonian fluid flow and various special cases have been developed to describe several common non-Newtonian viscoelastic materials [65-68].

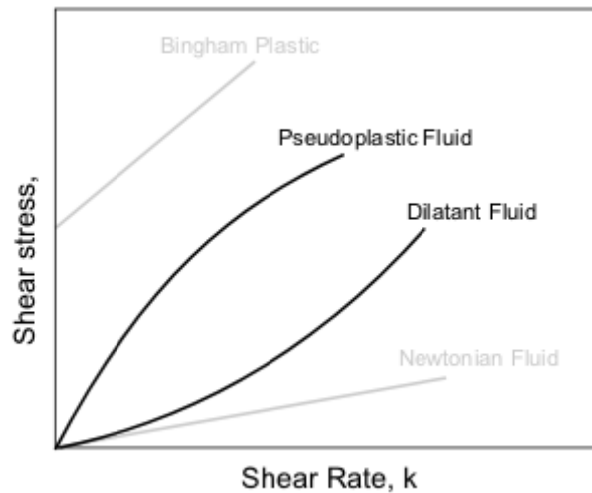


**Figure C.5:** Shear stress to strain rate graph for some special case viscoelastic materials

### C.3 Testing Methods for Viscoelastic Materials

As mentioned, testing of viscoelastic engineering materials is open to many approaches that are not applicable to or not practical in quasi-static testing. For this reason, testing the time dependent mechanical properties of materials can be done with basic methods, advanced or unorthodox methods or a number of techniques in between.

Most often, standard feedback controlled quasi-static testing equipment (Instron etc.) can be used to gather time dependent data pertaining to creep or stress relaxation. Feedback control is important to obtain the constant strain state or constant stress state required to measure

viscoelasticity in a “static” test. Also, the equipment must obviously be able to track measurements with respect to time. This is often an excellent option for viscoelastic testing due to the accessibility of equipment and standardization of testing procedures with said equipment. Micro/nano indentation is often used to measure material properties on small scale structures. These methods are adaptable to measure viscoelasticity in a similar manner to full scale testing.

Dynamic methods (DMA etc.) which measure the phase shift angle phenomena are also often employed. The concept and execution of this type of testing are quite simple and therefore another excellent option when measuring viscoelastic properties. In a dynamic mechanical test, a uniaxial harmonic forcing function is transmitted through a sample from one end; the function that the sample emits on the other end is then measured and compared to the input function. The phase shift between the two functions is proportional to the viscous properties of the material as described above, and as such can be used to characterize the sample material. This technique is often used concurrently with heating of a polymer sample to determine the characteristic glass-transition temperature [68, 69].

The most advanced methods for measuring viscoelasticity, also reviewed briefly in Chapter 3, involve ultrasound spectroscopy. In essence, these methods are similar to other dynamic methods and only differ in that the frequency of the function that is transmitted is much higher, generally in the kilohertz range. Also, higher frequencies allow the tests to take advantage of the resonance effect to improve accuracy and reduce sensitivity to uncontrollable external conditions.

#### **C.4 Quasi-physical Viscoelastic Models**

Representation of a material’s mechanical properties with theoretically ideal springs and dampers allows the tester to fit a quasi-physical model to the behavior of the material being tested. After hypothesis of a particular model, the solution for the proposed model is compared to the experimental data for the same mechanical input. Some standard models including:

Maxwell, Kelvin-Voigt and Standard Linear Solid are already established, but a material can be more precisely modeled by adding, subtracting or rearranging the mechanical elements.

The Maxwell and Kelvin-Voigt models are the most basic since each consists of only one spring and one damper. A Maxwell model, Figure C.6, calls for the spring and damper to be arranged in series. When mechanical elements are arranged in series, load is equal in both elements; however, total deformation equals the sum of the deformation of each element. The resulting solution predicts a linear relationship between deformation and time (creep) and an exponential behavior of natural unloading with time (stress relaxation). As a final point, upon instantaneous removal of load, the solution has a point of undefined slope corresponding to instantaneous recovery of the ideal spring.

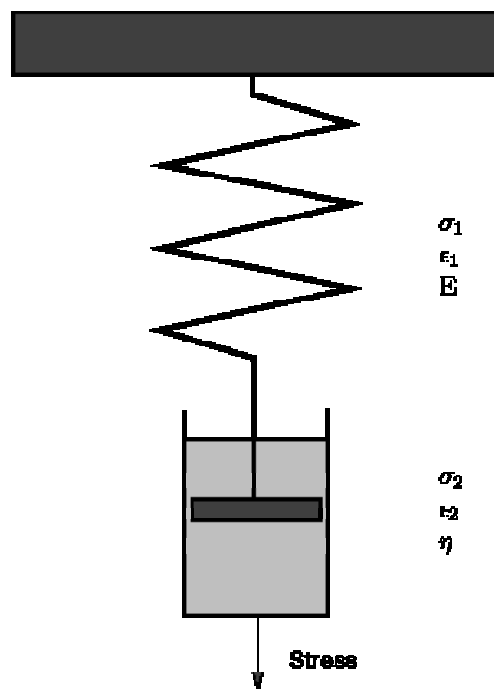
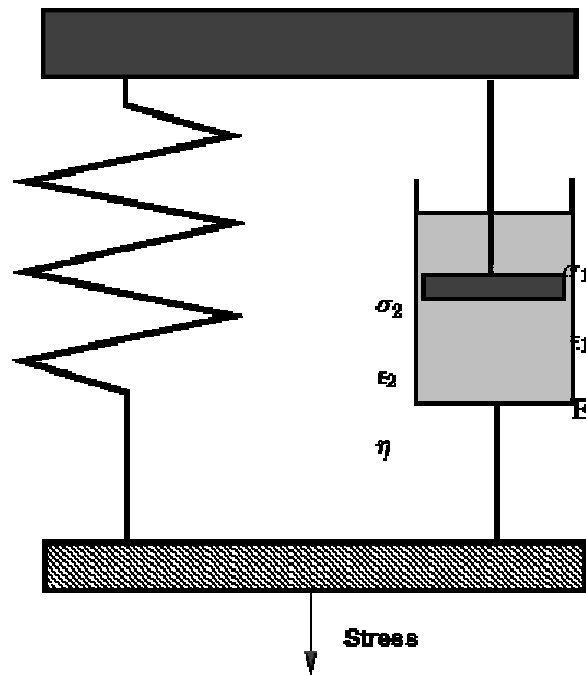


Figure C.6: Maxwell Model

The Kelvin-Voight Model, Figure C.7, also uses only one spring and one damper. The arrangement however, is in parallel instead of series. In this case, the deformation state of each element is equal, but the loads carried by each element are not constrained to be equal. The individual loads must still add to equal the total load transmitted through the model. The Kelvin-Voight Model predicts exponential creep behavior, but stress relaxation does not occur in the parallel arrangement.



**Figure C.7:** Kelvin-Voight Model

Obviously, each model has its limitations. The Maxwell Model does not provide an appropriate approximation of creep behavior while the Kelvin-Voight does not provide a solution for dynamic stress relaxation. To overcome these issues, both models are combined by switching a Maxwell element for the damper of the Kelvin-Voight Model. This combination is termed the Standard Linear Solid Model. The solution shows exponential behavior in both creep and stress relaxation, but as in the Maxwell Model has an undefined point of deformation per time upon complete instantaneous removal of load.

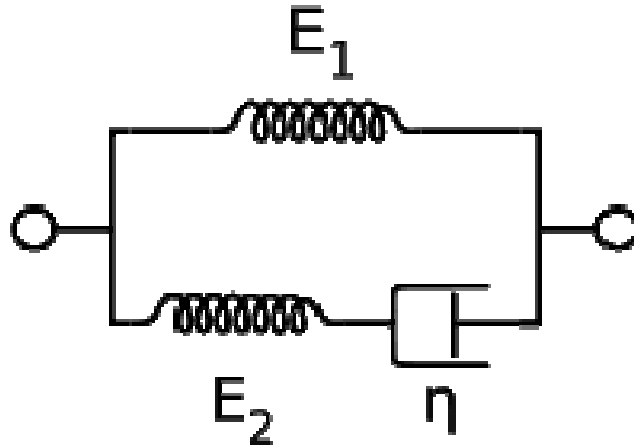


**Figure C.8:** Standard Linear Solid Model

As mentioned, springs and dampers may be added or rearranged to more closely approximate the behavior of the particular material being tested. For instance, in order to correct the instantaneous deformation recovery predicted by the Standard Linear Solid Model, one may add a damper in parallel to the arrangement. The possible combinations are limitless, but at some point the model may become overcomplicated for little enhancement of accuracy.

## C.5 Model Solutions and Tensor Analysis

Solution of the above described models begins with the creation of a first order differential equation using the equations that govern each element. A spring is modeled ideally with Hooke's Law according to Equation C.1:

**Equation C.1:** Ideal spring equation

Where:  $F_{\text{Spring}}$  is force in the element;  $k$  is the characteristic spring constant, most often called stiffness, and  $x$  is the deformation from the spring's equilibrium length. An ideal damper is modeled by Equation C.2:

$$F_{\text{Damper}} = c \frac{dx}{dt}$$

**Equation C.2:** Ideal damper equation

Where:  $F_{\text{Damper}}$  is the force in the element;  $c$  is the characteristic damping constant (not necessarily linear) and  $\frac{dx}{dt}$  is the time rate of deformation. The second order mass-acceleration term corresponding to the inertial body force is conspicuously missing, but it is often ignored for solution of the quasi-physical models. Further in terms of material test arrangements, the sample inertial body forces are minimally influential due to either very low acceleration of deformation or very low amplitude of deformation.

After defining the characteristic equations of each element, the differential equation can be formed based on the arrangement of the elements either in series or parallel. Series elements add directly, see Equation C.3:

$$F_{\text{Total}} = F_{\text{Element 1}} + F_{\text{Element 2}}$$

**Equation C.3:** Adding mechanical elements in series

While parallel elements add according to Equation C.4:

$$\frac{1}{F_{\text{Total}}} = \frac{1}{F_{\text{Element 1}}} + \frac{1}{F_{\text{Element 2}}}$$

**Equation C.4:** Adding mechanical elements in parallel

Reduction, simplification and solution of the differential equation yield a model that can be compared to experimental data for final material characterization.

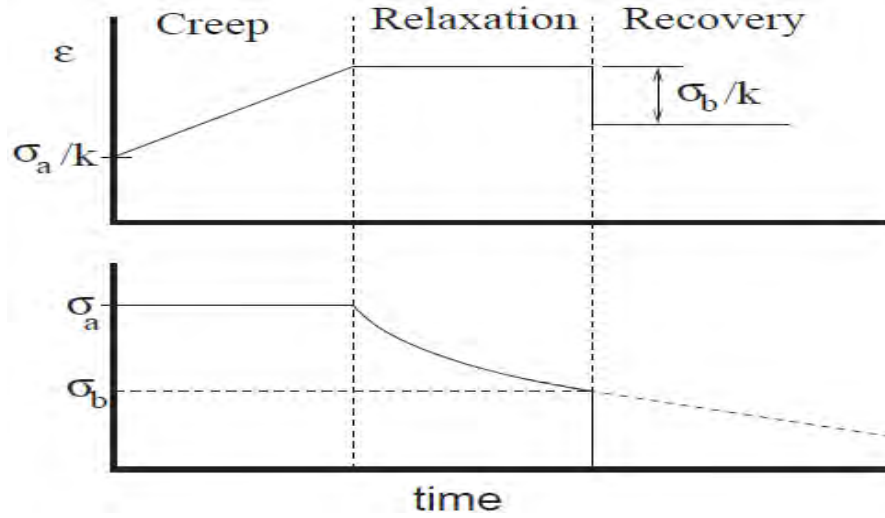


**Figure C.9:** Graphical representation of solution to Maxwell Model

\*Shown with constant stress differential

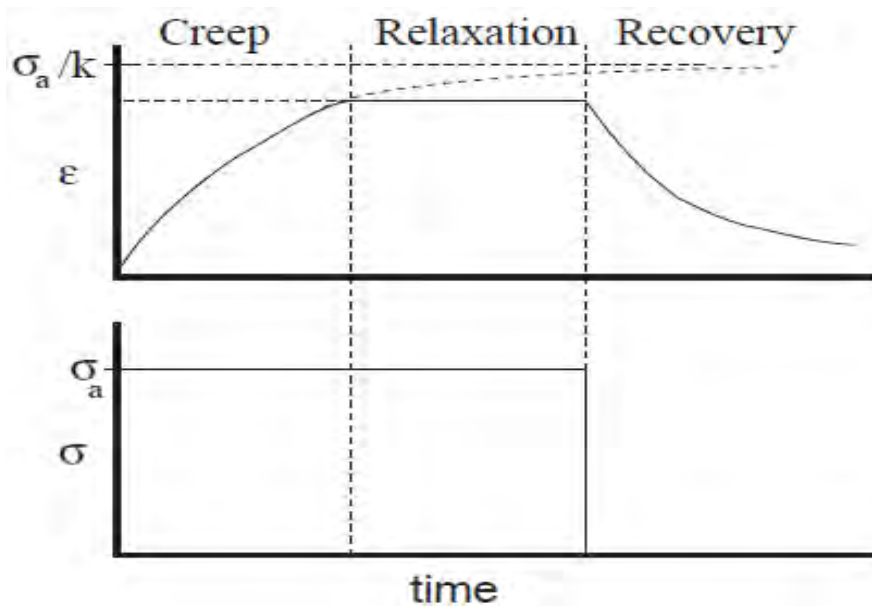


**Figure C.10:** Graphical representation of solution to Kelvin-Voigt Model

\*Shown with constant strain differential

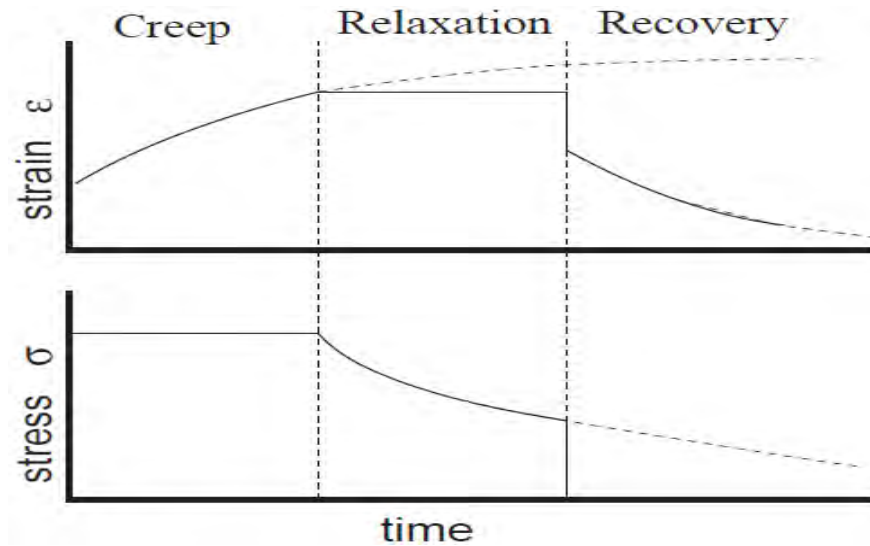


**Figure C.11:** Graphical representation of solution to Standard Linear Solid Model

\*Shown with coincident time scale

Departing from the quasi-physical model concept, the general solution to the viscoelastic phenomenon calls for tensor analysis by coupled equations. Coupled equations are used when two distinct but interdependent behavior are influential on a system. They are used in various analyses including mechanical dynamic systems, thermo-electrical systems etc. Tensor elements are employed to fully generalize the directionality of the material properties. The general coupled equations for viscoelastic behavior are given by Equation C.5:

$$\begin{aligned}
& \begin{bmatrix} \epsilon_{11}(t)\epsilon_{12}(t)\epsilon_{13}(t) \\ \epsilon_{21}(t)\epsilon_{22}(t)\epsilon_{23}(t) \\ \epsilon_{31}(t)\epsilon_{32}(t)\epsilon_{33}(t) \end{bmatrix} \\
& \begin{bmatrix} \sigma_{11}(t)\sigma_{12}(t)\sigma_{13}(t) \\ \sigma_{21}(t)\sigma_{22}(t)\sigma_{23}(t) \\ \sigma_{31}(t)\sigma_{32}(t)\sigma_{33}(t) \end{bmatrix} \\
= & \frac{\begin{bmatrix} \sigma_{11}(t)\sigma_{12}(t)\sigma_{13}(t) \\ \sigma_{21}(t)\sigma_{22}(t)\sigma_{23}(t) \\ \sigma_{31}(t)\sigma_{32}(t)\sigma_{33}(t) \end{bmatrix}}{\begin{bmatrix} Ci_{11} Ci_{12} Ci_{13} Ci_{14} Ci_{15} Ci_{16} Ci_{17} Ci_{18} Ci_{19} \\ Ci_{21} Ci_{22} Ci_{23} Ci_{24} Ci_{25} Ci_{26} Ci_{27} Ci_{28} Ci_{29} \\ Ci_{31} Ci_{32} Ci_{33} Ci_{34} Ci_{35} Ci_{36} Ci_{37} Ci_{38} Ci_{39} \\ Ci_{41} Ci_{42} Ci_{43} Ci_{44} Ci_{45} Ci_{46} Ci_{47} Ci_{48} Ci_{49} \\ Ci_{51} Ci_{52} Ci_{53} Ci_{54} Ci_{55} Ci_{56} Ci_{57} Ci_{58} Ci_{59} \\ Ci_{61} Ci_{62} Ci_{63} Ci_{64} Ci_{65} Ci_{66} Ci_{67} Ci_{68} Ci_{69} \\ Ci_{71} Ci_{72} Ci_{73} Ci_{74} Ci_{75} Ci_{76} Ci_{77} Ci_{78} Ci_{79} \\ Ci_{81} Ci_{82} Ci_{83} Ci_{84} Ci_{85} Ci_{86} Ci_{87} Ci_{88} Ci_{89} \\ Ci_{91} Ci_{92} Ci_{93} Ci_{94} Ci_{95} Ci_{96} Ci_{97} Ci_{98} Ci_{99} \end{bmatrix}}{\begin{bmatrix} K_{11}(t)K_{12}(t)K_{13}(t)K_{14}(t)K_{15}(t)K_{16}(t)K_{17}(t)K_{18}(t)K_{19}(t) \\ K_{21}(t)K_{22}(t)K_{23}(t)K_{24}(t)K_{25}(t)K_{26}(t)K_{27}(t)K_{28}(t)K_{29}(t) \\ K_{31}(t)K_{32}(t)K_{33}(t)K_{34}(t)K_{35}(t)K_{36}(t)K_{37}(t)K_{38}(t)K_{39}(t) \\ K_{41}(t)K_{42}(t)K_{43}(t)K_{44}(t)K_{45}(t)K_{46}(t)K_{47}(t)K_{48}(t)K_{49}(t) \\ K_{51}(t)K_{52}(t)K_{53}(t)K_{54}(t)K_{55}(t)K_{56}(t)K_{57}(t)K_{58}(t)K_{59}(t) \\ K_{61}(t)K_{62}(t)K_{63}(t)K_{64}(t)K_{65}(t)K_{66}(t)K_{67}(t)K_{68}(t)K_{69}(t) \\ K_{71}(t)K_{72}(t)K_{73}(t)K_{74}(t)K_{75}(t)K_{76}(t)K_{77}(t)K_{78}(t)K_{79}(t) \\ K_{81}(t)K_{82}(t)K_{83}(t)K_{84}(t)K_{85}(t)K_{86}(t)K_{87}(t)K_{88}(t)K_{89}(t) \\ K_{91}(t)K_{92}(t)K_{93}(t)K_{94}(t)K_{95}(t)K_{96}(t)K_{97}(t)K_{98}(t)K_{99}(t) \end{bmatrix}} \times \frac{d \begin{bmatrix} \sigma_{11}(t)\sigma_{12}(t)\sigma_{13}(t) \\ \sigma_{21}(t)\sigma_{22}(t)\sigma_{23}(t) \\ \sigma_{31}(t)\sigma_{32}(t)\sigma_{33}(t) \end{bmatrix}}{dt} \Bigg\} dt
\end{aligned}$$

**Equation 1**

$$\begin{aligned}
& \begin{bmatrix} \sigma_{11}(t)\sigma_{12}(t)\sigma_{13}(t) \\ \sigma_{21}(t)\sigma_{22}(t)\sigma_{23}(t) \\ \sigma_{31}(t)\sigma_{32}(t)\sigma_{33}(t) \end{bmatrix} \\
& = \begin{bmatrix} Ci_{11}Ci_{12}Ci_{13}Ci_{14}Ci_{15}Ci_{16}Ci_{17}Ci_{18}Ci_{19} \\ Ci_{21}Ci_{22}Ci_{23}Ci_{24}Ci_{25}Ci_{26}Ci_{27}Ci_{28}Ci_{29} \\ Ci_{31}Ci_{32}Ci_{33}Ci_{34}Ci_{35}Ci_{36}Ci_{37}Ci_{38}Ci_{39} \\ Ci_{41}Ci_{42}Ci_{43}Ci_{44}Ci_{45}Ci_{46}Ci_{47}Ci_{48}Ci_{49} \\ Ci_{51}Ci_{52}Ci_{53}Ci_{54}Ci_{55}Ci_{56}Ci_{57}Ci_{58}Ci_{59} \\ Ci_{61}Ci_{62}Ci_{63}Ci_{64}Ci_{65}Ci_{66}Ci_{67}Ci_{68}Ci_{69} \\ Ci_{71}Ci_{72}Ci_{73}Ci_{74}Ci_{75}Ci_{76}Ci_{77}Ci_{78}Ci_{79} \\ Ci_{81}Ci_{82}Ci_{83}Ci_{84}Ci_{85}Ci_{86}Ci_{87}Ci_{88}Ci_{89} \\ Ci_{91}Ci_{92}Ci_{93}Ci_{94}Ci_{95}Ci_{96}Ci_{97}Ci_{98}Ci_{99} \end{bmatrix} \times \begin{bmatrix} \epsilon_{11}(t)\epsilon_{12}(t)\epsilon_{13}(t) \\ \epsilon_{21}(t)\epsilon_{22}(t)\epsilon_{23}(t) \\ \epsilon_{31}(t)\epsilon_{32}(t)\epsilon_{33}(t) \end{bmatrix} \\
& + \int_0^t \left\{ \begin{bmatrix} F_{11}(t)F_{12}(t)F_{13}(t)F_{14}(t)F_{15}(t)F_{16}(t)F_{17}(t)F_{18}(t)F_{19}(t) \\ F_{21}(t)F_{22}(t)F_{23}(t)F_{24}(t)F_{25}(t)F_{26}(t)F_{27}(t)F_{28}(t)F_{29}(t) \\ F_{31}(t)F_{32}(t)F_{33}(t)F_{34}(t)F_{35}(t)F_{36}(t)F_{37}(t)F_{38}(t)F_{39}(t) \\ F_{41}(t)F_{42}(t)F_{43}(t)F_{44}(t)F_{45}(t)F_{46}(t)F_{47}(t)F_{48}(t)F_{49}(t) \\ F_{51}(t)F_{52}(t)F_{53}(t)F_{54}(t)F_{55}(t)F_{56}(t)F_{57}(t)F_{58}(t)F_{59}(t) \\ F_{61}(t)F_{62}(t)F_{63}(t)F_{64}(t)F_{65}(t)F_{66}(t)F_{67}(t)F_{68}(t)F_{69}(t) \\ F_{71}(t)F_{72}(t)F_{73}(t)F_{74}(t)F_{75}(t)F_{76}(t)F_{77}(t)F_{78}(t)F_{79}(t) \\ F_{81}(t)F_{82}(t)F_{83}(t)F_{84}(t)F_{85}(t)F_{86}(t)F_{87}(t)F_{88}(t)F_{89}(t) \\ F_{91}(t)F_{92}(t)F_{93}(t)F_{94}(t)F_{95}(t)F_{96}(t)F_{97}(t)F_{98}(t)F_{99}(t) \end{bmatrix} \times \frac{d \begin{bmatrix} \epsilon_{11}(t)\epsilon_{12}(t)\epsilon_{13}(t) \\ \epsilon_{21}(t)\epsilon_{22}(t)\epsilon_{23}(t) \\ \epsilon_{31}(t)\epsilon_{32}(t)\epsilon_{33}(t) \end{bmatrix}}{dt} \right\} dt
\end{aligned}$$

## Equation 2

### Equation C.5: Coupled equations defining viscoelasticity

The tensor equations can be written more concisely as:

$$[\epsilon(t)] = \frac{[\sigma(t)]}{[Ci]} + \int_0^t [K(t)]x \frac{d[\sigma(t)]}{dt} dt \quad \text{Equation 1}$$

$$[\sigma(t)] = [Ci]x[\epsilon(t)] + \int_0^t [F(t)]x \frac{d[\epsilon(t)]}{dt} dt \quad \text{Equation 2}$$

Note that the fourth order tensor  $[Ci]$  is the instantaneous stiffness matrix for a given material and is not required to be equal in both equations. The functions  $[K(t)]$  and  $[F(t)]$  are known as the creep and stress relaxation function respectively and are both fourth order tensors in their most general forms. The generalized coupled equations can be solved under the formulation of Volterra Equations where if material properties are known, behavior can be

predicted, or if behavior is known from experimentation, material constants can be extrapolated for characterization.

The mathematical analysis used for processing the results of forced dynamic testing is based on the phase shift angle that can be easily measured from recorded data. Since phase shift is most commonly measured first in units of time, the angle must be extracted based on frequency according to Equation C.6:

$$\delta = \frac{2\pi(\Delta t)}{f}$$

**Equation C.6:** Phase angle calculation

Where:  $\delta$  is the phase shift angle in radians;  $\Delta t$  is the measured phase shift in seconds and  $f$  is frequency. Typically,  $\delta$  is referred to as the loss angle and  $\tan(\delta)$  is referred to as the loss tangent. Dynamic modulus is a second key value for characterization of viscoelasticity. It is defined by the following complex equation, Equation C.7:

$$\frac{\sigma}{\epsilon_0} = E' + iE''$$

**Equation C.7:** Dynamic modulus relationships

In this case,  $\sigma$  and  $\epsilon_0$  are harmonic functions in time;  $E'$  and  $E''$  are the values of dynamic modulus where  $E''$  represents an imaginary value. In the field of materials testing,  $E'$  is often referred to as the storage modulus and  $E''$  as the loss modulus. Further, the values of dynamic modulus are related by Equation C.8:

$$\tan \delta = \frac{E''}{E'}$$

**Equation C.8:** Dynamic modulus relation to phase angle

\*This relationship assumes that all values are taken at the same frequency